The Final Report

Next Generation Affordable Small-Payload Launch System

R.J.F. van den Berg 4268997
D.A. Foulds 4298152
Z.X. Ge 4272358
N.A. Johnson 4195787
J. Negro Vadillo 4356845
S.J. Park 4120817
M. Reverda 4276299
G. Salvi 4347137
B.S. Sanghera 4356608
A. Shambalov 4362780

DESIGN SYNTHESIS EXERCISE
Spring 2017 Group S17

TU Delft Delft University of Technology

This page is intentionally left blank.

SMALL PAYLOAD LAUNCH SERVICE

NEXT GENERATION AFFORDABLE SMALL-PAYLOAD LAUNCH SYSTEM

by

A. Shambalov	**4362780**
B.S. Sanghera	**4356608**
D.A. Foulds	**4298152**
G. Salvi	**4347137**
J. Negro Vadillo	**4356845**
M. Reverda	**4276299**
N.A. Johnson	**4195787**
R.J.F. van den Berg	**4268997**
S.J. Park	**4120817**
Z.X. Ge	**4272358**

Tutor: Ir. Marc Naeije
Coaches: Dr. Claudio Lettieri
Paul Lancelot, MSc.

Wednesday 5 July, 2017

Version	Date	Changelog
1	27 June 2017	Initial Version

TU Delft Delft University of Technology

This page is intentionally left blank.

PREFACE

Before you lies the bachelor's thesis 'Next Generation Affordable Small-Payload Launch System'. The bachelor's thesis has been written to fulfil the graduation requirements of the Aerospace Engineering bachelor given at the Technology University of Delft. The authors of this report have been engaged in designing and reporting this bachelor's thesis from the end of April till the first week of July, 2017.

The thesis subject has been derived from the actual and ever increasing need of an affordable small payload launch service. The assigned task was to establish the preliminary definition of the affordable small-payload launch system. The search for this particular launch service was difficult, but after conducting extensive research, we were able to find a sustainable and revolutionary launch service with the required performance.

We hope you enjoy your reading.

DSE Group 17
Delft, Wednesday 5 July, 2017

This page is intentionally left blank.

ACKNOWLEDGEMENTS

The authors of this report would like to express their gratitude towards and appreciation of the professionalism of the supervisor Ir. Marc Naeije and the coaches Dr. Claudio Lettieri and Paul Lancelot, MSc. for providing the necessary guidance. Moreover, the authors would like to express their gratitude towards the client of this project, Bertil Oving; and the co-client Arnaud van Kleef for their general support. Additionally special thanks goes out to the staff of the University of Delft for providing us with their academic experience. Last but not least, we would also like the express our deepest appreciation to our families for supporting us at all times.

This page is intentionally left blank.

SUMMARY

Over the course of the last few years, the market for small satellites has grown considerably. However, there are almost no launch systems that are dedicated to this smaller size of satellites. This has as a consequence that small satellites have to ride piggy-back with other, bigger satellites on larger launch vehicles. This leads to very low flexibility in launch schedule as well as costs, as they are secondary payloads. Moreover, the small satellites have to stick to the same orbit the main payload is launched into, which often is far from ideal for the smaller payloads. To solve this issue, ALTAR took on the challenge to design an affordable and sustainable launch system that can put small satellites into orbit. Originally, the goal was set for payloads up to 20 kg up to a 700 km orbits. However, after a thorough market analysis, the payload weight was extended to 35 kg, while the maximum orbit altitude was decreased to 600 km with a sun-synchronous inclination, in accordance with the client. Furthermore, to be competitive in the future market, the launch costs should not exceed 50 k$/kg. With these top-level requirements in mind, the ALTAR team set out to find and design a concept that could deliver the flexibility for smaller satellites that was envisioned.

After an all-encompassing literature study into possible design options, the decision was made to go with the stratospheric balloon concept as it was deemed to have the potential to be the cheapest, while being relatively environmentally friendly and was deemed to be a big innovation to the space industry. For this concept a rocket is connected to a stratospheric balloon through a gondola. The balloon brings the rocket to an altitude of almost 40 km where the rocket is launched. This has a lot of advantages; the rocket experiences almost no aerodynamic drag, no static launch facilities are required, there are no emissions in the lower atmosphere and the balloon can be reused. Overall this was deemed to lead to the most sustainable and cheapest design.

After this design choice was made, the different subsystems were designed in more detail, which led to more detailed design choices. These choices will be qualitatively summarised below, divided into the three main components; Balloon, Gondola and Rocket.

Figure 1: A render of the balloon including the pressure vents, film and load tapes. Fewer load tapes than in reality are shown for clarity.

Balloon
The balloon will be made out a film of high density polyethylene (HDPE) reinforced with Zylon load tapes to support the film. The connection between the balloon, gondola and rocket will be done with polyester threads. Furthermore, the balloon will be filled with helium, mostly because that is the safest option. Six vents to keep the pressure equal to the local atmospheric pressure will be installed at the bottom of the balloon and a duct on the top to release helium before descent and retrieval. A render of the balloon showing the load tapes and pressure vents can be seen in fig. 1. The balloon can be steered during descent using a wing connected by a tether that is at a significantly lower altitude than the balloon. This Balloon Guidance System (BGS) will allow the balloon to be landed within a target area and can steer it away from populated areas during descent.

Gondola
The gondola connects the rocket to the balloon and is the interface between them. It will house the communication, which will mostly be done through S-Band. Furthermore, it will include the separation mechanism that separates the rocket and points the rocket in the right direction in both pitch and heading. The gondola also includes a parachute, which can be deployed in case of balloon or rocket failure to save the payload. The payload will stay connected to the gondola, while connections to the rest of the rocket and balloon are severed. It also houses one of the two lithium ion batteries, which will power all systems (the other battery is located within the rocket).

Rocket
The rocket will consist of three stages all of which will use a solid propellant consisting of aluminium powder, ammonium perchlorate and HTPB (a common binder). The third stage will also feature a mono-propellant orbital manoeuvring system to circularise and fine tune the final orbit. Stage one and two propellant grains will be moulded into a cylindrical mould with a hollow internal star shape. The third stage solid grain is end burning, without an internal cavity. The combustion chambers feature hemispherical endcaps and they are made from 7075 aluminium. A render of the propellant grains for each stage can be seen in fig. 2.

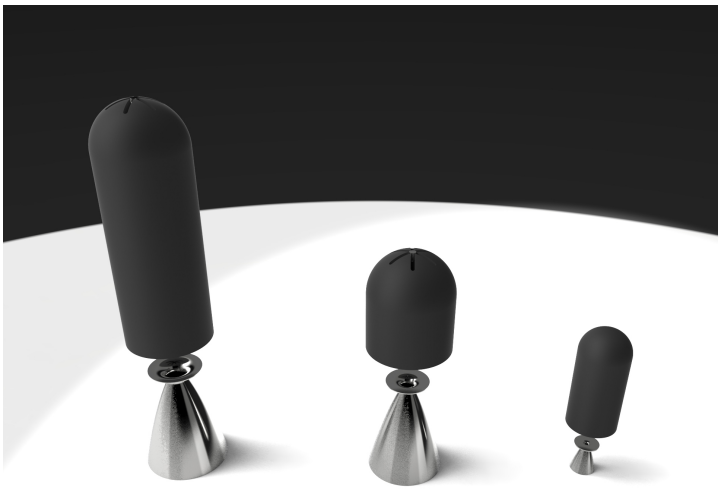

Figure 2: The solid propellant grains of each stage and their respective nozzle. Going from the first stage on the left to the final stage on the right.

Due to the lack of a dense atmosphere to balance or steer the rocket aerodynamically, this must be done by thrust vectoring. Thrust vectoring will be performed by four jet vanes inside the nozzle,

which will be made out of a tungsten-molybdenum alloy. The nozzles themselves will be made out of steel with an ablative material inner coating (e.g. Silica Fibres). The final stage will also have twelve ADCS thrusters and two Orbital Manoeuvring thrusters to accurately bring multiple payloads into orbit. Both types of thrusters will be mono-propellant hydrazine thrusters. The payload will be dispensed through either CubeSat dispense pods or a spring based separation system, depending on the type of payload(s). The fairing will be conical in shape and made out of reinforced HDPE. The upper stages and the fairing will burn up in the atmosphere while the first stage of the rocket will make a controlled splash down into the ocean.

To make the development of ALTAR possible a time line has been made. This time line includes testing, launch location, business plan, logistics and regulations concerning the production of an orbital class launch system. Over a five year period the rocket and balloon will be developed, tested and certified. After this period an initial market share of 2% will be available to the newly developed launch system. This share will grow to the market share goal of 20% of new satellites under 50 kg after 15 years. This growth with follow along a S-curve as can be seen in fig. 3. The ALTAR system will have a break even point of 5 years after begin of operation.

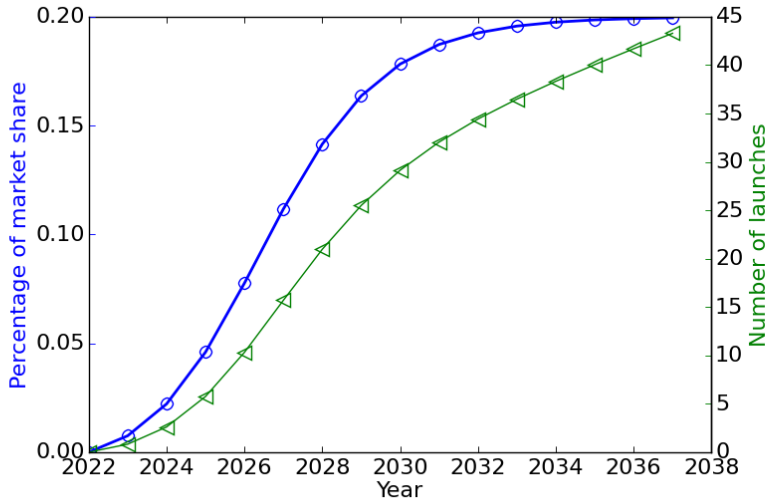

Figure 3: The expected evolution of the market share over ALTAR mission life

The system will be able to launch up to 35 kg into a sun-synchronous orbit at an altitude of 600 km while having an estimated reliability of around 91.5 %. Furthermore, it will be a sustainable design as nothing will be emitted into the lower atmosphere and very few non-renewable resources are wasted. With this performance, ALTAR will meet the requirements and will be a highly profitable launch system that can innovate the space market by offering a service tailored to the needs of the small satellites. This gives them more flexibility for a competitive price.

This page is intentionally left blank.

CONTENTS

This page is intentionally left blank.

List of Abbreviations

Abbreviation	*Stands for*
ADCS	Attitude determination & control system
ALTAR	A lighter than air rocket
AOA	Angle of attack
APRS	Automatic packet reporting system
BGS	Balloon guidance system
BPSK	Binary phase shift keying
CG	Center of gravity
COGS	Cost of goods sold
COTS	Commercial-Off-The-Shelf
CTPB	Carboxy-terminated Polybutadiene
DoD	United States department of defense
EBIT	Earnings before interest and tax
EBT	Earnings before tax
ECB	European central bank
ER	Exchange rate US Dollar to Euro
ESA	European space agency
FEM	Finite element method
FIR	Fixed interest rate
FTS	Flight termination system
GPS	Global positioning system
GUI	Graphical user interface
HDPE	High density PolyEthelyne
HTPB	Hydroxyl-Terminated PolyButadiene
IMU	Inertial Measurement Unit
IPMT	Interest payment
LLP	Limited liability partnership
LP	Launchpad
MEOP	Maximum expected operating pressure
NI	Net income
OMS	Orbit manoeuvre system
PBAN	Polybutadiene acrylonitile
PD&D	Project design and development
PPMT	Principal payment
RCS	Reaction control system
ROI	Return on investment
RX	Receiver
SN	Serial number
SSO	Sun synchronous orbit
TM&C	Telemetry and communications
TSOT	Trajectory simulation and optimisation tool
TVC	Thrust vector control
TX	Transmitter

This page is intentionally left blank.

List of Symbols

Symbol	*Stands for*	*Unit*
A	Aspect ratio	–
A^*	Nozzle throat area	m^2
A_b	Burning surface area	m^2
A_B	Balloon cross-sectional area	m^2
A_e	Nozzle exit area	m^2
A_{stage}	Surface area of a stage	m^2
A_t	Nozzle throat area	m^2
A_w	Contact surface of the engine with combustion gases	m^2
$\boldsymbol{a}$	Acceleration vector	m/s^2
a	Constant factor in the equation of the burning rate	$m/s/MPa^n$
a_{max}	Maximum acceleration	m/s^2
b	Wing span	m
bl	Slope of the learning curve	–
C_{B_P}	Production cost of the balloon	€
C_D	Drag coefficient	–
C_{D_B}	Drag coefficient of the balloon	–
C_f	Friction coefficient	–
C_{He}	Price of Helium per flight	€
C_L	Lift coefficient	–
C_p	Pressure coefficient	–
C_{sal}	Cost of salaries	€
$C_{STRATOS}$	Acquisition cost of the Stratos balloon financed by Redbull	€
C_T	Thrust coefficient	–
C_y	Production cost of the considered serial number	€
$\boldsymbol{c}(\boldsymbol{u})$	Vector of constraint violations	–
c	Wing chord	m
c^*	Characteristic velocity of the propellant	m/s
C_0	First unit production cost	€
D	Diameter of the engine	m
D	Drag	N
D_{sys}	Drag of the system	N
D_{tether}	Drag of the tether	N
D_{wing}	Drag of the wing	N
d_{drift}	The horizontal distance to drift the rocket till it launches	km
$d_{control}$	The horizontal distance to control the balloon during decent	km
$d_{platform}$	The maximum horizontal distance that balloon has travelled	km
d_{tether}	Diameter of the tether	m
E	Young's modulus	Pa
$\frac{E_b}{N_o}$	Energy per bit to noise power spectral density ratio	–
e	Oswald efficiency factor	–
EH	Cost of an engineering hour	€
$F(\boldsymbol{u})$	Cost function for the optimisation routine	–

Symbol	*Stands for*	*Unit*
$F_{control}$	Control force due to BGS	N
$F.R.$	Fineness ratio	–
F_{SL}	Strength of suspension lines	kg
F_T	Thrust force magnitude	kg
$\hat{\boldsymbol{f}}$	Pointing direction state vector	–
f_{ni}	Natural frequency	Hz
g_0	Acceleration due to gravity	$m/(s \cdot s)$
HPY	Hours worked per year	h
H_s	Total enthalpy	J
H_w	Enthalpy of the wall	J
h	Altitude above sea-level during launch	m
h_s	Stage altitude at burn-out	m
I	Impulse	$kN \cdot s$
I_{sp}	Specific impulse	s
I_{xx}	Moment of Inertia about the x-axis	$kg \cdot m^2$
j	Index of the currently active stage during simulation	–
i	Target inclination	rad
J	Jacobian of the constraint violations with respect to the control inputs	–
L	Length of the engine	m
L_{bell}	Divergent nozzle length	m
L_{cyl}	Cylindrical propellant grain length	m
L_{gr}	Propellant grain length	m
L_{nozz}	Nozzle length	m
L_S	Length of suspension lines	m
L_{sub}	Percentage of nozzle submerged in the combustion chamber	–
L_{wing}	Lift of the wing	N
l_{tether}	The length of the tether	m
M_C	Maintenance Cost	€
$M_{cylinder}$	Mass of the cylindrical part of the solid propellant tanks	kg
MDT	Mean down time	h
MLH	Maintenance labour hours	h
M_{para}	Mass of the parachute	kg
M_R	Total mass of the rocket	kg
$M_{sphericalend}$	Mass of the spherical end of the solid propellant tanks	kg
$MTBT$	Mean time between maintenance	h
$MTTM$	Mean time to maintain	h
M_W	Molecular weight	g/mol
M_x	Moment around the x-axis	$N \cdot m$
$\dot{m}$	Propellant mass flow	kg/s
m	Total vehicle mass	kg
m_{insul}	Mass of the motor insulator	kg
m_{nozz}	Mass of the nozzle	kg
m_{payload}	Mass of the payload	kg
m_{prop}	Mass of the propellant	kg
$N_{platform}$	Number of landing platforms	–
N_{SL}	Number of suspension lines	–
n	Exponent in the equation for the burning rate	–

Symbol	*Stands for*	*Unit*
n_{star}	Number of propellant grain stars	–
p_a	Atmospheric pressure	Pa
p_c	Combustion chamber pressure	Pa
p_e	Nozzle exit pressure	Pa
PHe	Price per kg of Helium	\$/kg
PP	Percentage of production cost over total cost	–
Q_A	Heat dissipating to the air	J
Q_B	Heat dissipating to the stage	J
R	Code rate	–
R_A	Universal gas constant	J/(kmol·K)
R_B	Balloon radius	m
R_e	Mean radius of the earth	m
$\boldsymbol{r}$	Position state vector	m
r^*	Nozzle throat radius	m
r_a	Apogee radius	m
r_b	Propellant burn rate	m/s
r_e	Nozzle exit radius	m
r_f	Final radius	m
r_c	Nozzle convergent radius	m
r_d	Nozzle divergent radius	m
r_{gr}	Propellant grain radius	m
r_i	Nozzle inlet radius	m
r_p	Perigee radius	m
$r_{star,i}$	Propellant grain inner star radius	m
$r_{star,o}$	Propellant grain outer star radius	m
S_0	Surface area of the canopy	m^2
St	Stanton number	–
$\boldsymbol{s}^c$	Search direction to minimise the constraint violations	–
$\boldsymbol{s}^o$	Search direction to minimise the cost function	–
s	curve length	m
t	Simulation time	s
T	Thrust	N
T_0	Stagnation temperature	K
T_c	Combustion chamber temperature	K
t_b	Burn time of the engine	s
$t_{control}$	The time for balloon to arrive at one of the platforms	s
t_{rot}	Time of rotation	s
t_{star}	Propellant grain star thickness	m
$\boldsymbol{u}$	Vector of control inputs in the optimisation routine	–
V_B	Velocity of the balloon	m/s
$V_{control}$	Control velocity	m/s
V_{rel}	The relative velocity	m/s
V_p	Propellant volume	m^3
V_s	Free stream velocity for re-entering stage	m/s
$\boldsymbol{v}$	Velocity state vector	m/s
v_{eq}	Equivalent exit velocity	m/s
v_e	Exit velocity	m/s
v_f	Magnitude of the final velocity vector	m/s

Symbol	*Stands for*	*Unit*
W	Weight	N
w_c	Specific mass of the canopy	kg/m^2
w_{SL}	Specific mass of suspension lines	kg/m^2
α	Angle of the control velocity acting on the balloon	°
α_B	Deviation of balloon from original trajectory due to BGS	°
α_i	Real part of a complex number	–
$\ddot{\alpha}$	Angular acceleration about the x-axis	rad/s^2
β_i	Complex part of a complex number	–
γ	Ratio of specific heats	–
Γ	Vandenkerckhove function	–
δ	Axial displacement	m
Δd	Distance between two consecutive contour curves	m
Δt	Burn time between two consecutive contour curves	m
ε	Nozzle expansion ratio	–
η	Efficiency factor for the combustion chamber	–
θ	Pitch angle	rad
$\dot{\theta}$	Pitch rate	rad/s
θ_i	Nozzle contour angle at I	rad
θ_e	Nozzle exit angle at E	rad
λ	Nozzle efficiency factor	–
μ_e	Gravitation parameter of Earth	m^3/s^2
ρ	Air density	kg/m^3
ρ_{prop}	Density of the propellant	kg/m^3
σ_{hoop}	Hoop stress due to internal pressure	Pa
σ_{yield}	Yield stress	Pa
ς	Optimisation step size	–
φ	Latitude of the launch site	rad
Ω	Angular rotation rate of the Earth	rad

1

INTRODUCTION

Due to the rapidly decreasing cost and size, and increasing capability of electronics, the operation of microsatellites and satellite swarms has become increasingly feasible for private companies and research institutions. Companies like Planet Labs and Astrocast operate large constellations of CubeSats for Earth observation or communications purposes[1]. Since 1998, over 1600 nanosatellites have been launched into orbit [1]. This amount is expected to increase rapidly over the coming years [2–4]. Up to this time, most of these satellites are launched piggyback with larger satellites on launchers with excess capacity available [1]. Launching piggyback limits the payload to the same orbit as the primary satellite. Therefore, the ALTAR team have been assigned the task to design and develop an affordable small-payload launcher service.

In the previous Midterm Report [5], three concepts have been traded off to come to the design choice of a rocket launched from a stratospheric balloon. This Final Report will continue on the basic outline of this concept that has already been sketched and work out all subsystems as well as procedures, financing and logistics that are deemed necessary to produce a successful launch system.

The structure of the report is as follows; it will start with an overview of the current system in chapter 2 as well as a recap of the previous design efforts. These efforts can be found in more detail in the Midterm Report. After stating the requirements, this report will continue with a thorough analysis of the trajectory of the launch system found in chapter 3. After the trajectory of the launch system has clearly been defined, an in-depth analysis of all major components of the system will follow. This is done in chapter 4, where the balloon, gondola and rocket and their major subsystems are worked out one by one. After the design concept has been given shape with clearly defined (sub)systems, the performance of the launch system is analysed, while also looking at the sensitivity of the complete model for the launch system in chapter 5. Moreover, this chapter includes the cost analysis in which the costs for all major components will be estimated. Furthermore the operational and development costs are estimated after which the cost analysis is concluded with a total financial plan that follows the whole mission time-line. This cost analysis is followed by a short look into the RAMS aspects of this design as well as its sustainability and risks. Chapter 5 is concluded with a check on each requirement that has been defined at the start of the report. Subsequently, the verification and validation efforts of all models are summarised in chapter 6. Having almost concluded the whole design, a business plan is suggested in chapter 8, which carefully details the process with which profit will be made from the design. Lastly, the report is concluded in chapter 9, in which the final design and its performance are discussed, as well as recommendations for future development of ATLAS.

[1] More information on these companies can be found at https://www.planet.com/ and http://www.astrocast.net/

This page is intentionally left blank.

2

System Overview

2.1. Trade-off Summary

During the initial phase of the project, many design options capable of satisfying the mission need statement have been identified and evaluated. Three design concepts remained after a high level trade-off as the most attractive for mission performance. These options are a ground based multi-stage rocket, a rocket launched from a stratospheric balloon and a rocket with a beam powered propulsion system using a heat exchanger. Representation of those concepts can be seen in fig. 2.1.

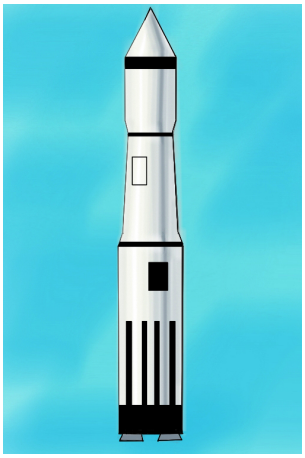

(a) Multi-stage rocket concept

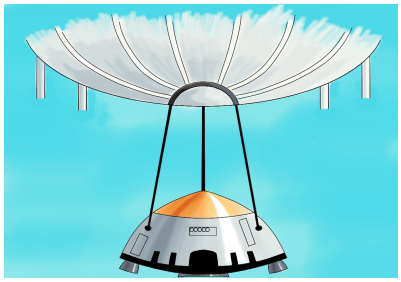

(b) Stratospheric balloon concept

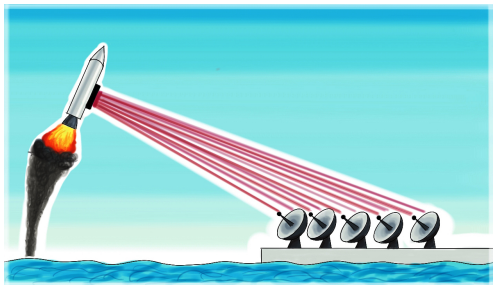

(c) Heat exchenger concept

Figure 2.1: A schematic overview of considered concepts

The main criteria that have been used during the trade-off process were mission risk, sustainability, cost per launch and development risk. The component that had the most influence on the trade-off table was cost per launch. The only concept that met the cost per launch requirement was the stratospheric balloon concept, therefore getting the highest score in the final trade-off and being chosen for the mission accomplishment. Detail design of the stratospheric balloon launcher is going to be discussed in chapter 4.

2.2. Mission Profile

In this section the mission profile is given for the ALTAR launch system. A brief illustrative overview of the mission profile will be displayed in fig. 2.2. Where the duration, velocity and altitude of the mission phases will be given. A more detailed mission profile is given in the form of a Functional Flow Block Diagram (FFBD) in fig. 2.3 and fig. 2.4, where every process involved in the launch system is given. Also a Functional Breakdown Block Diagram (FBBD) was created, which can be seen in fig. 2.5. In the mission FBBD, elements of the mission FFBD are grouped together to identify necessary hardware and software components.

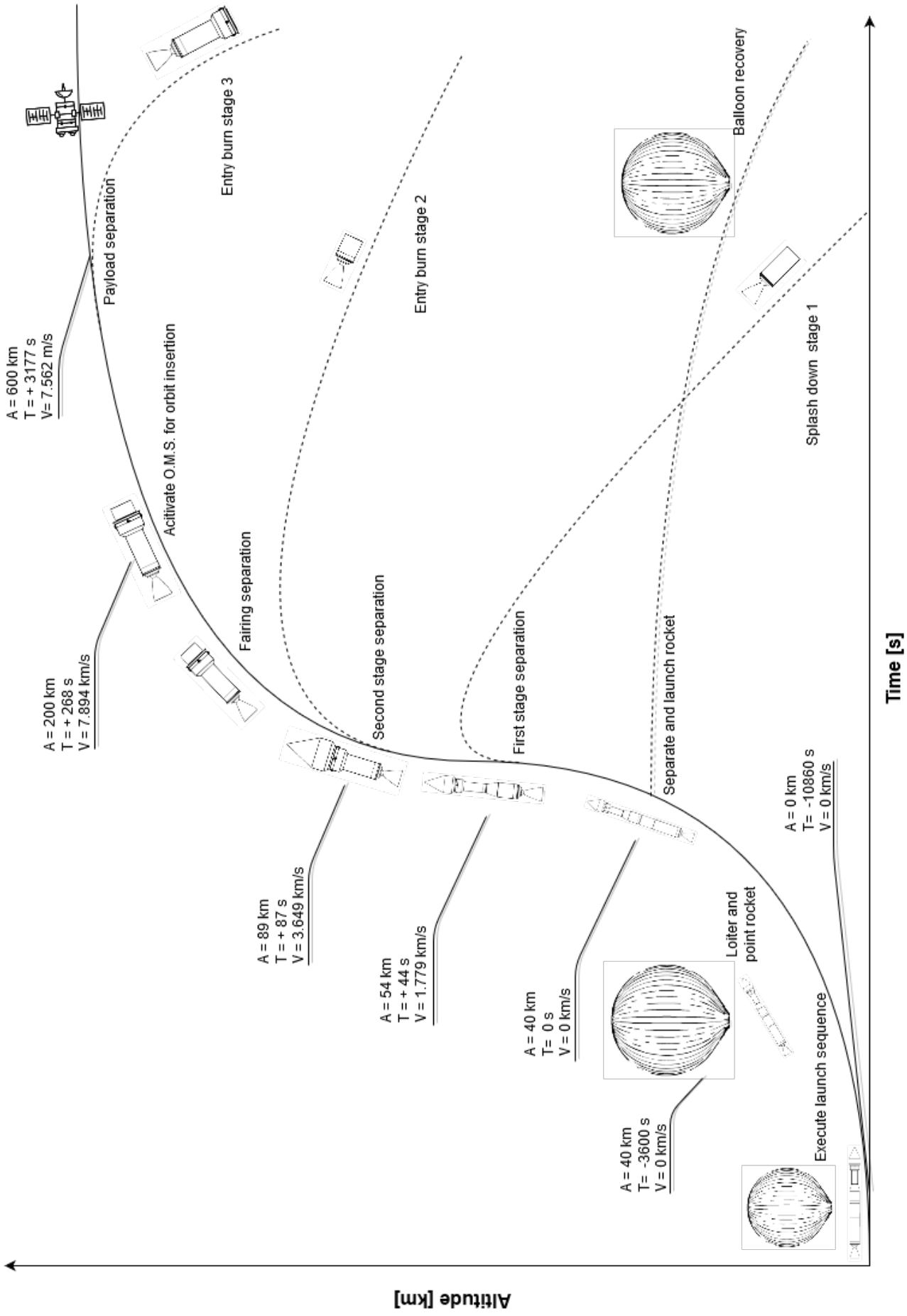

Figure 2.2: A mission profile overview. The overview is not to scale, it is meant for illustrative purposes of displaying the mission phases. The letters A, T, V, indicate altitude, time and velocity respectively.

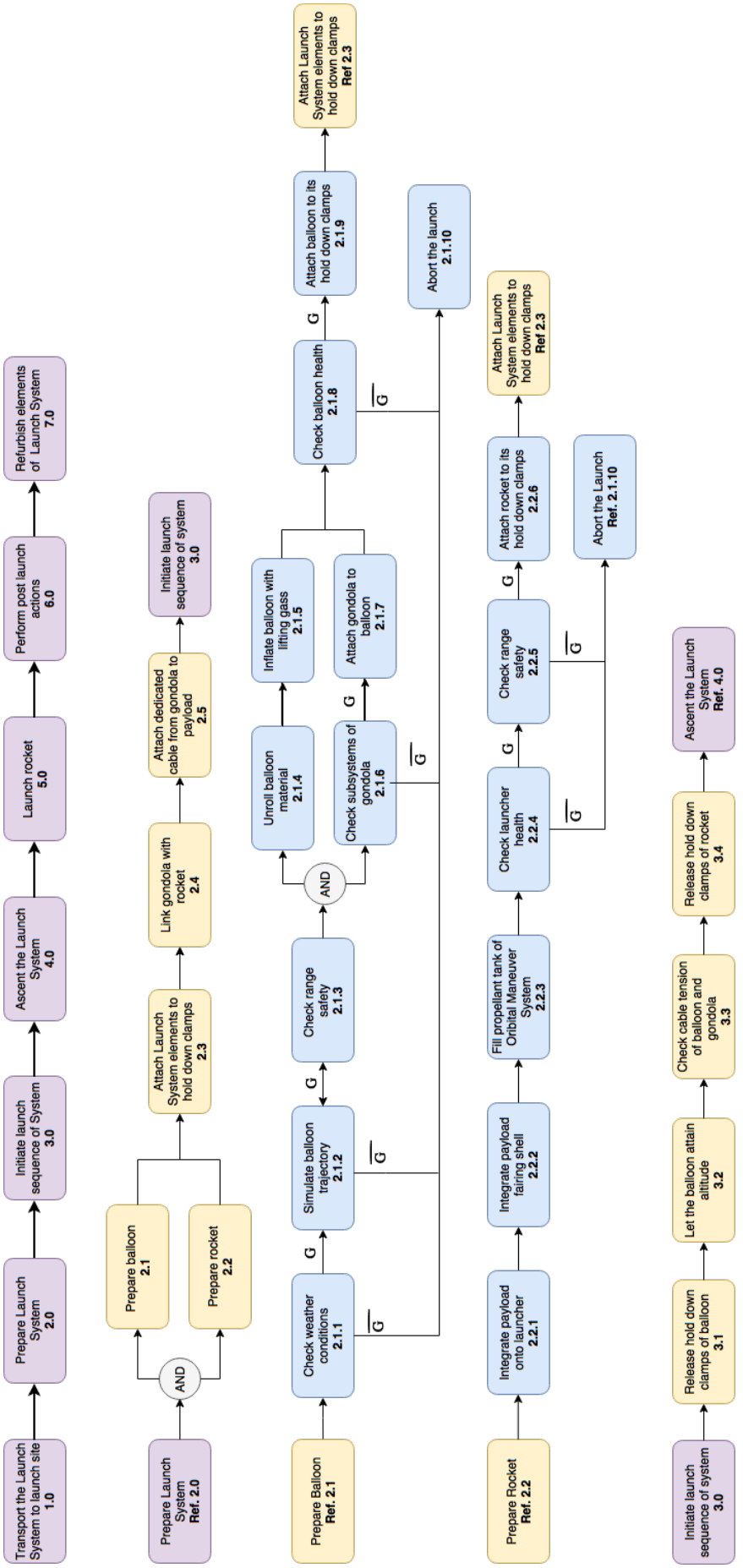

Figure 2.3: Part one of a functional flow block diagram of the mission. This shows a sequential order of processes that must be executed, such that the ALTAR launch can be operated correctly.

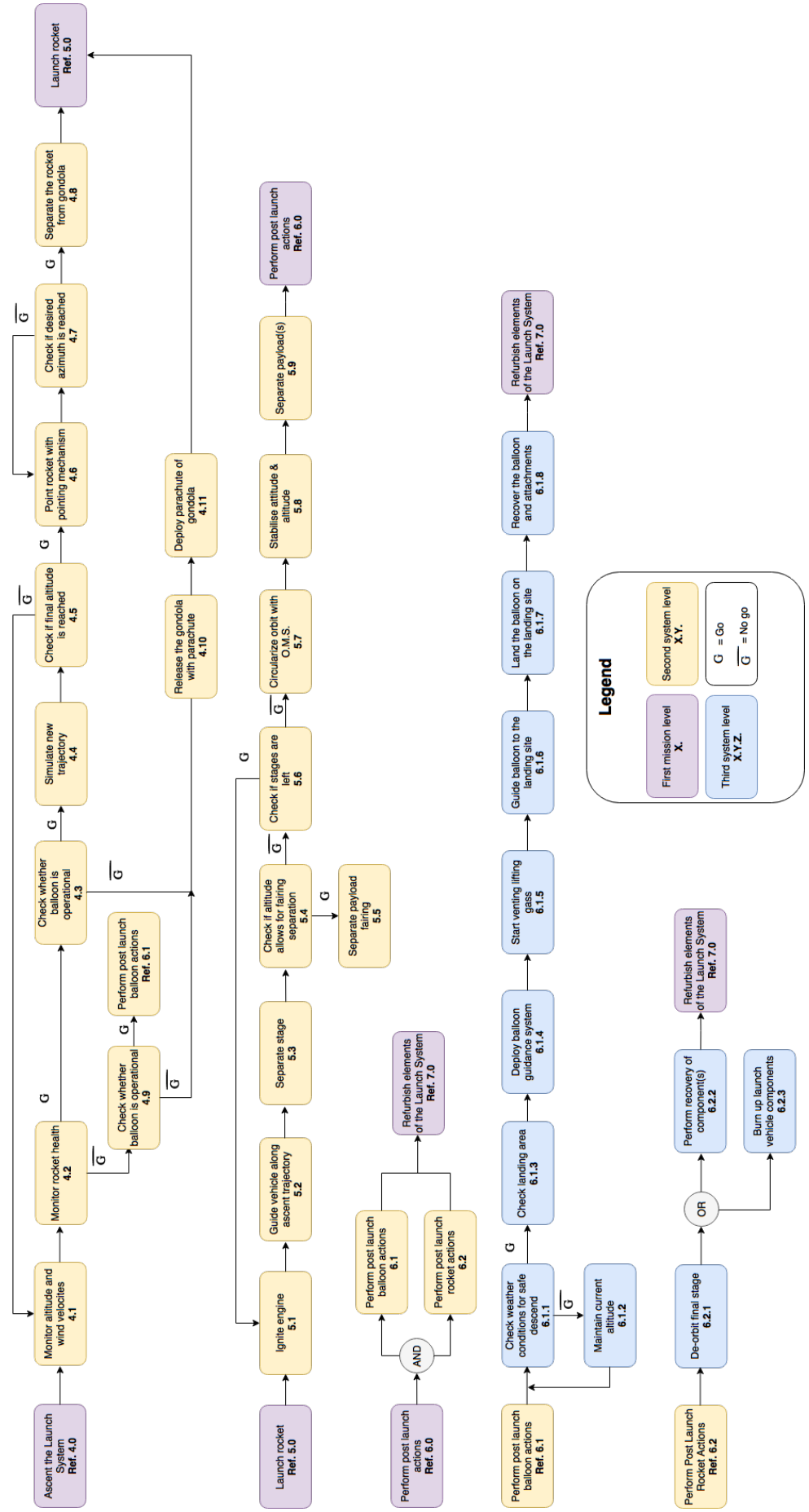

Figure 2.4: Part two of a functional flow block diagram of the mission.

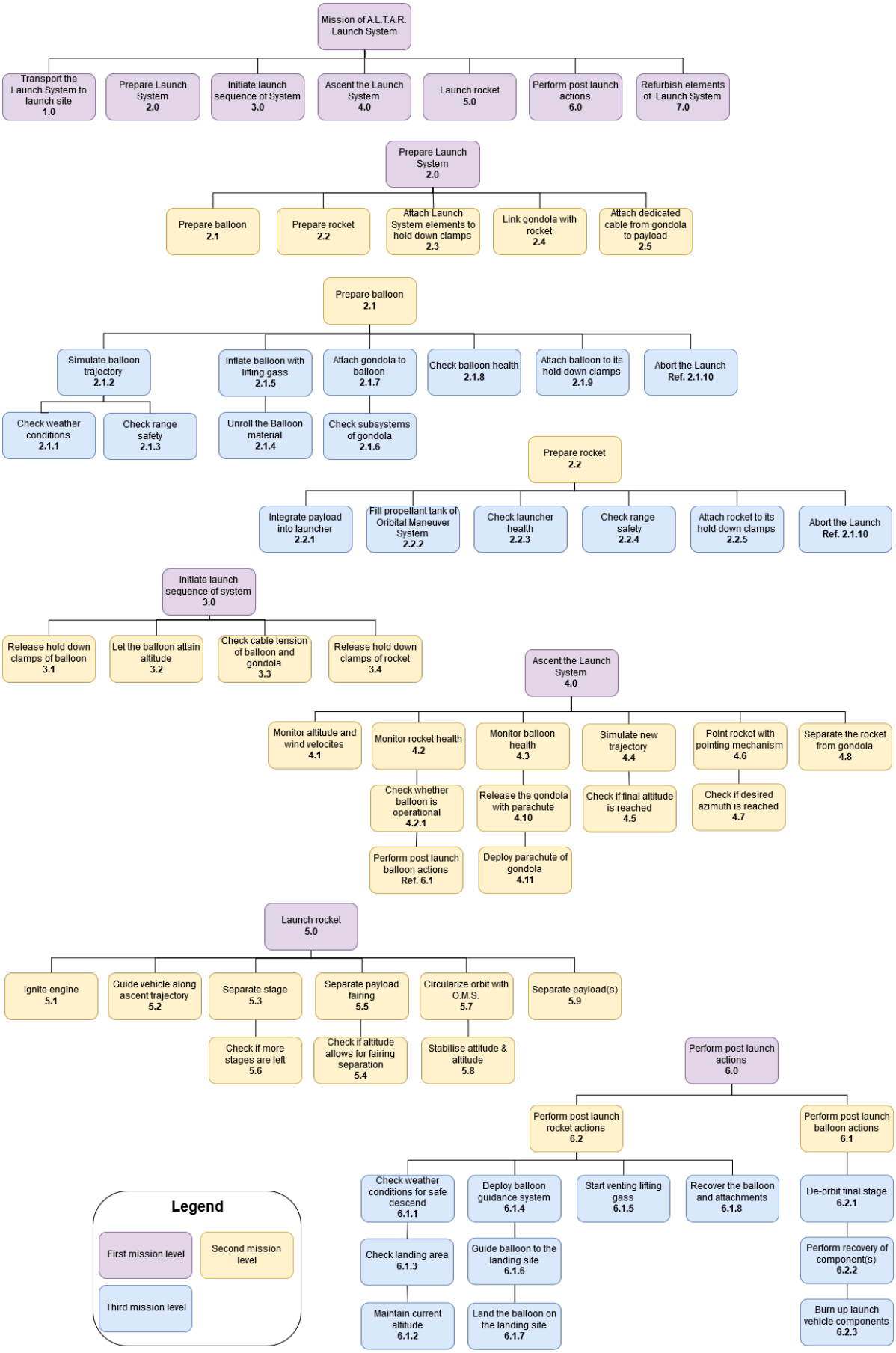

Figure 2.5: The mission functional breakdown block diagram (FBBD). This is based on the mission flow block diagram. The logic of the numbers can be found in the previous two figures. The mission FBBD helps with identifying the software and hardware needed for the mission execution. The blocks that are grouped together and the blocks that are aligned in the same vertical axis. These can be replaced with one hardware or software component.

This page is intentionally left blank.

3

Trajectory Simulation and Optimisation Tool

For the conceptual design of the launch vehicle, a trajectory simulation and optimisation tool was developed. It is separated into two main components: the trajectory simulation and the optimisation routines.

3.1. Simulation of Trajectories

The purpose of the simulation component is to use the initial state, data about the vehicle, and the steering profile, to propagate the position and velocity of the vehicle until some specified end condition. The main assumptions that are made in the simulation are the following:

- **The Earth is a perfect sphere.**
  This allows for the modelling of the Earth as a single point gravity source, neglecting non-uniformities in the gravity field. The largest contribution to this effect is the J_2 term, which models the oblateness of the Earth. It causes a precession of the line of nodes around the poles. For a low Earth orbit, the acceleration due to the J_2-effect is two to three orders of magnitude smaller than the acceleration of the point-mass Earth [6]. Since the simulation of a launch to orbit is short (on the order of a few minutes), this term (and therefore all other non-spherical terms) can be safely neglected.
- **Only the gravity of the Earth acts on the vehicle.**
  This means that the effect of the Sun, Moon and other planets is ignored in the simulation. The gravity of the Earth is six orders of magnitude higher than that of the Sun, Moon and other planets combined [6]. Since the simulation time is short, these other gravity sources have a very small effect. For this reason, this was considered a reasonable assumption.
- **The atmosphere can be sufficiently modelled by the ISA up to 100 km in altitude; above this, the atmospheric pressure and density are zero.**
  This means that variations in the atmosphere due to latitude, time of day, and seasonal effects are neglected. Also, the atmospheric forces due to the atmosphere above 100 km are neglected. From the simulation of the ascent trajectory, the drag losses were almost negligible (on the order of 0.1 %). Therefore, small changes in the drag force due to a different atmosphere model can be neglected.
- **The drag coefficient of the vehicle depends only on the Mach number.**
  As another simplification in the aerodynamic model, the effect of a changing Reynolds number is neglected. Also, the drag coefficient of a vehicle is considered independent of its angle of attack. Most space launch vehicles exit the lower part of the atmosphere fairly quickly. The angle of attack is kept close to zero while aerodynamic forces are large. These two reasons make that the effect of this assumption is small for most launch vehicles.

- **There are no lift or side force components to the aerodynamic force.**
  Due to the fact that the angle of attack is kept small while the dynamic pressure is high, this can be reasonably assumed for a first order estimate.
- **Engines are ignited and shut down instantly.**
  In real life, engines take time to start up. However, this time is small with respect to the total burn time of each stage. Therefore, this assumption was made, to simplify the overall thrust calculations.
- **Thrust is always directed through the center of gravity in the direction of the nose of the vehicle.**
  In reality, this is not always true, since thrust vectoring is used to steer the vehicle. The offset angle is usually small though, so this assumption does not have a large effect. An extreme example where this is not the case is the Space Shuttle. The Space Shuttle vehicle was highly asymmetric, and the thrust was not aligned with the longitudinal axis of the vehicle. Since this tool will (for now) only be used to simulate axis-symmetric vehicles, this assumption is reasonable.
- **Only one engine is active at a time.**
  This simplification makes the implementation of the vehicle model less complex. Stages in series are supported; to create stages in parallel, the vehicle has to be split into multiple logical stages. In case of multiple engines in one stage, their thrusts can be simply added in the case that their specific impulses are the same. Otherwise, a thrust-weighted average of the specific impulse of each engine must be used as the specific impulse of the full stage.

As input data, some data about each stage of the vehicle are needed, as well as the initial conditions.

- For each stage:
  - Dry mass.
  - Fuel mass.
  - Maximum thrust in vacuum; either constant, or as a function of remaining propellant mass.
  - Specific impulse, both sea level and vacuum.
  - Drag coefficient; either constant, or as a function of Mach number.
  - Reference area, corresponding to the drag coefficient.
- The initial conditions: position, velocity and pointing direction, specified as one of:
  - Position, velocity and pointing vectors in the Earth-centered inertial frame.
  - Position as a location above the Earth's surface, given in latitude, longitude and altitude coordinates. In this case, velocity is assumed to be zero relative to the rotating Earth's surface. Pointing is then given as a combination of pitch and azimuth angles.
- A function to calculate the pointing direction from the current simulation state. This function is used to steer the vehicle during the ascent.

During simulation, at each time step, the simulation routine outputs the following data to a data file:

- t, the simulation time.
- $\boldsymbol{r}$, the position vector.
- $\boldsymbol{v}$, the velocity vector.
- $\hat{\boldsymbol{f}}$, the pointing direction vector.
- $\boldsymbol{F_a}$, the total aerodynamic force vector.
- $\boldsymbol{a}$, the total acceleration vector due to gravity, thrust and aerodynamic forces.
- m, the total mass of the vehicle.
- F_T, the thrust magnitude of the vehicle; the thrust vector is then defined as $\hat{\boldsymbol{f}} \cdot F_T$.
- j, the index of the currently active stage.

Vectors are given in their cartesian components in an Earth-centered inertial reference frame.

The position and velocity state vectors are propagated using a fourth order Runge-Kutta method. Let h be the time step size, and $\boldsymbol{a}_n = \Lambda(t_n, \boldsymbol{r}_n, \boldsymbol{v}_n)$ the method that calculates the acceleration vector from the state vectors. Then

$$\boldsymbol{r}_{n+1}^{(0)} = \boldsymbol{r}_n + \frac{h}{6}(\boldsymbol{k}_1 + 2\boldsymbol{k}_2 + 2\boldsymbol{k}_3 + \boldsymbol{k}_4) \tag{3.1}$$

$$\boldsymbol{v}_{n+1}^{(0)} = \boldsymbol{v}_n + \frac{h}{6}(\boldsymbol{l}_1 + 2\boldsymbol{l}_2 + 2\boldsymbol{l}_3 + \boldsymbol{l}_4) \tag{3.2}$$

With

$$\boldsymbol{k}_1 = \boldsymbol{v}_n \tag{3.3}$$

$$\boldsymbol{l}_1 = \Lambda(t_n, \boldsymbol{r}_n, \boldsymbol{v}_n) \tag{3.4}$$

$$\boldsymbol{k}_2 = \boldsymbol{v}_n + \frac{h}{2}\boldsymbol{k}_1 \tag{3.5}$$

$$\boldsymbol{l}_2 = \Lambda\left(t_n + \frac{h}{2}, \boldsymbol{r}_n + \frac{h}{2}\boldsymbol{k}_1, \boldsymbol{v}_n + \frac{h}{2}\boldsymbol{l}_1\right) \tag{3.6}$$

$$\boldsymbol{k}_3 = \boldsymbol{v}_n + \frac{h}{2}\boldsymbol{k}_2 \tag{3.7}$$

$$\boldsymbol{l}_3 = \Lambda\left(t_n + \frac{h}{2}, \boldsymbol{r}_n + \frac{h}{2}\boldsymbol{k}_2, \boldsymbol{v}_n + \frac{h}{2}\boldsymbol{l}_2\right) \tag{3.8}$$

$$\boldsymbol{k}_4 = \boldsymbol{v}_n + \frac{h}{2}\boldsymbol{k}_2 \tag{3.9}$$

$$\boldsymbol{l}_4 = \Lambda(t_n + h, \boldsymbol{r}_n + h\boldsymbol{k}_3, \boldsymbol{v}_n + h\boldsymbol{l}_3) \tag{3.10}$$

The simulation is ended on one of three conditions:

1. The current stage has burned out (no more fuel mass), and there are no more stages left;
2. The norm of the position vector on the next time step is less than the radius of the Earth (i.e. the vehicle has impacted the ground); or
3. The maximum simulation time has been reached.

3.2. TRAJECTORY OPTIMISATION ROUTINE

For optimising a trajectory with respect to some cost function, a projected gradient method is used [7]. Given the control inputs $\boldsymbol{u}$, the cost function $F(\boldsymbol{u})$, and the vector of constraints $\boldsymbol{c}(\boldsymbol{u})$, the algorithm to minimise $F(\boldsymbol{u})$ with respect to $\boldsymbol{u}$ is as follows:

1. The derivatives of the cost and constraint functions with respect to the control inputs are estimated by a finite difference. These are arranged in the gradient vector ∇F and the Jacobian J, such that
$$\nabla F_i = \frac{\partial F}{\partial \boldsymbol{u}_i} \tag{3.11}$$
and
$$J_{ij} = \frac{\partial \boldsymbol{c}_i}{\partial \boldsymbol{u}_j} \tag{3.12}$$

2. If the error is small, an optimisation step is performed; otherwise, the algorithm skips to step 6.

3. The step direction for optimisation $\boldsymbol{s}^o$ is calculated using
$$\boldsymbol{s}^o = -P\nabla F(\boldsymbol{u}) \tag{3.13}$$
with
$$P = I - J^T\left(J \cdot J^T\right)^{-1} J \tag{3.14}$$

4. The step size ς is determined such, that the estimated value of the cost function on the next time step is minimised. This is done by minimising the function
$$h_o(\varsigma) = F\left(\boldsymbol{u} + \varsigma \boldsymbol{s}^o\right) - F(\boldsymbol{u}) + \nabla F \cdot \left[-J^T\left(J \cdot J^T\right)^{-1} \boldsymbol{c}\left(\boldsymbol{u} + \varsigma \boldsymbol{s}^o\right)\right] \tag{3.15}$$
with respect to ς

5. The control vector is updated: $\boldsymbol{u} = \boldsymbol{u} + \varsigma \boldsymbol{s}^o$

6. The step direction for constraint direction is calculated; this direction is the shortest possible step, such that the constraints are satisfied. This direction is calculated using
$$\boldsymbol{s}^c = -J^T\left(J \cdot J^T\right)^{-1} \boldsymbol{c} \tag{3.16}$$

7. The step size for the constraint correction ς is determined such, that the norm value of the constraint errors is minimised. This means minimising the function
$$h_c(\varsigma) = |\boldsymbol{c}\left(\boldsymbol{u} + \varsigma \boldsymbol{s}^c\right)|^2 \tag{3.17}$$
with respect to ς.

8. The control vector is updated: $\boldsymbol{u} = \boldsymbol{u} + \varsigma \boldsymbol{s}^c$ and the algorithm jumps back to step 1.

3.3. VERIFICATION AND VALIDATION

To verify and validate the simulation component, a comparison was set up between it and the TU-DAT astrodynamics library [1]. For this, a simplified vehicle and trajectory were created. The input

[1] TU Delft Astrodynamics Toolkit, tudat.tudelft.nl

Table 3.1: Verification input data for the TSOT and the TUDAT library.

Input parameter	**Value**
Vehicle initial mass	2500 kg
Vehicle thrust	100 kN
Vehicle specific impulse	225 s
Vehicle drag coefficient	0.5
Vehicle reference area	3.14 m^2
Vehicle pointing direction	Calculated from constant pitch and yaw angles.
Initial altitude	38 km
Initial latitude	30°
Initial longitude	0°
Initial heading	45°
Initial pitch angle	45°
Simulation time	44 s
Simulation time step	0.01 s

data can be found in table 3.1. For verification of the simulation, similar simplifications were used in the TUDAT simulation: only the gravity of the Earth was considered, the Earth was approximated as a perfect sphere, and the atmosphere model was the ISA extended up to 100 km. For validation, the TUDAT simulation model was expanded to include also the gravity of the Sun and the Moon. The gravity field of the Earth was modeled with a more complete spherical harmonics model. Finally, the atmosphere was modelled with the NRLMSISE-00 model provided by the TUDAT library.

It was assumed that if the final position and velocity results of the TSOT simulation are close to those of the TUDAT verification and validation simulations, that the tool was accurate enough to be used for further design work. A position error of 100 m and a velocity error of 40 m/s will be tolerated for verification; for validation, these tolerances are 250 m and 60 m/s, respectively. As can be seen in table 3.2, the results for both the verification and the validation fall within these tolerances. Given that the verification and validation simulations are only 44 s long, compared to the simulation of the ALTAR vehicle of 270 s, it can be expected that the errors after the full launch are approximately six times larger than these tolerances.

3.4. USAGE FOR THE ALTAR VEHICLE

In applying the TOST for the design of the ATLAR vehicle, one further simplification was used: the effect of atmospheric pressure on the specific impulse and thrust is neglected: the thrust was always the vacuum thrust. Since the launch starts at a high altitude (approximately 40 km), this assumption has a small effect. The first and second stages were modelled with a full thrust versus propellant mass curve, as determined by the grain design tool (section 4.4.2). The third stage was modelled with a constant thrust from ignition to burnout. The trajectory was further designed such, that the third stage places itself, the OMS and the payload into an elliptical orbit with a periapsis of 200 km and an apoapsis at the altitude of the target orbit. Steering of the vehicle during launch is done using a stepwise function for the pitch rate $\dot{\theta}$, changing value at six predetermined times during the burn. Two additional control variables were the initial pitch angle and the payload mass. This gives nine control inputs in total:

$$\boldsymbol{u} = \left[\theta_0,\ m_{\text{payload}},\ \dot{\theta}_1 \ldots \dot{\theta}_7\right]^T \tag{3.18}$$

Table 3.2: Verification and validation comparison data for the TSOT tool. Position and velocity are in the Earth-centered corotating frame.

		TSOT Simulation	**TUDAT Verification**		**TUDAT Validation**	
			Value	Error	Value	Error
Final position (m)	x	5 563 151	5 563 170	–19	5 563 093	58
	y	3 245 005	3 245 099	–94	3 245 224	–219
	z	29 048	29 031	17	28 871	17
Total position error (m)				97.4		227.2
Final velocity (m/s)	x	905.46	910.82	–5.38	899.51	5.95
	y	2527.17	2541.77	–14.60	2561.03	–33.86
	z	1763.46	1786.44	–22.98	1763.76	–0.30
Total velocity error (m/s)				27.75		34.38

The constraints specified were the final altitude, horizontal velocity and vertical velocity, calculated such that the vehicle is at the periapsis of the required orbit. Finally, the cost function was defined as the negative of the payload mass $F = -m_{\text{payload}}$. The results of the optimisation of the trajectory can be found in section 4.7.1.

4

ALTAR SYSTEM DESIGN & SPECIFICATIONS

In this chapter, the deign of the ALTAR system design is described. The technical resource budgets are described in section 4.1 and the balloon subsystem is described in section 4.2. The interfaces and separation system are described in section 4.3 and the propulsion systems are described in section 4.4. The payload integration and aerodynamic characteristics are described in sections 4.5 and 4.6, respectively. The guidance, navigation and control characteristics are described in section 4.7 and the telemetry and communications characteristics are explained in section 4.8. Sections 4.9 and 4.10 describe the electrical power system and the recovery subsystem, respectively. The flight termination system is described in section 4.11 and the structures and materials characteristics are described in section 4.12. Lastly, the system configuration and layout is described in section 4.13.

4.1. TECHNICAL RESOURCES AND BUDGETS ALLOCATION

This chapter deals with the allocation and budgeting of mission technical resources. To facilitate the successful development of the launch system and to attract customers these technical resources must be identified and managed. For this purpose, so called technical performance measurement (TPM) parameters are used. In this chapter these parameters are identified and their final values are presented.

4.1.1. TECHNICAL RESOURCE IDENTIFICATION AND ALLOCATION

In the baseline report, ΔV and cost per launch were identified as TPM parameters [8]. In this section, updated values of these TPM parameters are provided, along with the values of newly determined TPM variables in table 4.1.

Customers want a low cost per launch, high technical readiness level and high success rate for launches. Based on these top-level system requirements, the TPM parameters are selectively chosen. The top-level requirements state that the launch service shall have a specified launch cost and launch success rate and that it shall be able to be operational by 2022, as mentioned in section 5.9. To achieve the specified launch cost, the launch cost will be calculated throughout the whole design phase. To make sure the launch service has the specified launch success rate, the reliability of the different subsystems will be analysed with time. Lastly, to ensure that the launch service is able to reach the intended orbit by 2022, the ΔV will be tracked at different phases of the design.

Table 4.1: TPM parameters during the different design phases.

	Cost per launch (k€/kg)	**Launch success rate**	**ΔV (km/s)**
Baseline report	44.7	0.9	9.2
Final report	32	0.915	8.5

In table 4.1, the current TPM values are compared to initial estimated TPM values, but only for the

TPM parameters that were initially used in the baseline report. The first TPM parameter which drives the design of the vehicle is the cost per launch. The objective of this launch system is to generate profit, and if the launch system is not profitable to operate this will not be feasible. Therefore, each aspect of the launch system must be budgeted a cost such that during development, the launch system can be designed to the budgeted cost. At the current stage of the design, the cost per launch is estimated at 32 k€/kg and the cost analysis can be found in section 8.3.

The second TPM parameter for this system is Delta-V. This is a measure of a launch vehicles ability to change its own velocity by exhausting propellant at a high velocity. This is important because an orbit is defined by an inclination, height and longitude of ascending node with respect to the earth. A customer will dictate their desired orbit, and the launch vehicles ability to reach this orbit will depend on its ΔV value. At this stage of the design, the required Delta-V value is estimated as 8.5 km/s. To estimate this value, a trajectory simulation and optimisation tool was used and it can be found in chapter 3.

None of the customers are willing to invest a lot of money with a low launch success rate. The customer has expressed the need for high reliability, therefore the launch success rate is the last TPM parameter. It is highly dependent on the engine failure rate and the value is estimated in section 5.3.

4.1.2. CONTINGENCY MANAGEMENT

To make sure the design meets the specified requirements upon completion, it is of utmost important to closely track the TPM parameters throughout the different design phases by means of a contingency management. This section is dedicated to establishing the contingency management plan.

As mentioned before, the TPM procedure will ensure that the launch service will achieve the specified performance upon delivery. The contingency management is a technique that achieves this by specifying the contingency for parameters that determine the success of the launch service at different phases of the design. The size of the contingency depends on the amount of uncertainty that a certain TPM parameter carries. As the different TPM parameters carry different amounts of uncertainty, the contingencies also differ for each TPM parameter.

As the design becomes more mature, the level of detail and accuracy increases so the contingency factors decrease. The design phase and corresponding contingency of each TPM parameter is shown in table 4.2. The current design phase is between preliminary design and detailed design.

It is of utmost importance that the launch cost is within the attractive price of the client. To ensure this, the aim is to have a launch cost that is within 1-3% from the target launch cost during the detail design phase. The launch cost is allowed to differ slightly more than other TPM parameters during the final phase. This is because the target launch cost is set lower than the cost requirement states. Therefore, slight deviations will prevent the launch service from violating the cost requirement. For the initial phases, the contingencies are highest. This can be explained by the high uncertainty in the associated costs, which also holds for many engineering projects. The launch cost contingencies are derived from NASA's typical values for the cost contingencies of space system engineering projects and have been slightly adjusted to the current project [9].

The target launch success rate was set at above 0.9. To ensure this value is met in the final product, a contingency factor of 1-3% is added in the final design phase.

To avoid mission failure and to reach a desired orbit, a certain contingency is required for ΔV. In the final design phase, 1% of contingency was estimated due to low performance of each subsystems

Table 4.2: Contingencies for the TPM parameters during the different design phases.

Contingency management	Cost per launch	Launch success rate	Δ V
Conceptual design	35%	15%	15%
Preliminary design	25%	10%	10%
Detailed design	10%	5%	5%
Final design	1-3%	1-3%	1%

component through out the mission.

4.2. BALLOON SUBSYSTEM CHARACTERISTICS

In this section, the balloon subsystem will be designed. First, the gas selection will be explained in section 4.2.1. Afterwards, the balloon ascent dynamics will be investigated and the balloon will be sized in section 4.2.2. Once done, the structure and material characteristics of the subsystem will be explained in section 4.2.3 and the overview of the balloon will be presented in section 4.2.4. To conclude, the balloon communication system and the positioning system are explained.

4.2.1. BALLOON LIFTING GAS

The only lifting gasses that are contenders to fill the balloon with are helium and hydrogen. These two gases have the lowest density and therefore create the most lift. Using Archimedes Principle, one can calculate that at sea-level 1 m^3 of helium creates 10.27 N of buoyancy force, while hydrogen creates 11.13 N. So a hydrogen balloon would be able to carry around 8% more than helium balloon of same volume. Furthermore, the cost of helium per cubic meter is 29 times higher than the cost of hydrogen. In terms of sustainability, hydrogen can be generated, while helium is a non-renewable gas. The drawback of hydrogen, however, is the large increase in risk with respect to helium. Hydrogen is very flammable, especially when mixed with air. Since static sparks can ignite Hydrogen, many measures would have to be taken in order to prevent catastrophic events. Due to this risk, the helium was chosen as the lifting gas for the mission.

4.2.2. BALLOON ASCENT DYNAMICS AND SIZING

In order to define important characteristics of the balloon used for the mission, a basic Python code simulation of the mission was implemented. At this stage of the design, this simulation is simple and approximated but it aims to describe the ascent of the balloon, as illustrated in the fig. 4.1, to the target altitude by basic parameters.

As it can be seen from fig. 4.1, the balloon has variable mass and volume. This is a characteristic of a zero-pressure balloon, which was chosen over the super pressure balloons mainly for two reasons. The first motivation is that super pressure balloons are more complex and heavier than zero pressure ones because their structure needs to withstand a pressure differential between the gas contained inside the balloon and the atmosphere. The second reason is that super pressure balloons are designed to stay in the stratosphere for extremely long periods (e.g. over 100 days), which is neither essential nor desirable for the purpose of the mission.

Referring to fig. 4.1, the balloon at ground level has the minimum volume and maximum mass and at this moment it lifts off and begin the ascent. Once it reaches an intermediate altitude, indicated as $H1$, it cannot climb more without releasing some of its internal gas. At this moment, the mass begins to reduce and the volume stays constant until the balloon reaches the float altitude, indicated

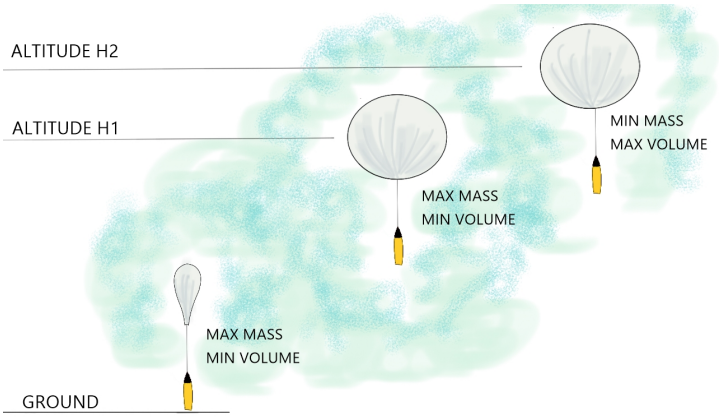

Figure 4.1: The ascent of the balloon illustrated at three representative altitudes associated with changes in mass and volume. The volume of the balloon changes due to the expansion of the filling gas. The mass of the balloon decreases from altitude $H1$ onward due to the release of the gas itself through exhaust vents to reach altitude $H2$.

as $H2$. At this moment, the balloon has still some momentum and it will begin to oscillate around the floating altitude. This oscillation will cause the balloon to lose its internal gas and gradually decrease its floating altitude. Nonetheless, this oscillation is supposed to happen at a slow rate as explained in the "Scientific Ballooning" book [10], therefore, it should not affect the deployment of the orbital rocket considerably.

The balloon motion described above can be simulated by the Python program and in the following list, the assumptions used in the program are presented as well as their consequences on the results obtained from the software.

- **The International Standard Atmosphere (ISA) is used.** This means that atmospheric properties are considered not to vary due to factors such as seasons, solar mimima or maxima, etc. In fact, the ISA parameters represent an average and therefore, the balloon could experience a variation in its lifting capabilities depending on the weather conditions of the launch day. In the later stages of the design, a proper margin should be considered in the sizing of the balloon to account for this atmospheric variations.
- **The Earth's gravitational acceleration is constant (g_0=9.80665 m/s^2).** Between 0 km and 30 km altitude, the variation of the gravitational acceleration is less than 1% and therefore can be assumed constant with no major consequences on the results of the simulation.
- **The wind direction is constant but unknown.** This is considered to be the worst case scenario because the balloon will have the maximum drift in a direction that is unknown. This could lead to an overestimation of the drift, and therefore of the control radius as will be further explained in section 4.10.
- **The lifting gas is a perfect gas.** This can be considered to be a valid assumption because the temperatures of the gas stay within a relatively restricted range. The main consequence is that two properties of the gas are enough to describe its behaviour completely, such that the temperature and pressure of the gas determine its density.
- **Only the gas contained in the balloon has lifting capabilities.** The rocket and all the structural elements of the balloon are considered to have a volume that is negligible when compared to that of the gas contained in the balloon. Therefore, the buoyancy force in the simulation results is slightly smaller than to be expected in reality. Furthermore, the effects of drag

Table 4.3: The inputs required by the simulation software that reflect the design choices or external parameters.

Input	Symbol	Value
Helium gas constant	R_{He}	2077.0 J/(kg·K)
Total mass at target altitude	M_{total}	7750.0 kg
Target altitude	$H2$	40 km
Balloon initial velocity	V_0	0.0 m/s
Positive lift factor	PLF	1.1
Balloon drag coefficient	C_D	0.3
Film thickness	t_{film}	0.02 mm
Wind velocity	V_{wind}	30.0 m/s
Max vertical acceleration encountered in flight	a_{maxB}	0.83 m/s^2

Table 4.4: The outputs generated by the simulation software that are relevant for the design of the other subsystems of ALTAR.

Output	Symbol	Value
Radius of the balloon	R_B	78.2 m
Lifting capability	M_{lift}	5006.4 kg
Mass of Helium	M_{He}	1178.2 kg
Max drift radius	d_{drift}	215.7 km
Ascent time	t_{ascent}	121 min
Max vertical acceleration	$a_{B_{MAX}}$	0.8 m/s^2

are slightly greater in reality too.

- **The balloon is a perfect sphere.** This is an assumption that could influence greatly the aerodynamic properties of the balloon, given the fact that its shape changes continuously during the ascent. This will add some aerodynamics penalties to the design, when keeping a constant C_D equal to 0.3, as suggested by the "Scientific Ballooning" book [10].

- **The gas cannot leak out of the balloon.** This assumption can be valid considered that it is a zero-pressure balloon and that the ascent occurs in a relatively short amount of time (in the order of few hours).

In table 4.3 the inputs of the Python simulation software are presented. V_0 was assumed to be zero because the payload attached to the balloon is steady on the ground at lift off. The PLF was assumed to be equal to 1.1. Finally, V_{wind} was assumed to be the maximum average at varying altitude during the period 1948-1953 in the skies above Belmar, New Jersey, that is 30 m/s [11]. The data contained in "Winds at Altitudes up to 80 Kilometers" [11], were selected for their extensiveness and completeness but, for a later stage of the design, wind data relative to the launch location will be used. The outputs resulting from the simulation software are presented in table 4.4.

Given the fact that the mass estimated for the rocket is equal to 4179.1 kg, the balloon is capable of lifting an extra 827.3 kg that have to account for the mass of the recovery system, gondola and suspending ropes. The ascent profile of the balloon can be seen in fig. 4.2, where it can be noticed that the last part of the ascent is characterised by a decrease in velocity which is caused by the release of the helium from the vents present in the balloon.

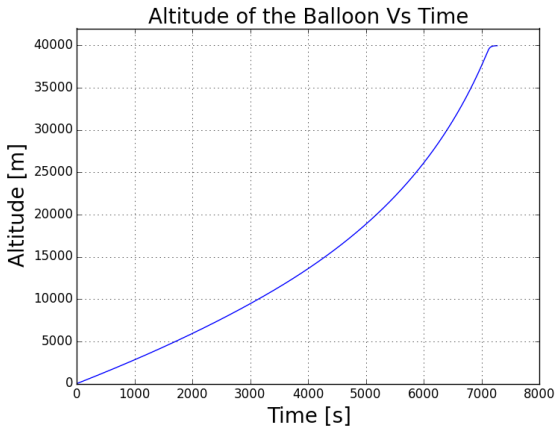

Figure 4.2: The altitude plotted as a function of time that describes the vertical motion of the balloon during the ascent phase.

4.2.3. BALLOON STRUCTURE

The weight of the rocket and the gondola is transmitted to the ropes and then to the balloon's film by means of multiple high-tensile strength fibers, the so called load tapes. Load tapes span from the bottom of the balloon all the way to the top, just like the meridians of the Earth.

For this stage of the design, a preliminary structural sizing is performed to estimate the total mass of the balloon given by eq. (4.1).

$$M_{struct} = M_{film} + M_{tapes} + M_{SH} \tag{4.1}$$

M_{film} is the mass of the thin material that contains the gas, M_{tapes} is the total mass of the load tapes and M_{SH} is the mass of the suspending ropes. Now these terms will be analysed separately to get an estimation of the M_{struct}.

A preliminary material selection was performed for the film of the balloon and the load tapes. The film of the balloon will be made from a commonly used ballooning material called high density polyethylene (HDPE), the same one used for the Stratos mission financed by Redbull [1]. The material of the load tapes is selected to be poly-phenylene-benzobisoxazole, commonly known as Zylon® [12], due to its low mass and high tensile strength. The material of the ropes suspending the rocket is selected to be polyester because it does not lose strength if wet and it has overall good chemicals and UV resistance[2]. Finally, the gas contained inside the balloon was decided to be Helium for the reasons explained in section 4.2.1. In table 4.5, the materials selected and their relevant properties are reported.

The first term of the right hand side of eq. (4.1) can be calculated inserting the properties of HDPE in eq. (4.2), M_{film} can be calculated as follows:

$$M_{film} = 4\pi \cdot R_B^2 \cdot t_{film} \cdot \rho_{HDPE} = 746.4\,\text{kg} \tag{4.2}$$

Where R_B is taken from table 4.4, and t_{film} is assumed to be the same of the balloon used by the Stratos mission and equal to 0.0232 mm. The mass of the tapes that need to withstand the load,

[1] http://www.redbullstratos.com/technology/high-altitude-balloon/
[2] http://www.christinedemerchant.com/rope_material_comparison.html

Table 4.5: The preliminary selected materials for the structural sizing of the balloon system and their relative mechanical and physical properties that are used in section 4.2.3, as taken from a materials engineering book [13].

	Symbol	Value	Unit
HDPE			
Density	ρ_{HDPE}	970	kg/m^3
Tensile yield strength	$\sigma_{yield_{HDPE}}$	26.2	MPa
Maximum shear	$\tau_{max_{HDPE}}$	3000	Pa
Zylon			
Density	ρ_{zylon}	1540	kg/m^3
Tensile yield strength	$\sigma_{yield_{zylon}}$	2700	MPa
Maximum shear	$\tau_{max_{zylon}}$	6895	Pa
Polyester			
Density	ρ_{pol}	1380	kg/m^3
Tensile yield strength	$\sigma_{yield_{pol}}$	850	MPa
Maximum Shear	$\tau_{max_{pol}}$	–	Pa

M_{tapes}, is calculated by first deciding the number needed. This is dependent on the shear stress that the film can withstand, in fig. 4.3 the load case for the film is illustrated.

From the top view, it can be seen that the out of plane shear in the film, which causes the film to wrinkle, is maximum where the load tapes are and then it decreases rapidly towards the centre line. This shear stress is dependant on the amount of load tapes that are present in the structure and it acts on the surface, A_1, represented in the side view of fig. 4.3. The in plane shear is assumed to be zero because the tapes are considered to carry the same tensile load. Therefore, the number of load tapes can be calculated with eq. (4.3):

$$n_s = \frac{F_{max}}{\tau_{max_{HDPE}} \cdot A_1} \cdot FS = \frac{4305.0}{3000 \cdot 0.0050} \cdot 1.5 = 431 \tag{4.3}$$

Where n_s is the total number of load tapes, F_{max} is the maximum vertical force acting on the balloon during the ascent, and FS is the safety factor used. At this point, the width of the load tapes, w_{tape}, can be calculated assuming that the film under them carries the same tensile strength of the tapes themselves. The cross sectional area of interest, A_2, can be seen in the front view of fig. 4.3. Using eq. (4.4), the width of the 431 tapes can be calculated:

$$w_{tape} = \frac{F_{max}}{n_s \cdot \sigma_{yield_{HDPE}} \cdot t_{film}} = \frac{4305.0}{431 \cdot 26,200,000 \cdot 0.0000232} = 0.0188\,\text{m} \tag{4.4}$$

At this point, the minimum thickness of the load tapes can be calculated but, using Zylon® as material, it results to be too small to be manufactured and therefore a value of 0.05 mm is used for the thickness, as suggested by the materials engineering book [13]. This results in a total mass of the load tapes equal to 153 kg.

The ropes serving as the connection in between the balloon and the gondola should be as short as possible for stability reasons, but at the same time they should comply with the measures imposed by the system's safety. The melting temperature of HDPE, which is used as film's material, is 126 °C

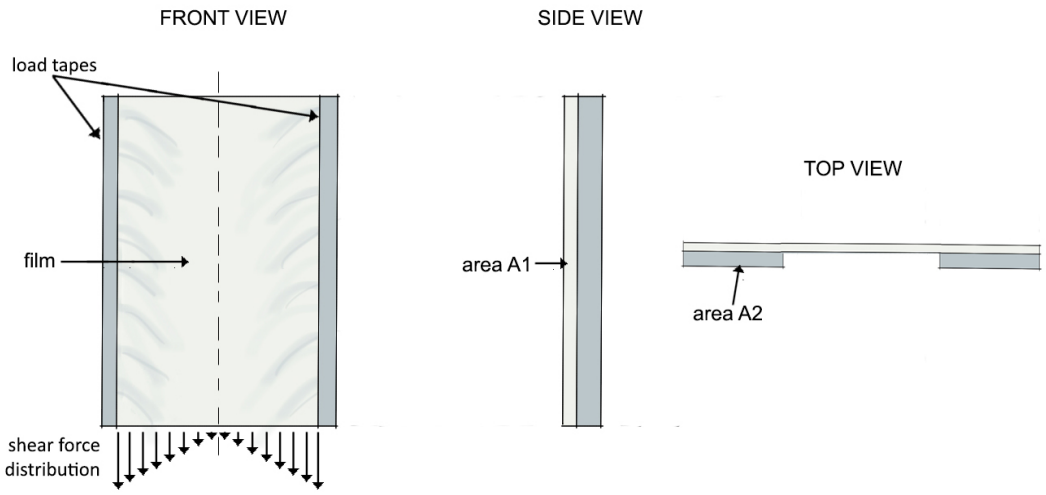

Figure 4.3: Three views of a section of the structure of the balloon containing the lifting gas. In dark grey the load tapes are indicated and the film is indicated in light grey.

[3]. It has to be made sure that the heat from the rocket ignition will not lead to the destruction of the balloon by applying a safety distance between the nozzle of the rocket and the balloon itself. Another reason for the increase in the rope length, is the required clearance angle. In fact, the pointing mechanism described in section 4.3.2 can vary the pitch of the rocket up until 45°, therefore, this is considered to be the clearance angle required. For the balloon with radius of 78.2 m the required rope length would be equal to 32.4 m.

Three polyester ropes with diameter of 12 mm are going to be used in order to support 6 tons of payload, taking into account the safety margin of 1.5[4]. With the rope length of 32.4 m, the total weight of the ropes, M_{SH} is going to be 5 kg.

Summing together all the values so far calculated, a value for M_{struct} can be computed using eq. (4.1). This is equal to 4367 kg.

4.2.4. BALLOON LAYOUT

The layout of the balloon is quite simple, it features a duct on the top of it that is necessary to release the gas during the descent, the six vents described in section 4.10.3, and a supporting structure that connects the load from the load tapes to the ropes.

In fig. 4.4, a rendering of the balloon can be seen, it has to be noticed that the load tapes, in reality, should be many more but due to convenience only few of them are shown. In fig. 4.5, a front view of the balloon, together with a detail of the vents necessary to keep the pressure inside the balloon in equilibrium with the outside one, are presented.

4.2.5. BALLOON COMMUNICATION SYSTEM

The communication system of the balloon is an essential part of the on-board equipment which is separated into the data transmission system and the command acquisition and execution system.

[3] http://www.plasticmoulding.ca/polymers/polyethylene.htm
[4] http://www.lanex.cz/en/polyester-ropes—rope-strength-table

Figure 4.4: A render of the balloon where the vents and load tapes can be seen. Number of load tapes and their spacing does not represent the reality because of hardware limited computing capabilities.

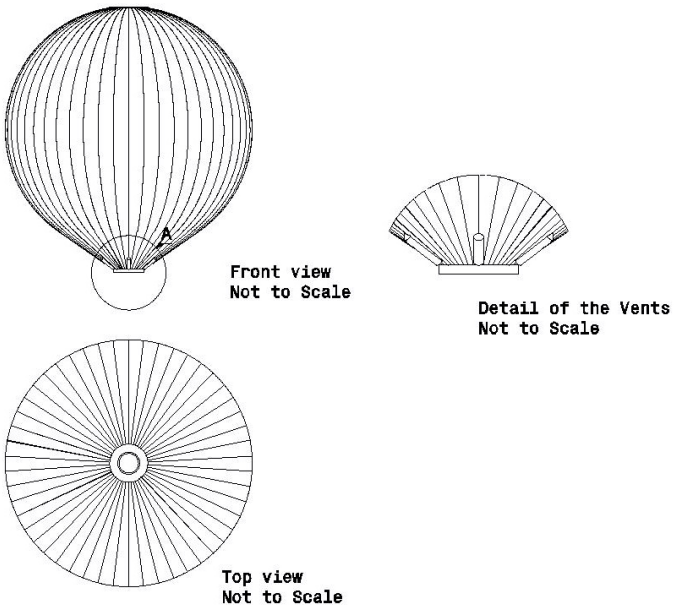

Figure 4.5: Some views of the balloon, where the vents can be seen in detail. Not to scale.

Data Transmission System

The data transmission system sends output data from the observational equipment to the ground station. Such data could combine information about the surrounding atmosphere and the position of the balloon. As an example, a telemeter is a device for data transmission system. The components of the data transmission system are a transmitter, encoder, antenna, multiplexer and power source. The digital data are controlled by a carrier wave and transmitted to the ground station.

Signals are going to be transmitted via a VHF radio link, which has a frequency range of 30 MHz to 300 MHz. Usually, the high-altitude balloon transmitter uses 2 m band. This is a suitable choice, as the balloon will not travel extremely far from the ground station and there is no need for a more expensive system. As further mentioned in section 4.8, the transmitter output power of the instrument antenna that the Pegasus used was 25 W [14]. The maximum horizontal distance that the balloon has travelled with respect to the launch site is 200 km. Since the output power is proportional to square of the travelled distance. The transmitter output power of the BGS system can be estimated as 0.75 W without an antenna efficiency, thus the total output power is re-estimated as 2 W with an antenna efficiency of 40% [15].

Command Acquisition and Execution System

The command acquisition and execution system receives signals from the ground station and executes the received command. The principal commands could include mission termination, change in altitude, or control of the recovery system. It is important to include the command acquisition system in order to consider safety and reliability of the balloon flight. Such system consists of three devices: telecommand receiver, telecommand decoder and the command control unit.

- **Telecommand receiver**

  The voltage of the receiver indicates that the command has been received by the system. Output from the receiver is fed to the telecommand decoder.

- **Telecommand decoder**

  The output from the receiver is going to be passed through a band pass filter and translated into logic levels, with 0 corresponding to 0 V and 1 corresponding to 9 V. Each command is represented by a 16 bit code. Depending on the received command, the decoder will output a pulse onto one of the output lines. This pulse is used to actuate a corresponding sub-system.

- **Command control unit**

  A command control unit reads the decoder output and executes the command sent from the ground station.

4.2.6. Positioning System

The positioning system is responsible for continuous determination of the balloon position during the flight. As the balloon is not moving at high velocities, a mounted global positioning system (GPS) receiver is going to be sufficient for determining the flight position of balloon. The data from GPS receiver is going to be sent to the ground station with the use of the data transmission system.

An APRS system developed for the use on high altitude balloons called Tracksoar[5] is going to be implemented on the design. With a weight of 230 g it is able to determine balloon location and

[5] https://www.tracksoar.com

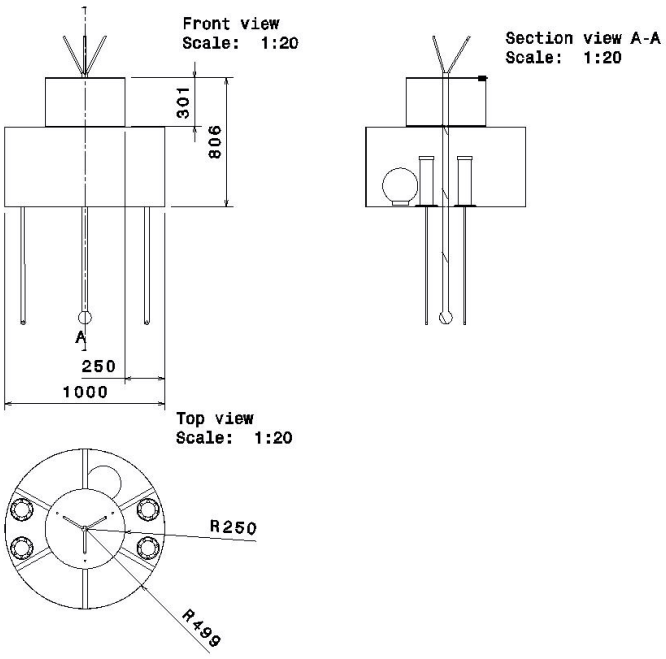

Figure 4.6: A preliminary layout of the gondola with key elements of the structure and separating mechanism. Dimensions are expressed in millimiters.

collect data on temperature and pressure. Ready to fly model costs €173, and it requires 5 V of power. Two models are going to be installed in order to keep the design redundant.

4.3. INTERFACE AND SEPARATION SYSTEM

In this section, the design of the gondola and the separation mechanism which it contains will be discussed. The gondola is the part of the launcher system suspended between the balloon and the rocket. A cross section of the preliminary design of this subsystem is presented in In section 4.3.1, the gondola interface will be briefly explained, then, in section 4.3.2, the separation mechanism will be described and sized.

4.3.1. GONDOLA DESIGN

The gondola has to provide structural support to the communication, abortion, batteries, recovery, etc.; as well as protect them from the environment (temperature gradients and eventually rain). Moreover, the gondola has to support the detaching mechanism of the rocket. Therefore, its dimensions and features depend on the subsystems that it has to contain. The outer structure of the gondola was chosen to be composed by two concentric cylinders of different radii. One of which needs to contain the rotation and inclination mechanism, the other one all the other subsystems. As illustrated in fig. 4.6, the two parts of the gondola are connected via a central rod which is also the main support of the rocket. The rod is separated from the lower part of the gondola by ball bearings and it is connected to the rocket by a ball joint. In this way, the lower part of the gondola can rotate freely with respect to the upper part, reducing the inertia around the rods axes, which is one of the sizing factors for the rotating mechanism that make sure that the rocket ignites in the correct direction, as will be discussed later in section 4.3.2. The rod has a circular cross section and it is sized to support the mass of the rocket and the lower part of the gondola, under a maximum acceleration of

10.64 m/s^2. This acceleration resulted to be the highest one encountered by the gondola during the mission, according to the results obtained by the Python simulation program of the balloon ascent (see table 4.3). The upper part of the gondola also contains a structure that connects the three ropes attached at the balloon to the central rod and transfers the loads generated by the upper part of the gondola to the ropes. This structure was sized based on maximum tension stress because it is composed by three one-force members which have forces acting parallel to their axes. This means that, using Aluminium 7075 (see table 4.23) the structure will have a cross sectional area as calculated by eq. (4.5).

$$A_{suppmech} = FS \cdot \frac{M_{susp} \cdot a_{max}}{3 \cdot \sigma_{yield}} = 3.0 \cdot \frac{5833.7 \cdot 10.64}{3 \cdot 5.03E+08} = 1.234 \times 10^{-4}\,\mathrm{m}^2 \tag{4.5}$$

Therefore, assuming a circular cross section for the structural members, they result to have a diameter of 1.25 cm. FS was chosen to be equal to three because these are primary structural members with very limited redundancy.

Moreover, the upper part of the structure needs to have sufficient volume to contain the rope necessary for the control mechanism for recovery of the balloon and for the parachute as described in section 4.10. In addition, on the top of the upper part of the gondola needs to lay the wing necessary for the recovery phase and its deployment mechanism, which is simply a spring loaded ejector.

The bottom part of the gondola contains the pointing and rotating mechanism of the rocket. It is enclosed by an open upper cap to minimise weight due to the fact that the parts that it contains do not need any particular shield against low temperature nor pressures.

4.3.2. SEPARATION MECHANISM

The separation mechanism has to perform three different tasks: first of all it has to rotate the rocket on the horizontal plane towards the correct direction, secondly it has to regulate the pitch of the rocket and finally it has to detach the rocket from the gondola. All these movements are regulated by the computer carried by the gondola which uses attitude inputs from the sensors inside the rocket used for guidance and telemetry, as explained in section 4.7.

To rotate the rocket, cold gas thrusters were selected to be the most suitable option. In fact, if using electrical motors, there could be a problem determining the required rotation because the inertia of the balloon is not big enough to be assumed infinite. Therefore, when trying to rotate the rocket, also the balloon would rotate due to the reaction forces generated inside the electrical motor. This could result to be a problem for achieving a precise pointing of the rocket, especially for the wind acting on the big surface of the balloon that could create additional torques and or unbalanced forces. Also, to have a more stable rocket during the ascent, it is preferable to keep its rotational motion independent of the one of the balloon, therefore a central rod with ball bearings is used as primary structure, as already explained in section 4.3.1 and illustrated in fig. 4.8. This independent motion is suitable for the use of cold gas thrusters and that's another reason why they were selected.

In order to size the thrusters, it has to be decided how many of them are needed. To have only pure torque acting around one axis of the rocket during the rotational manoeuvre, a minimum of four thrusters are needed. Consequently, this number of cold thrusters was selected, with two pairs of nozzles pointing in opposite direction. It has to be noticed that this nozzles configuration has redundancy embedded in its design because just two opposing thrusters could manoeuvre the balloon effectively if needed. The moment necessary to rotate the rocket was found using

eq. (4.6):

$$\sum_{i=1}^{n} M_x = I_{xx} \cdot \ddot{\alpha} = 16.08\,\mathrm{N \cdot m} \tag{4.6}$$

where:

$$\ddot{\alpha} = 2 \cdot \frac{\Delta\alpha}{t_{rot}^2} = 2 \cdot \frac{\pi}{2 \cdot 90^2} = 7.757 \times 10^{-4}\,\frac{\mathrm{rad}}{\mathrm{s}^2} \tag{4.7}$$

$$I_{xx} = \frac{1}{4} \cdot M_R \cdot R_R^2 + \frac{1}{12} \cdot M_R \cdot L_R^2 = 21\,253\,\mathrm{kg \cdot m}^2 \tag{4.8}$$

In eq. (4.6), M_x is the moment around the x-axis, I_{xx} the moment of inertia and $\ddot{\alpha}$ is the angular acceleration about the x-axis. In eq. (4.7), α is the angle of rotation, assumed to be of 90° because for the other part of the rotation the rocket would be slowing down to come to a rest. t_{rot} is the total time required for half a rotation, that means a total time of 180 s would be needed to perform the rotation manoeuvre. In eq. (4.8), M_R is the total mass of the rocket, R_R is the average radius and M_R is the mass of the rocket. Some assumptions were made to compute the necessary moment M_x:

- zero drag is assumed to act on the rotating body of the rocket due to the elevated altitude of 40 km at which the manoeuvre occurs;
- the rocket is assumed to be a cylinder with constant density and radius and to be rotated around its center of gravity;
- the bearings suspending the rocket are frictionless and therefore they do not cause any reaction torques.

All of the assumptions listed above can be assumed to be valid considering the early stage of the design process. At this moment, the thrust required from the cold gas nozzles can be estimated. This is done by dividing M_x by the number of thrusters acting in the same rotational direction (=2) and the arm of the nozzles, which is assumed to be equal to maximum 0.4 m in order to maintain the lower part of the gondola as light as possible. As a result, thrusters of 20.1 N are necessary. Cold gas thrusters of this size could be bought instead of designed, reducing this way the cost development cost of the gondola. The mean operative pressure of such nozzles is typically in the order of 100 bar [16] and this could be used in the later stages of the design to size the required feed system size and specifications. But for now, this operating pressure can be used to size the propellant tank mass and volume. For this, a storing pressure of 1.5 times the mean operating pressure is assumed. Moreover, the burn time (t_b) is assumed to be twice the time needed to complete a full rotation of the rocket, that is equal to 360 s. Now, the total mass of propellant (M_{CG})can be calculated with eq. (4.9).

$$M_{CG} = t_b \cdot T \cdot \frac{1}{I_{sp} \cdot g_0} = 360 \cdot 20.1 \cdot \frac{1}{80 \cdot 9.81} = 9.22\,\mathrm{kg} \tag{4.9}$$

Where I_{sp} it taken from a typical value for nitrogen thrusters [16]. The volume of the tanks containing the gas can now be calculated using the ideal gas law and assuming a maximum storing temperature of 20 °C. This is equal to 53.5L.

To regulate the pitch of the rocket, pneumatic pistons are selected. This is mainly due to the fact that these are relatively simple when compared to other kinds of linear actuators, especially because pressurised gas is already being used for the cold thrusters. Therefore, the gas contained in the tank has just to pass through a pressure regulator and then being fed to the pistons that alter the pitch of the rocket. There is a big variety of pneumatic pistons on the market that could serve this purpose and therefore it is chosen to buy them to save on development costs. Four pistons will be used for

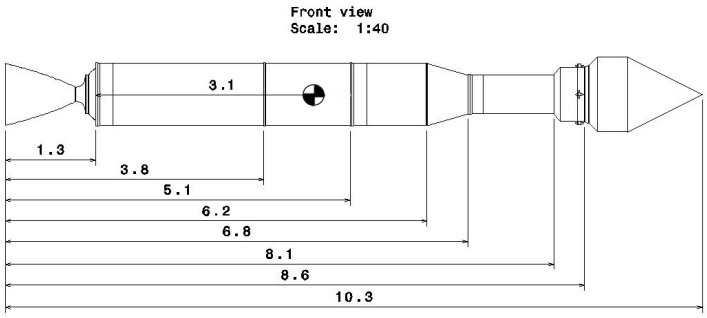

Figure 4.7: The dimensions of the rocket and the position of the CG.

redundancy, two per side, and the cylinders will have a minimum length calculated to be 28.3 cm, based on a maximum pitch of 45°. The mechanism is attached to the centre of gravity of the rocket that is shown in fig. 4.7 and was calculated by assuming each part of the rocket (i.e. stage, interstage, oms, etc.) to have its specific constant density. To conclude, a rendering of the preliminary sized gondola and mechanism can be seen in fig. 4.8.

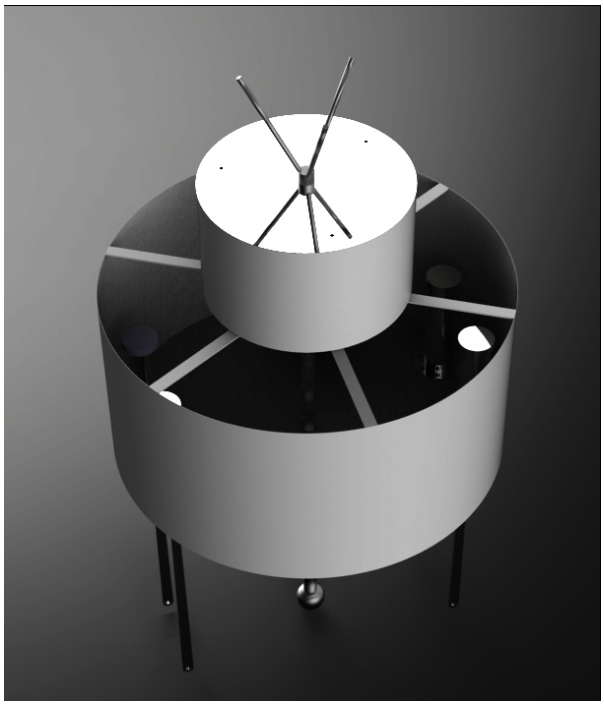

Figure 4.8: A rendering of the preliminary design of the gondola and separation mechanism.

4.4. PROPULSION SUBSYSTEM CHARACTERISTICS

The rockets main propulsion systems are solid propelled rocket motors. These will be used for stages one, two and three. There is an orbital manoeuvring system (OMS) attached to the third stage which is powered by mono-propellant engines. After release from the balloon, the first three rocket stages will accelerate the rocket to a 200 x 600 km orbit, after which, the OMS will circularise and fine tune the orbit to that which is required. It will also serve to deorbit the third stage and will limit the contribution to space debris. Solid propellant motors were chosen for a number of reasons including cost, complexity, propellant handling characteristics, etc with respect to liquid, hybrid

and beam powered ones. The engine thrust, propellant mass and total impulse requirements per stage have been set by the system integration tool and are shown in table 4.6. All requirements for the propulsion system are checked for compliance in section 5.9.

Table 4.6: Engine Requirements

Requirement	**Stage 1**	**Stage 2**	**Stage 3**	**Stage 3+ (OMS)**
Nominal Thrust (T)	160 952 N	92 900 N	6702 N	44 N
Impulse (I)	5779 kNs	2289 kNs	1010 kNs	22.6 kNs
Propellant Mass (m_p)	2356 kg	933 kg	443 kg	9.9 kg

4.4.1. HTPB PROPELLANT

The solid propellant to be used is a composite mixture of oxidiser crystals and fuel which are bound together with a a binder. The heterogeneous propellant grain consists of 18% aluminium powder (Al) as fuel, 71% ammonium perchlorate (AP) as oxidiser and 11% hydroxyl-terminated polybutadiene (HTPB) as a binder. In literature this mixture is refereed to as TP-H-3340 Propellant B [17]. Double base propellants are not used due to their high hazards, low density and low performance. HTPB is one of the most common solid propellant binders and its performance is better than propellants with CTPB and PBAN binders. HTPB propellants have the widest ambient temperature limits, good burn-rate control, stable combustion, medium cost, good storage stability and a hazard classification of 1.3. A hazard classification for detonation of 1.3 is the lower hazard level for solid propellants, as these type of propellants will not keep burning or gasify and explode under a combustion chamber rupture. This DoD rating determines the labelling, costs, and limits of shipping and storing this propellant. [18]

This propellant can be cast into the correct shape of the grain and inserted into the motor or be cast directly into the motor casing. For internal burning engines, it can be cast with a mould of the cavity shape inside, which is removed after. The burn characteristics of 'Propellant B' are given in Table 4.7. The value of the molecular mass of the combustion products are taken from the University of Colorado Colorado Springs solid and liquid propulsion examples [6]. The Vandenkerckhove function, which is dependent on the specific heat ratio, is calculated in eq. (4.10) and the characteristic velocity is calculated in eq. (4.11). The characteristic velocity is a measure of the performance of the propellant and it is a function of the chamber conditions. St. Robert's Law, quantifying the burn rate, is shown in eq. (4.12) and is a function of the chamber pressure in MPa, burn rate coefficient and exponent. The maximum operating chamber pressure ($MEOP_c$) is chosen to be 3.5 MPa to keep the combustion chamber mass down while motor performance high.

$$\Gamma = \sqrt{\gamma \cdot (\frac{1+\gamma}{2})^{\frac{1+\gamma}{1-\gamma}}} = 0.6485 \tag{4.10}$$

$$c^* = \frac{1}{\Gamma}\sqrt{\frac{R_A}{M_W}T_c} = 1471.6\,\frac{\mathrm{m}}{\mathrm{s}} \tag{4.11}$$

$$r_b = a p_c^n = 0.00581\,\frac{\mathrm{m}}{\mathrm{s}} \tag{4.12}$$

[6] Taken From Solid & Liquid Propulsion Examples http://eas.uccs.edu/~aketsdev/MAE%205391_files/Solid_Liquid%20Propulsion%20Examples.pdf

Table 4.7: TP-H-3340 'Propellant B' Characteristics [17]

Combustion Temperature (T_c)	3396 K
Fuel Density (ρ_{prop})	1800 kg/m^3
Burn Rate Coefficient (a)	0.00399 m/s/MPa^n
Burn Rate Exponent (n)	0.30
Combustion Pressure Range (p_c)	2.75 MPa to 5 MPa
Universal Gas Constant (R_A)	8314 J/(kmol·K)
Gas Molecular Mass (M_W)	31 g/mol
Specific Heat Ratio (γ)	1.2

4.4.2. GRAIN DESIGN TOOL

Solid rocket motors can have a variety of grain configurations that provide different thrust curves. The initial internal cross section (and length) determines the evolution of the burning surface area with time. The burning surface area can increase, remain constant or decrease over the burn. These are called progressive, neutral and regressive burning grains, respectively, because the mass flow (and thrust) is directly related to the burning surface area shown in eq. (4.22).

This tool works by inputting the initial the grain configuration shown in fig. 4.9. First, the construction or center lines of are given a outer radius ($R_{star,o}$), then the stars are given a thickness. The star thickness is the distance from the center line to the outside of the star. For the rounded star, this will offset the outer edges of the star arm in all directions by this amount. For the wide star, there is a setting for the radial star width, which is the width of the tip of the star arms shown in fig. 4.12. Setting an inner star radius will cause the configuration to have a circular arc between the star arms as shown in fig. 4.12. If this radius is set below the radial distance to the intersection of two adjacent star arms edges, this arc is not present and a corner is, as shown in fig. 4.11.

The GUI of the grain design tool specifies the core shape as a polygon, with the corners specified as (x, y)-coordinate pairs. From this polygon, the contour lines at specified distances from the core are calculated. These contour lines correspond to the burning surface areas when that amount of web has been burned away. Using eq. (4.13), the length of these contour curves is calculated; multiplied by the length of the grain, this gives the burning surface area as a function of web thickness burned. Examples of these contour lines are plotted in figs. 4.10 to 4.12.

The nozzle throat area is calculated such, that the maximum allowed chamber pressure of 3.5 MPa is reached when the burning area is maximal (eq. (4.14)). This throat area can then be used to calculate the chamber pressure at the other web burn-back distances (eq. (4.15)). From this, the instantaneous regression rate at the specified burn-back distances can be calculated (eq. (4.12)).

$$s = \sum \sqrt{(x_n - x_{n-1})^2 + (y_n - y_{n-1})^2} \tag{4.13}$$

$$A^* = \frac{A_{b,\max} \cdot \rho_{\text{prop}} \cdot c^* \cdot a}{p_{c,\max}^{1-n}} \tag{4.14}$$

$$p_c = \left(\frac{A_b \cdot \rho_{\text{prop}} \cdot a \cdot c^*}{A^*} \right)^{\frac{1}{1-n}} \tag{4.15}$$

$$\tag{4.16}$$

With
- a the constant value in the equation for the regression rate eq. (4.12)
- A_b the burning area
- A^* the nozzle throat area
- c^* the characteristic exhaust velocity of the propellant
- n the exponent in the equation for the regression rate eq. (4.12)
- p_c the chamber pressure
- ρ_{prop} the density of the solid propellant

The regression rates are averaged between two contour lines, such that the time to burn from one contour to the next can be calculated as $\Delta t = \frac{\Delta d}{r_{b,\text{avg}}}$ with Δd the distance between two contour curves. This gives the times corresponding to the burn-back distances, and thus the chamber pressure over time.

The thrust of the engine is given by eq. (4.17), and can now be calculated as a function of time. The thrust coefficient C_T is a constant for a given nozzle design, and is given by eq. (4.18). λ and η are an efficiency factor for the nozzle and the combustion chamber, respectively. They are assumed to be 0.97 and 0.93. The engine is assumed to be operating in a vacuum; since the vehicle is launched at 40 km altitude, this assumption has only a small effect on the thrust of the engine. Finally, the total impulse is calculated using a numerical approximation to eq. (4.19), with the burnout time t_b set to occur when $p_c < 10\% p_{c,\max}$.

$$F_T = \eta\lambda C_T \cdot A^* \cdot p_c \tag{4.17}$$

$$C_T = \Gamma\sqrt{\frac{2\gamma}{\gamma-1}\left[1-\left(\frac{p_e}{p_c}\right)^{\frac{\gamma-1}{\gamma}}\right]} + \frac{p_e - p_a}{p_c}\frac{A_e}{A^*} \tag{4.18}$$

$$I_{\text{total}} = \int_0^{t_b} F_T\, dt \tag{4.19}$$

Sharp, rounded and wide star gain configurations were analysed with the grain design tool and they are shown in figures 4.10 - 4.12. With the tool, one is able to change the parameters of the shapes in the GUI including the star outer radius, the star inner radius, star thickness (only applicable for rounded and wide star shapes) and the number of star points. Also, one can change the nozzle expansion ratio, grain radius and length. With changes to these parameters, the grain shape and the outputs are updated shown in fig. 4.13. Changing these values and reflecting on the changes to the tool's outputs is the process used to choose the internal shape, grain diameter and length. This shape was chosen based mainly on the thrust curves. To minimise steering losses (for the first stage) and to keep the final thrust to weight ratio low, a high initial thrust, neutral burning grain shape was to be found. The best option for this is the rounded star pattern. This shape was also chosen for the (2^{nd}) stage grain because it fulfils the requirements and will reduce the costs. The development cost and the production costs for the first two stages will cost less than the production of motors with different grains because the grain shape and grain radius is exactly the same, while only the lengths are

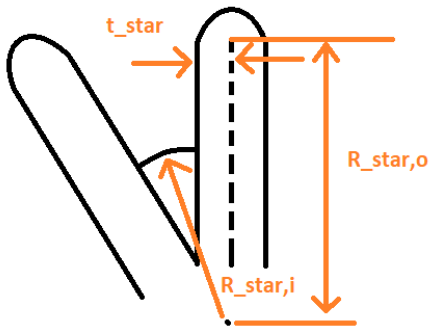

Figure 4.9: Grain Design Tool Geometry.

different. This tool is not used for the third stage motor because it is an end burning grain which has a constant burning surface area and thrust. The chosen grains and their specifications are described in the next section 4.4.3.

Figure 4.10: Star Shaped Grain

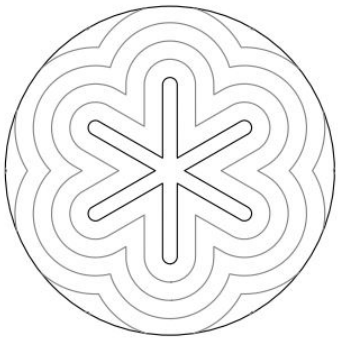

Figure 4.11: Rounded Star Shaped Grain

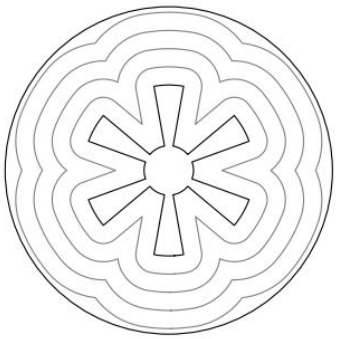

Figure 4.12: Wide Star Shaped Grain

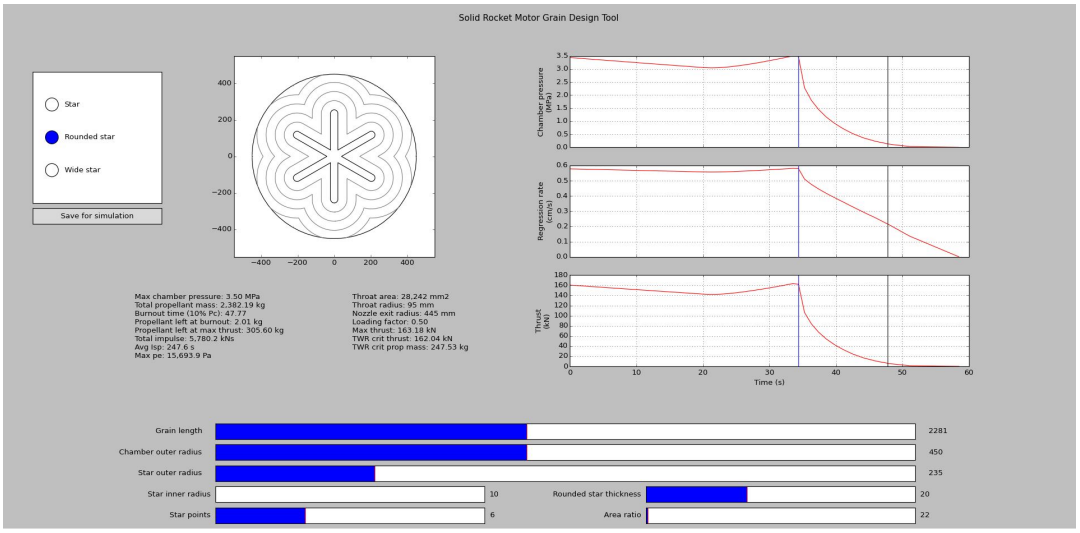

Figure 4.13: Stage 1 Engine Details, Showing the Tool's GUI.

4.4.3. ENGINE SPECIFICATIONS

With the engine requirements defined, a engine may be designed to fulfil them. The grain design tool is used to deign the 1^{st} and 2^{nd} stage internal burning grains, while the 3^{rd} stage is designed by hand.

1ST & 2ND STAGE GRAIN

The propellant grain for the 1^{st} and 2^{nd} stage grains is the internal burning star shape with rounded edges shown in fig. 4.11. One can also see the perimeter lines of the burning surface as time progresses. The star grain dimensions are shown in table 4.8 for stage 1 and stage 2. Stage one star dimensions are chosen to have a high initial thrust which is relatively constant over time (neutral burning). The design chamber pressure is 3.5 MPa. The first stage needs a high initial thrust to minimise steering losses during the initial manoeuvre. This manoeuvre is needed to raise the angle of

the airspeed vector after release from the balloon. The star dimensions for stage 2 are also chosen to have a thrust curve that is almost constant. The stage 2 grain star shape is identical to that of the the first stage, only with a shorter grain length and different nozzle expansion ratio. The curves of the chamber pressure, regression rate and thrust for stages 1 and 2 can be seen in fig. 4.14 and fig. 4.15. The blue line in the curves indicates the when the critical thrust occurs and the grain design tool outputs the thrust and remaining propellant mass at this point. This allows the calculation of the critical thrust to weight ratio. This critical thrust to weight is the maximum value throughout the burn. The second line indicates the burn-out time which occurs at 10% of the chamber pressure. The important information regarding these stages can be found in table 4.9. These engines with these specifications will fulfil the requirements. The igniter for these engines is at the top of the combustion chamber, within the star cavity. These will require a small amount of power from the electrical power system.

Table 4.8: Star Grain Dimensions

Dimension	**Stage 1**	**Stage 2**
Grain Outer Radius (r_{gr})	0.45 m	0.45 m
Grain Length (L_{gr})	2.281 m	0.9 m
Star Outer Radius ($r_{star,o}$)	0.235 m	0.235 m
Star Thickness (t_{star})	0.02 m	0.02 m
Number of Stars (n_{star})	6 –	6 m
Nozzle Expansion Ratio (ε)	22 –	45 –

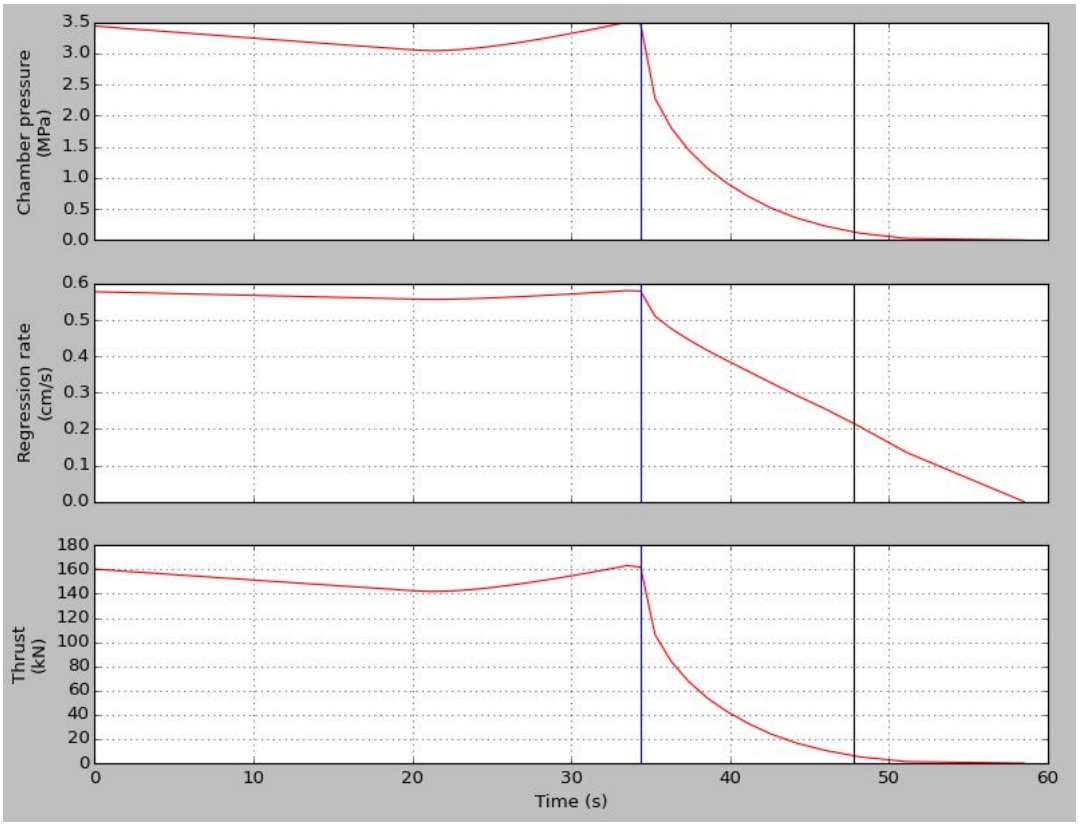

Figure 4.14: Stage 1 Chamber Pressure, Regression Rate and Thrust Curves.

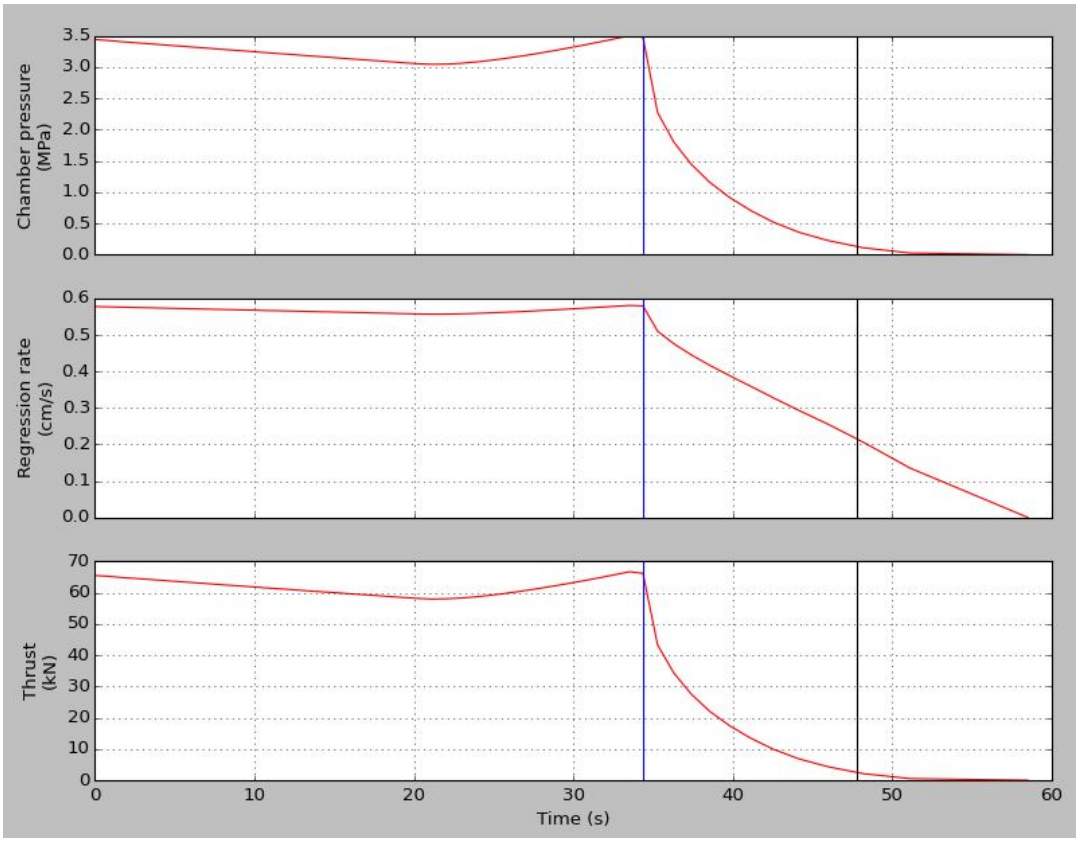

Figure 4.15: Stage 2 Chamber Pressure, Regression Rate and Thrust Curves.

Table 4.9: Stage 1 and 2 Engine Specifications

Dimension	**Stage 1**	**Stage 2**
Initial Thrust (T_{init})	160.3 kN	65.5 kN
Maximum Thrust (T_{max})	163.2 kN	66.6 kN
Initial Thrust to Weight $[T/W]_{init}$	3.89 –	4 –
Critical Thrust to Weight $[T/W]_{crit}$	7.98 –	8.3 –
Propellant Mass (m_p)	2382 kg	940 kg
Burn Time (t_b)	47.8 s	47.8 s
Impulse (I)	5.78 MNs	2.3 MNs
Average Specific Impulse ($i_{sp,avg}$)	247.6 s	256.3 s

3RD STAGE GRAIN

The propellant grain to be used for the third stage is the end burning geometry shown in fig. 4.16. This grain configuration has a constant burning surface area and as a result of this, the chamber pressure is constant for this grain. This stage was not designed with the grain design tool but by hand because the chamber pressure and mass flow is constant. The design chamber pressure is also 3.5 MPa. The constant burning surface area and chamber pressure cause a constant mass flow seen in eq. (4.22). With eq. (4.21), the thrust is also constant over the burn which means it is neutral burning. It must be ignited from the end nearest to the nozzle, and the burning linearly progresses away from the nozzle. The igniter requires little power from the electrical power system.

To design the end burning grain, eq. (4.21) is used to calculate the mass flow needed to reach the

required thrust. This is done using the equivalent exit velocity calculated in eq. (4.20). To meet the required thrust (or mass flow), there must be a minimum burning surface area shown in eq. (4.22) and with a cylindrical grain shape, the required grain radius ($r_{gr,3}$) can easily be found. The grain will have a spherical end cap, so the length of the cylindrical part of the grain (L_{cyl}) is calculated in eq. (4.23) using the volume of the propellant. The burn time can be calculated with eq. (4.24). When the burning of the grain reaches the start of the end cap, the burning surface area will start to reduce. This is not taken into account for this design phase.

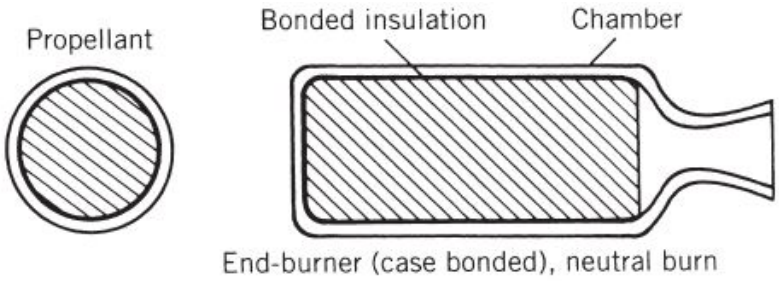

Figure 4.16: End Burning Propellant Grain [18]

$$v_{eq} = i_{sp} \cdot g_0 = 285 \cdot 9.81 = 2795.85\ m/s \tag{4.20}$$

$$\dot{m}_{req} = \frac{T_{req}}{v_{eq}} = \frac{6701.58}{2795.85} = 2.397\,\frac{\text{kg}}{\text{s}} \tag{4.21}$$

$$A_b = \frac{\dot{m}}{\rho_{prop} \cdot r_b} = \frac{2.397}{1800 \cdot 0.00581} = 0.229\,\text{m}^2 \Rightarrow r_{gr,3} = \sqrt{\frac{A_b}{\pi}} = 0.2701\,\text{m} \tag{4.22}$$

$$V_p = \frac{m_p}{\rho_{prop}} = \pi r_{gr}^2 L_{cyl} + 0.5(\frac{4}{3})\pi r_{gr}^3 \Rightarrow L_{cyl} = \frac{V_p - (\frac{2}{3})\pi r_{gr}^3}{\pi r_{gr}^2} = \frac{0.2465 - (\frac{2}{3})\pi 0.2701^3}{\pi \cdot 0.2701^2} = 0.8955\,\text{m} \tag{4.23}$$

$$t_b = \frac{L_{gr,3}}{r_b} = \frac{1.075}{0.00581} = 185\,\text{s} \tag{4.24}$$

4.4.4. NOZZLES

1ST & 2ND STAGE NOZZLE

While designing the 1^{st} & 2^{nd} stage grains, the expansion ratio is also chosen to meet the engine requirements. This leads to the exit radius with eq. (4.25). Bell shaped nozzles have been chosen for the first two stages because they are the most common shape, and more efficient than conical nozzles [18]. A 80% length bell nozzle is chosen because it provides slightly more efficiency than a full length conical nozzle with the same area ratio [18]. The length of the 80% bell nozzle can be estimated as a fraction of the length of a reference 15° half angle conical nozzle. The equation to estimate the length of the 80% bell nozzle is shown in eq. (4.26). This is the length of the divergent section from the throat to the exit. In fig. 4.17, the radius of the convergent section and divergent section are shown as a function of the throat radius. At point I in the figure, there is an inflection point and the curve between this point and the exit (point E) can be approximated with a parabola [18]. The nozzle characteristics are shown in table 4.10 below. The inlet radius is defined as the

throat radius plus the convergent section radius. The inlet is flat beyond the inlet radius, and starts converging to the throat radius as one moves aft in the nozzle. The mass of the nozzle may be estimated with a relation shown in eq. (4.27) [17]. In this equation, the chamber pressure in in MPa and θ_{cn} is the nozzle divergence half angle for a reference 15° conical nozzle. The nozzles will reasonably weigh more than this due to the TVC system inside of them. The nozzle will be made from a steel structural shell which is lined on the inner side with an ablative material such as carbon, Kevlar or silica fibers with an epoxy resin, ablative plastics or carbon-carbon. Ablation must be used to keep the nozzle structure's temperature within it's material limits.

$$A_e = \varepsilon \cdot A^* \tag{4.25}$$

$$L_{bell} = 0.8 \cdot L_{cone} = 0.8 \, \frac{r_e - r_t}{\tan(\alpha)} \tag{4.26}$$

$$m_{nozz} = 0.256 \cdot 10^{-4} \left[\frac{(m_p \cdot c^*)^{1.2} \varepsilon^{0.3}}{p_c^{0.8} \cdot t_b^{0.6} (\tan(\theta_{cn}))^{0.4}} \right] \tag{4.27}$$

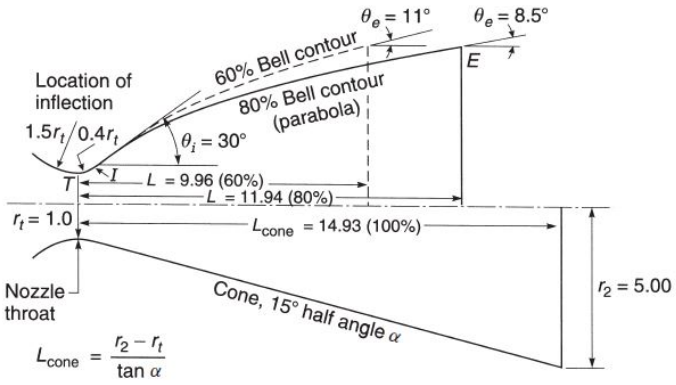

Figure 4.17: Nozzle Geometry [18]

Table 4.10: Stage 1 and 2 Nozzle Specifications

Dimension	**Stage 1**	**Stage 2**
Divergent Length (L_{bell})	1.045 m	1.015 m
Expansion Ratio (ε)	22	45
Throat Radius (r^*)	0.095 m	0.060 m
Exit Radius (r^e)	0.445 m	0.4 m
Convergent Radius (r_c)	0.1425 m	0.09 m
Divergent Radius (r_d)	0.038 m	0.024 m
Inlet Radius (r_i)	0.2375 m	0.15 m
Total Length (L_{nozz})	1.188 m	1.105 m
Contour Angle at I (θ_i)	26°	26°
Exit Contour Angle at E (θ_e)	13.44°	9.31°
Nozzle Mass (m_{nozz})	73.5 kg	32.1 kg

3RD STAGE NOZZLE

The third stage nozzle is designed by hand and with Python to be able to quickly iterate and find the reduction in required exit velocity due to the pressure contribution to thrust. For a first iteration, the pressure term was neglected and the process below was applied. With this result, the pressure term was added to v_e and iterated until the exit pressure and area input to eq. (4.28) coincided with the output exit area and pressure. This code was verified by hand.

The equation for required exit velocity is shown in eq. (4.28). With this required exit velocity, eq. (4.29) can be rearranged for the required exit pressure. Next, the required expansion ratio to meet the exit pressure can be calculated with eq. (4.30). With the required mass flow defined from eq. (4.21), the throat area can be calculated with equation eq. (4.31). With these equations, the nozzle characteristics are defined.

As above, the nozzle will be an 80% bell shaped nozzle. The length of the nozzle can be calculated with eq. (4.26), and the convergent and divergent radii are still $1.5 \cdot r^*$ and $0.4 \cdot r^*$, respectively. The mass of the nozzle may be estimated with a relation shown in eq. (4.27) [17]. The nozzle specifications for the stage 3 nozzle can be seen in table 4.11. The nozzle will be made from a steel structural shell which is lined on the inner side with an ablative material such as carbon, Kevlar or silica fibers with an epoxy resin, ablative plastics or carbon-carbon. Ablation must be used to keep the nozzle structure's temperature within it's material limits. The grains and nozzles can be seen in fig. 4.18.

$$v_{eq} = I_{sp} g_0 = v_e + \frac{p_e A_e}{\dot{m}} \Rightarrow v_e = I_{sp} g_0 - \frac{p_e A_e}{\dot{m}} \tag{4.28}$$

$$v_e = \sqrt{\frac{2\gamma}{\gamma - 1} \frac{R_A}{M_W} T_c \left[1 - (\frac{p_e}{p_c})^{\frac{\gamma-1}{\gamma}} \right]} \Rightarrow p_e = p_c \cdot \left[1 - \frac{v_e^2}{\frac{2\gamma}{\gamma-1} \frac{R_A T_c}{M_W}} \right]^{\frac{\gamma}{\gamma-1}} \tag{4.29}$$

$$\varepsilon = \frac{A_e}{A_t} = \frac{\Gamma}{\sqrt{\frac{2\gamma}{\gamma-1} (\frac{p_e}{p_c})^{\frac{2}{\gamma}} \left[1 - (\frac{p_e}{p_c})^{\frac{\gamma-1}{\gamma}} \right]}} \tag{4.30}$$

$$A_t = \frac{c^* \dot{m}}{p_c} \tag{4.31}$$

4.4.5. ORBIT MANOEUVRE SYSTEM

In this section the features and specifications of the Orbit Manoeuvre System (OMS) are detailed. The thruster type and specifications are presented in section 4.4.5. The design of the OMS propellant feed system is discussed in section 4.4.5. A summary of the specifications of the OMS is provided in table 4.13.

OMS THRUSTERS

The OMS is integrated with the third stage bus of the rocket. It has two primary functions, to accurately bring the payload to the desired orbit and to deorbit the the third stage after separation of the payload. To fulfil the required functionality the OMS must posses multiple restart capability and operational adaptability to provide fine control of the orbit.

Table 4.11: Stage 3 Nozzle Specifications

Dimension	**Stage 1**
Effective Exhaust Velocity (v_{eq})	2679 m/s
Required Exit Pressure (p_e)	5724 Pa
Expansion Ratio (ε)	48.5 –
Throat Radius (r^*)	0.018 m
Exit Radius (r^e)	0.125 m
Convergent Radius (r_c)	0.027 m
Divergent Radius (r_d)	0.0072 m
Inlet Radius (r_c)	0.045 m
Divergent Length (L_{bell})	0.319 m
Total Length (L_{nozz})	0.346 m
Contour Angle at I (θ_i)	26°
Exit Contour Angle at E (θ_e)	14.12°
Nozzle Mass (m_{nozz})	6.8 kg

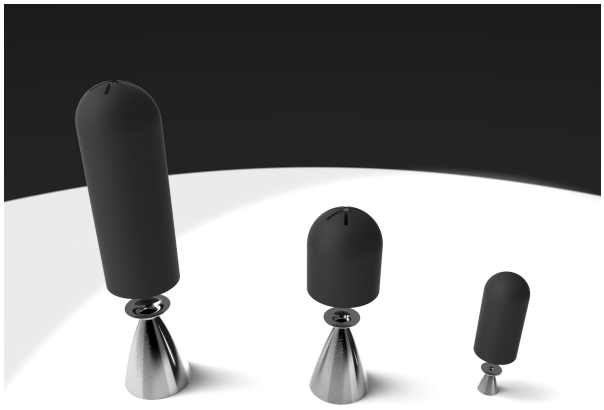

Figure 4.18: Renders of the Stage Grains and Nozzles.

To meet these criteria the OMS uses a monopropellant propulsion method with hydrazine propellant. Thrust is produced by decomposing the hydrazine molecule over a heated catalyst, releasing thermal energy and expanding the decomposition products. An unfortunate property of hydrazine is that is extremely toxic, however only a small amount of propellant is required so the danger is somewhat mitigated. Currently there are safer monopropellants being investigated as an alternative to hydrazine [19] but none of these are flight ready.

The OMS uses two MR-106E monopropellant engines depicted in fig. 4.19, the specifications are listed in table 4.12. It is designed and produced by Aerojet Rocketdyne, thus this component is sourced externally. The engine is flight proven and is assumed to have a high reliability due to the manufacturers experience. It requires power to operate the engine, 39.52 W to open the solenoid valve, 3.27 W to heat the valve, and 6.36 W to heat the catalyst bed. It is assumed that for operation all of these components are used, making for a total power consumption of 49.15 W.

To conclude, a render of the preliminary design is shown in fig. 4.20.

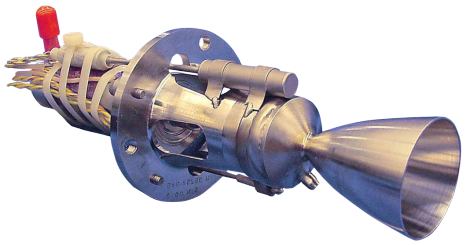

Figure 4.19: MR-106e thruster from Aerojet Rocketdyne. Obtained from: http://www.rocket.com/propulsion-systems/monopropellant-rockets

Table 4.12: MR-106E Monopropellant Engine Specifications

Thrust	**Isp**	**Operating Power**	**Max. Feed Pressure**	**Min. Feed Pressure**	**Unit Mass**
22.0 N	232.0 s	49.15 W	24.1 bar	6.9 bar	0.635 kg

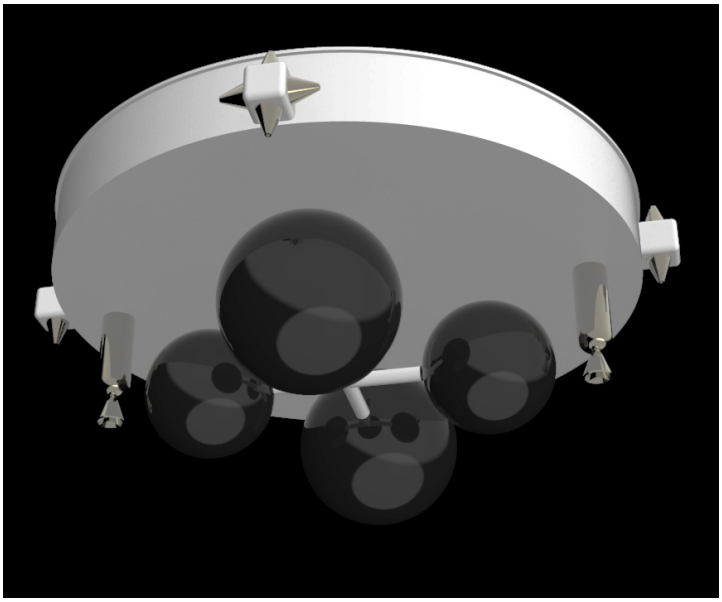

Figure 4.20: A rendering of the preliminary design of the OMS module. Figure is not to scale.

OMS Feed System

The feed system of the OMS is the mechanism responsible for feeding the propellant to the engine inlet valves. It has 3 main features, the propellant tanks, the pressurant & pressurant tanks, and the pressurisation manifold.

The propellant tank is a diaphragm type tank, whereby the propellant and pressurised gas are physically separated a flexible bladder inside the tank. Due to the complexity of these tanks, an empirical relation from [15] is used to size the propellant tank mass, it can be seen in eq. (4.32). The V in this relation represents the tank volume in litres, and it calculates the mass in kilograms. To balance the rocket, the propellant is divided into two tanks which are placed opposite each other in a symmetric manor.

The tank tank volume is determined by taking half the OMS propellant mass over the density of hydrazine, 4.95 kg and 1.02 kg/l respectively. It is prescribed in [15] to apply a 20% margin to the propellant tank volume to account for thermal expansion of the propellant and space for the bladder. This results in a tank volume of 6.07 l, including the contingency, applying this to eq. (4.32), a propellant tank mass of 1.05 kg is obtained, for a total mass of 2.1 kg. The diameter of the tank $\varnothing_{\text{tank}}$ is found from the volume with eq. (4.33), resulting in a tank diameter of 0.23 m.

$$M_{\text{propellant tank}} = 2.7086 \cdot 10^{-8} V^3 - 6.1703 \cdot 10^{-5} V^2 + 6.6290 \cdot 10^{-2} V + 1.391 \tag{4.32}$$

$$\varnothing_{\text{tank}} = 2 \cdot \left(\frac{3V}{4\pi} \right)^{1/3} \tag{4.33}$$

The required mass and tank volume of the pressurant for the OMS is calculated using the ideal gas law by identifying its initial and final states, and solving the coupled equations. The pressurant gas used is helium with a gas constant R_{He} of 2077 J/kgK. The state of the pressurant is defined by the volume, pressure, temperature, mass, and gas constant. The initial pressure P_i is set as the maximum inlet pressure of the engines 24.1 bar, likewise the final pressure P_f is the minimum inlet pressure of the engines 6.9 bar. The temperature of the initial condition T_i is set to 323 K and for the final condition T_f it is set to 293 K, these are recommended by [15]. The volume of the initial state is the undefined pressurant volume $V_{\text{pressurant tanks}}$, and the final state is the pressurant tank volume $V_{\text{pressurant tanks}}$ plus the total propellant tank volume $V_{\text{propellant tanks}}$, 12.14 l. The mass of pressurant $M_{\text{pressurant}}$ must be the same for both conditions. The total pressurant tank volume $V_{\text{pressurant tanks}}$ is solved for with eq. (4.34), and the total pressurant mass $M_{\text{pressurant}}$ is solved for with eq. (4.35) which yields 0.021 kg of pressurant.

$$V_{\text{pressurant tanks}} = V_{\text{propellant tanks}} \div \left(\frac{P_i}{P_f} \cdot \frac{T_f}{T_i} - 1 \right) \tag{4.34}$$

$$M_{\text{pressurant}} = P_i \cdot V_{\text{pressurant tanks}} \div (T_i \cdot R_{He}) \tag{4.35}$$

$$M_{\text{pressurant tank}} = 5.4548 \cdot (PV)^2 + 6.6092 \cdot PV + 1.862 \tag{4.36}$$

The pressurant tank mass $M_{\text{pressurant tank}}$ is estimated using an empirical relation from [15] shown in eq. (4.36). The input to the relation PV is the Pressure times the Volume of the tank in the units of MPa $\cdot$ m^3. Applying this to previous result yields a pressurant tank mass of 1.9 kg for total mass of 3.8 kg. The tank diameter $\varnothing_{\text{tank}}$ is determined by eq. (4.33), which yields 0.175 m.

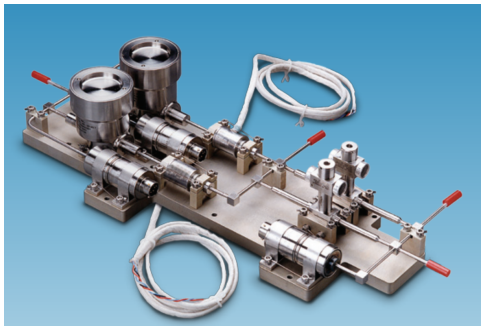

Figure 4.21: MOOG Propellant Management Assembly, Obtained from: http://www.moog.com/products/propulsion-controls/spacecraft/spacecraft-propulsion-components

Table 4.13: Orbit Manoeuvre System Specification Summary

Component	Power Consumption	Unit Mass	Unit Diameter
MR-106e Thruster (x2)	49.15 W	0.635 kg	*N/A*
Propellant Tank (x2)	*N/A*	1.05 kg	0.23 m
Helium Pressurant	*N/A*	0.021 kg	*N/A*
Pressurant Tank (x2)	*N/A*	1.9 kg	0.175 m
Feed System	13.5 W	3.75 kg	*N/A*
OMS Total	111.8 W	10.941 kg	*N/A*

The final major component of the OMS system is the pressurisation manifold, it is responsible for controlling the pressure level inside the propellant tanks and routing propellant to the thrusters. The *Propellant Management Assembly* manufactured by MOOG is used for the OMS, it is depicted in fig. 4.21. The assembly component specification are shown in table 4.13.[7]

4.5. PAYLOAD INTEGRATION

Payload integration is an important aspect of the launcher as it connects the payload to the final rocket stage while also making sure that the payload is released in a timely fashion. Furthermore, inertial and vibration loads are transmitted through the connection between payload and upper stage. All of the aforementioned aspects will be discussed more thoroughly in the following subsections.

4.5.1. PAYLOAD SEPARATION

An important design aspect for the payload is the separation of the payload from the final stage. This can be done in multiple ways, but mostly pyrotechnics or springs are used when a single satellite is launched. How multiple CubeSats are launched will be discussed in section 4.5.3 After investigating existing separation system options the decision was made to use the Lightband Mark II produced by Planetary Systems Corporation [20], which can be seen in fig. 4.22. This is a motorised spring based separation system, which has a long flight history with a 100% success rate over almost 30 missions. It is produced in diameters from 20 cm to 100 cm although it has been mostly used in its larger variants. Apart from its perfect success rate one of its major advantages is that it is a Commer-

[7] All specifications taken from manufacturer data sheet obtained from: http://www.moog.com/products/propulsion-controls/spacecraft/spacecraft-propulsion-components

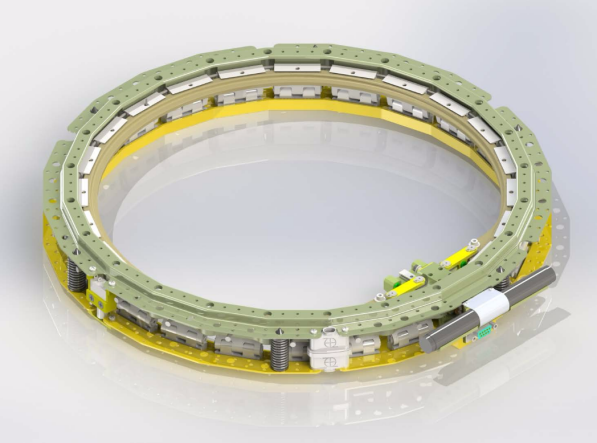

Figure 4.22: A render of the Mark II Lightband as produced by Planetary Systems Corporation

cial Off-The-Shelf (COTS) Technology and thus easily implemented. Other companies that provide separations systems (RUAG Space, Eurocot) produce unique designs for each mission, which would be a lot more expensive. The weight of the Lightband system with a 80 cm diameter will be 5.6 kg [20]. Of which 1.64 kg will be stuck to the payload or its dispension system.

4.5.2. PAYLOAD ADAPTOR

The main goal of this structure is to support the payload and adapt the diameter of the final stage to the diameter of the payload (separation) system. It was assumed it would have no further function. Therefore this component was modelled as a simple thin walled truncated cone. The axial loads were modelled and the adaptor was assumed to be made from aluminium 7075-T7. The necessary thickness found when assuming the adaptor fails in direct compressive stress was far below the production limit, which is around 1 mm for this very hardened version of aluminium. It is known, however that conventional adaptors are not produced this flimsy and thin. Therefore a 3 mm thickness was used to conform to conventional thicknesses [21]. The difference is most likely caused, because vibration and buckling loads play a large role for failure of this component. A thorough analysis of these loads was however deemed outside the current scope for this minor component. Combining this thickness with a height of 20 cm leads to a mass of 4.9 kg.

4.5.3. PAYLOAD DEPLOYMENT

For the deployment of CubeSats, conventionally pods are used for which multiple configurations are possible. This was mostly done to physically separate them from the main payload on piggyback launches. However, they should still be used for the design and can even replace the separation system if the payload exists of CubeSats only. Innovative Solutions In Space (ISIS) produces CubeSat pods called ISIPODs for 3, 6 or 12 Unit CubeSats. In the worse case scenario of having nine times 3U Pods it adds around 15 kg to the payload integration [8].

4.5.4. VIBRATION ISOLATION

Vibration can be a big problem for launchers, as these loads can cause damage to the payload and are hard to reduce. Therefore it might be necessary to isolate the payload from the main structure

[8] https://www.isispace.nl/product/isipod-cubesat-deployer/

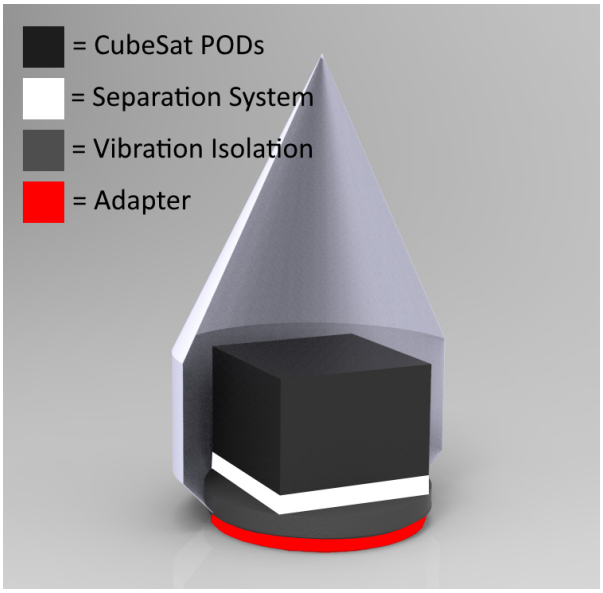

Figure 4.23: The complete payload integration consisting of the CubeSat PODs, Separation System, Vibration Isolation and Payload adaptor. Together they are encompassed by the fairing

of the final stage such that vibrations can not pass through to the payload. Technologies creating this vibration isolation are commercially available. One COTS vibration isolation system with the diameter required for the concept is the OmniFlex vibration isolation, produced by MOOG corporation, which can be seen in fig. 4.24. OmniFlex reduces vibration in both the axial as well as the lateral direction. They also make a ShockRing to damp shocks next to the vibration. These combined would weigh 9 kg [21]. Do mind this is optional for the customer to include in their launch as certain payloads might be able to withstand the vibration loads easily and thus do not require a vibration isolation system.

4.5.5. PAYLOAD CONFIGURATION

The payload configuration must be flexible for large and small payloads. The configuration is determined for the case that the launcher has to transport only 1U CubeSats, since this is the extreme case for the configuration. For this case, nine 3U ISIPODs are needed which also fits three separate 1U CubeSats. The ISIPODs are 13 cm by 18 cm by 42 cm. A margin of 3 cm has been applied for the distance between the ISIPODs both in the length and width. This margin is needed due to opening of the lids. These lids need more space than the respective length. The width also has a margin of 3 cm due to mounting the box on a platform. To assure that the fairing will encapsulate the payload without being in contact with it, an off set height from payload and fairing wall of 10 cm is used. The same off set is used for the diameter of the payload.

To determine the payload diameter, it is first investigated which CubeSat combinations are possible. From the market analysis it was concluded that 27U is preferable per launch. So the possible combinations has to add up to 27U. In table 4.14 different CubeSat combinations were investigated for three configurations, see fig. 4.25a, fig. 4.25b and fig. 4.25c. It must be noted that the option of putting one 27U satellite will result in less space needed than the combination of smaller CubeSat. From these configurations, two have the same critical radius. These radii are R2 and R5 and these are equal to 43.02 cm. So to support flexibility of all 3U ISOPOD box configurations, it was calculated that a cylinder with a radius of 43.02 cm and a height of 42 cm can support this.

Figure 4.24: OmniFlex vibration isolation as produced by MOOG Corporation

Table 4.14: The possible combinations of different CubeSat sizes for each configuration.

	Combination A	Combination B
Configuration 1	2× 3U	4× 6U + 1× 3U
Configuration 2	2× 12U + 1× 3U	1× 24U long version + 1× 3U
Configuration 3	2× 12U + 1× 3U	1× 24U short version + 1× 3U

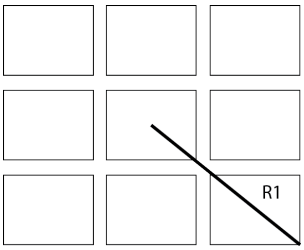

(a) A top view for configuration 1. Every cube is a ISO-POD which can contain three 1U CubeSats.

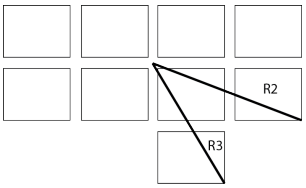

(b) A top view for configuration 2.

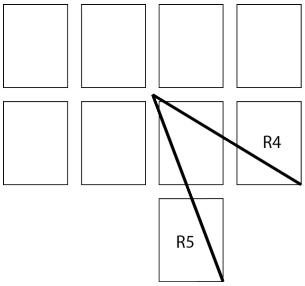

(c) A top view for configuration 3. This figure is similar to fig. 4.25b, but the boxes are rotated by 90 degrees.

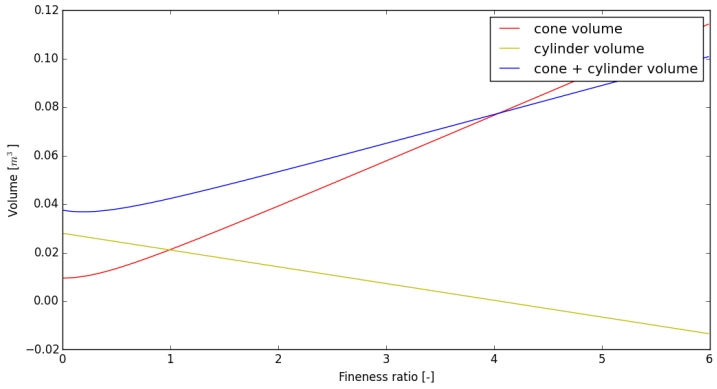

Figure 4.26: A plot generated in Python showing the quadratic relation between fineness ratio and volume. It can be seen that the graph is almost linear from the point where fineness ratio is equal to 1.

4.5.6. PAYLOAD FAIRING DESIGN

In section 4.6 it was determined that air density is sparse enough from 40 km altitude that it will not generate significant drag. While the design of the payload fairing still needs to be aerodynamic, it does not need to be optimally designed to reduce drag. So a less aerodynamic, but a more manufacturable nose cone design can be chosen. A less complicated shape will result in simple manufacturing, which in turn results in lower manufacturing costs. A conical nose cone design is chosen for this purpose.

The conical shape will be defined by a fineness ratio which is given in eq. (4.37). A high fineness ratio gives a low drag coefficient. The fineness ratio, F.R., is defined by the length and the radius which are L and R respectively. The radius needed for the payload was given in the previous section, where it was also determined that a radial margin of 10 cm between the payload and fairing will be used. So a radius of 0.55 m when rounded up to fives. The only unknowns left are the fineness ratio and the length of the conical nose cone.

$$F.R. = \frac{L}{2R} \tag{4.37}$$

For a good design choice, the nose cone design is not only dependent on the fineness ratio. It also depends on the mass, since more mass on the top of the rocket will result in a large snowball effect. To minimise the mass, the material used for the cone should be minimised. A higher fineness ratio means an increase in the amount of material needed, and thus the mass of the cone.

In order to have the payload fit in the fairing, a hollow cylinder will be fitted under the cone. This solution prevents the cone to be extraordinarily tall. To minimise the mass of the fairing, the volume of the material used was minimised. The thickness of the fairing is just a scaling factor of the area, as can be seen in eq. (4.39). So for determination of the minimum volume, an arbitrary thickness can be used. The thickness of the fairing is depended on the stresses acting on it, this will be determined in section 4.12.

To find the fineness ratio related to the minimal volume, a plot was generated in Python to find the minimal point. This plot can be seen in fig. 4.26. The relation between the fineness ratio and the volume of the cone material is quadratic. This is due to the fact that the area of the slant of the cone is described by eq. (4.38). The variable 's' is equal to the hypotenuse of a triangle.

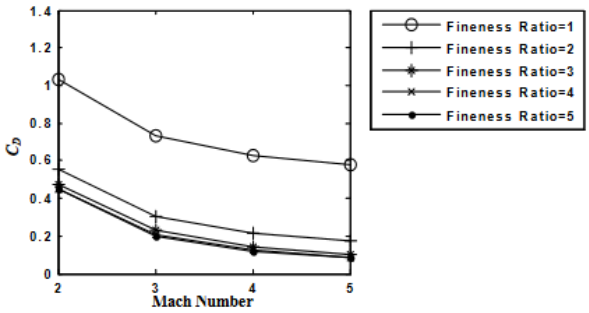

Figure 4.27: A plot showing the relation between the fineness ratio and drag coefficient. This plot is taken from Drag of Conical Nose at Supersonic Speedsarticle [22].

$$A_{slant} = \pi \cdot R \cdot s \tag{4.38}$$

When combining eq. (4.37) and eq. (4.38), the following relation is obtained for the volume of the nose cone:

$$V_{slant} = \pi \cdot R \cdot \sqrt{(2 \cdot R \cdot F.R.)^2 + R^2} \cdot t \tag{4.39}$$

The minimum volume is 0.03684 m^3, this corresponds to a fineness ratio of 0.2 which is below one. A fineness ratio below one means that the nose cone will have a blunt conical shape. This shape will near that of a flat plate. Since no experimental data is available on drag behaviour of blunt nose cone shapes and flat plates or blunt nose at supersonic speeds, this option must be disregarded. There are experimental data available for fineness ratio's of one to four. In article drag on different nose cone designs at supersonic speeds [22], the data are displayed. A fineness ratio of 1 will have the highest drag, but the lowest volume needed to make the nose cone. Since mass has the highest priority and drag is negligible, a fineness ratio of 1 will be chosen for the fairing design.

4.6. AERODYNAMICS & STABILITY CHARACTERISTICS

The aerodynamic forces such as lift and drag have different effects on a rocket than on an aircraft. For an aircraft, the lift is used to overcome the weight. For a rocket, the lift is a side force and it stabilises the rocket when the center of pressure is below the center of gravity. Whereas the thrust of the rocket is used to counteract its weight, more on stability of the rocket topic will be displayed in section 4.6.4. The center of pressure will be determined. In order to know if the rocket can stabilise with aerodynamic forces, it must be determined if the aerodynamic forces will be significant enough for stabilisation this will be done in section 4.6.1 and section 4.6.2. Also it should be checked if the drag is low enough such that a more manufacturable, but a less drag reducing design can be applied to the rocket. This section will be concluded with an analysis on burn-up of the stages at re-entry in section 4.6.5.

4.6.1. DRAG FORCES

Above 30 km altitude, 99 percent of the atmosphere has been covered. In fig. 4.28 it can also be seen that the density above 40 km altitude is very low. Thus one can conclude that the drag can be neglected. In this section it will be investigated if this is valid. At first sight this might be obvious, but the drag can become significant when high velocities are reached within low density atmosphere.

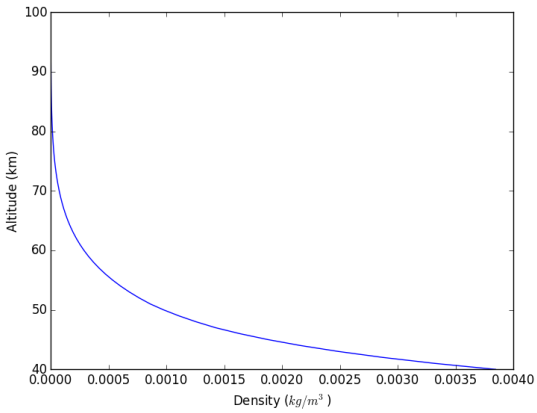

Figure 4.28: A plot of altitude versus density generated in Python. It shows that the density decreases with increasing altitude.

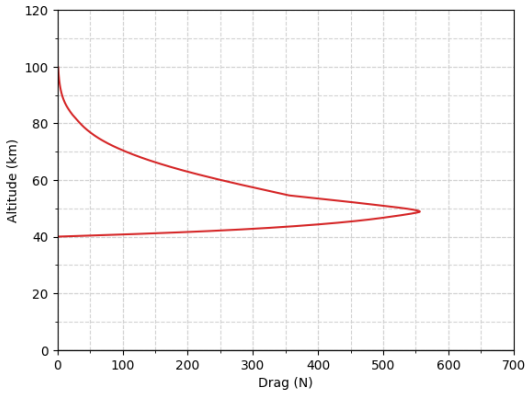

Figure 4.29: A plot of altitude versus drag generated in Python. The altitude has been put on the y-axis to make it intuitively.

To investigate this drag, eq. (4.40) is used. For the drag coefficient, C_D, a blunt conical nosecone with a fineness ratio of 1 has been chosen. This will result in minimum mass of the payload fairing. In fig. 4.27, it can be seen that the C_D decreases from 1.01 to 0.6 with increasing mach number 2 to 5, respectively.

In the determination of the drag, the upper boundary of the altitude will be the Kármán Line, which defines the physical boundary between Earth's atmosphere and outer space [23]. The Kármán Line is defined at 100 km altitude, above this point, the air is too thin to generate lift that is larger than the centrifugal forces generated by high velocity. For the first 85 km, a model of the International Standard Atmosphere is used to determine air density. For the range 85 to 100 km, an approximation was made based on the article: "New Static Models of the Thermosphere and Exosphere with Empirical Temperature Profiles" [24]. In section 4.5.6, it is established that the the diameter of the wet surface is 1.10 m, so $S = 0.95\,\text{m}^2$.

The velocity in the drag equation was determined by the trajectory model in section 4.7. The exact trajectory for the ALTAR launch system gave varying velocities during the ascent.

$$D = 0.5 \cdot C_D \cdot \rho(h) \cdot V(h)^2 \cdot S \tag{4.40}$$

A graph was made in Python, which can be seen in fig. 4.29. The maximum drag is less than 600 N. A thrust of 160 kN is generated by the first stage as mentioned in section 4.4. The drag is 0.375 % of the aforementioned thrust, so it can be concluded that the drag is low. Thus the shape of the nose cone can be designed such that it is not the most aerodynamically efficient design.

4.6.2. LIFT

The lift force for a rocket is much smaller than the drag force. This is especially true when the nose of the rocket is aligned with its flight path i.e. the air stream and rocket are not inclined with respect with each other. There is no lift force due to symmetry of the rocket in both axes. This can be seen in fig. 4.30 if the rocket has zero displacement angle. The fact that the rocket will operate in minimum atmospheric conditions and taking into account the aforementioned information, the lift force will be neglected.

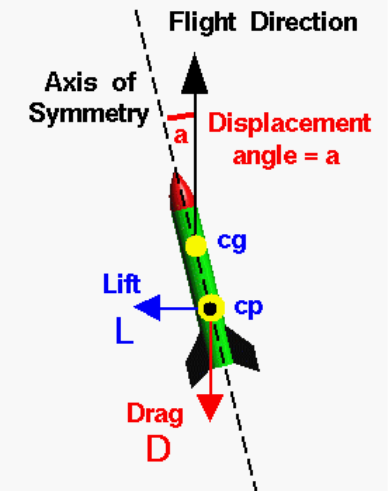

Figure 4.30: The aerodynamic forces are acting in the center of pressure. The weight is acting in the center of gravity. The center of pressure is behind the center of gravity. One can observe that the line of action of the aerodynamic forces are off set from the center of gravity. This causes the lift and drag forces to cause a moment in the opposite direction of the moment caused by the weight. This makes the rocket statically stable. This image is taken from NASA education [25].

4.6.3. CENTRE OF PRESSURE

The center of pressure (*C.P.*) is the point where the aerodynamic forces are acting on the rocket. An accurate estimation of *C.P.* can be performed when the pressure distribution of the rocket is known. The pressure distribution can be determined by experiments or complex numerical methods, in a preliminary design this is beyond the scope. Instead, a simplified method which is applied to small scale rockets will be used for a rough estimate. For this eq. (4.41) will be used. This equation determines the location of the *C.P.* with respect to the base of the rocket. Here the total lateral area, A. The distance between the average area of a section and the base is defined as x_i. The local lateral area is defined by a_i.

$$x_{c_p} \cdot A = x_{nose} \cdot a_{nose} + x_{body} \cdot a_{body} + x_{fins} \cdot a_{fins} \tag{4.41}$$

Using data from the CATIA drawing of the rocket displayed in fig. 4.7, this results in a x_{c_p}. equal to 5.11 m and a total lateral are of 6.992 m.

4.6.4. STABILITY

For flight stability, the *C.P.* should be below the centre of gravity (*C.G.*) of the rocket as shown and explained in fig. 4.30. The distance between the *C.P.*. and *C.G.* is called the static stability margin. The static stability margin can be increased by adding fins with a large sweep angle. In the case of ALTAR launch system, it is chosen not to attach fins to the rocket. Since the rocket will be launched at about 40 km altitude. At that altitude the air density is minimal. Due to this reason, fins would not be effective. During the ascent in the atmosphere, the rocket will be naturally unstable due to the lack of fins. Also it was determined in section 4.6.3 that the location of *C.P.* is at 5.11 m from the base of the rocket. In figure fig. 4.7 it can be seen that the *C.G.* is at 4.40 m from the base of the rocket. The fins would contribute to moving the center of pressure below the centre of gravity. An active control system will be used, namely a thrust vectoring system, for the handling of the natural instability.

4.6.5. RE-ENTRY

Although the rocket will not be reused nor landed in the same fashion as SpaceX it is important to investigate the re-entry of the stages as they descend through the atmosphere. This is to make sure they actually burn up and not crash down to Earth in pieces of half molten aluminium, which obviously would be rather dangerous. To analyse this, the kinetic and potential energy that is stored within the stage after it burns out and is separated from the rest of the rocket is calculated. All this energy needs to be dissipated as heat for the stage to reach zero velocity. Now the only question is how much of the heat is transferred to the air and how much to the stage itself. The ratio for this heat division can be found by the following eq. (4.42) as can be found in Hankey's *Re-entry Aerodynamics* [26].

$$\frac{Q_B}{Q_A} = \frac{St \cdot \rho \cdot A_{stage} \cdot V_s (H_S - H_W)}{\rho \cdot A_{stage} \cdot V_s \cdot H_S} \approx St \tag{4.42}$$

In this equation, Q_B is the heat flow into the stage Q_A is the thermal flow rate of the air stream, St is the Stanton number, A_{stage} the surface area of the stage, ρ the air density, V_s the relative air velocity, H_S the total enthalpy, and H_W the wall enthalpy.

Assuming the wall enthalpy is much smaller than the total enthalpy, this ratio can be simplified to only being the Stanton number as can be seen in eq. (4.42). In turn the Stanton number can be estimated with the friction coefficient using Reynolds analogy, given in eq. (4.43).

$$St = C_f/2 \tag{4.43}$$

With C_f the friction coefficient.

Knowing the ratio between the energy dissipated to the air and the energy that flows into the stage, the latter can be calculated. The potential and kinetic energy are calculated using the well known equations that can be seen in eq. (4.44).

$$KE = 0.5\rho V^2 \qquad PE = m \cdot g \cdot h_s \tag{4.44}$$

With KE the kinetic energy stored within the stage, PE the potential energy stored within the stage, m the mass of the empty stage, g the gravitational acceleration, and h_s the altitude of the stage at burn-out.

Another parameter of interest is the maximum temperature that is reached at the stagnation point of the flow around the stage. To find this temperature, shock relations are combined with the assumption that the free stream flow temperature is a lot smaller than the stagnation temperature and thus can be neglected. This leads to the simple relation given in eq. (4.45), with T_0 the stagnation temperature and C_p the pressure coefficient. For each stage, the results of using the equations mentioned above are summarised in table 4.15.

$$T_0 = V_\infty^2/2 \cdot C_p \tag{4.45}$$

While the above estimation is a decent first order estimation, it does not take into account drag forces ripping the stage apart into a lot of pieces, which highly increases the friction coefficient for each separate piece tumbling through the atmosphere and thus increasing the amount of heat each piece receives. It also does not take into account that at the end of the reentry parts can still have a (small) velocity and fthus not all kinetic energy has been dissipated as heat. It is however deemed

Stage #	Speed [m/s]*	Altitude [km]*	Amount of stage molten [%] **	Stagnation Temperature [K]
1	1776	54.09	-70.0	1568.9
2	3649	89.00	7.4	6625.4
3	7894	200.00	372.3	31003.0

Table 4.15: Reentry Heating parameters for all stages. *at burn-out, **Difference between heat dissipated to the stage and energy required to completely melt divided by the latter

an accurate enough estimation in this stage of the design. Looking at the results, one can see that the first stage is only molten for 30%, while the second and third stage are completely molten, but the second stage only barely so. Furthermore, enough heat will be dissipated to the third stage to vaporise around 25% of its mass. Additionally, for all stages, the stagnation temperatures are high enough to start the melting process at the stagnation point.

Now that it is clear that the second and third stage will not cause much problems while re-entering as they are completely liquefied, the focus shifts to the first stage. The first stage poses a clear problem as it is not completely disintegrated during re-entry and will probably fall down in multiple big pieces of half molten aluminium. This poses an unacceptable risk if the re-entry trajectory of the first stage is over a populated area. Thus, it is highly preferable to make sure this re-entry trajectory does not fly over populated areas, preferably over sea. This is one of the reasons launching from an island was chosen (e.g. Terceira Island) as a possible launch location, because in a 320 km radius (the downrange distance the first stage will land as calculated in section 4.7.1) there is only ocean. The sea routes still need to be cleared to make sure it does not accidentally land on a ship. Furthermore, it might be better to decrease the friction coefficient by using a very smooth coating so the first stage stays (almost) completely intact. This would be done to have a single part crashing down instead of having a spread of smaller parts over a larger region, which would increase the chance of an unwanted collision.

4.7. Guidance & Control Characteristics

The guidance, navigation and control (GNC) subsystem has as purpose to measure the position, velocity and attitude of the launch vehicle and to use these measurements to steer the launch vehicle to the correct target orbit. As the name implies, the system has three main components:

- **Navigation**, which determines the current position, velocity and attitude of the vehicle
- **Guidance**, which determines the required attitude, such that the vehicle will reach the intended target orbit at burnout
- **Control**, which applies control inputs such that the vehicle is steered to the required attitude.

Figure 4.31 gives an overview of how these three components are connected, forming a feedback loop.

4.7.1. Ascent Trajectory

The ascent trajectory was designed using the Trajectory Simulation and Optimisation Tool described in chapter 3. As explained there, a thrust-mass profile was used for the first two stages (see fig. 4.32), and a constant thrust for the third stage. The burn of the OMS stage at the first apogee, which raises

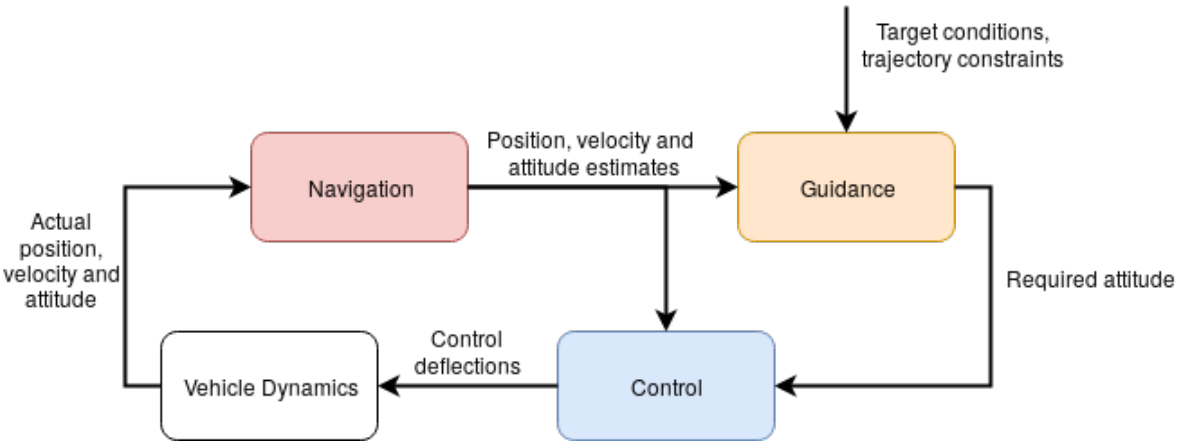

Figure 4.31: Overview of the guidance, navigation and control subsystem.

the perigee from 200 km to its final value, is not included in the simulation. An overview of the inputs to the simulation can be found in table 4.16. The drag coefficient was assumed to be the same function of Mach number for all three stages (see fig. 4.33). Finally, the change in thrust and I_{sp} due to the atmospheric pressure was neglected; since the pressure at 40 km is already less than 0.3 % of the value at sea level, this effect is considered negligible. The steering vector was calculated from a stepwise pitch rate function, changing at 30 s, 45 s, 60 s, 90 s, 150 s and 210 s, and an initial azimuth angle. This initial azimuth was calculated using eqs. (4.46) to (4.48).

$$\sin\alpha = \begin{cases} 1 & \text{if } \varphi < i \\ \frac{\cos i}{\cos\phi} & \text{if } \varphi \geq i \end{cases} \tag{4.46}$$

$$v_0 = \Omega(R_e + h)\cos\varphi \tag{4.47}$$

$$\tan(\text{azimuth}) = \frac{v_f \sin\alpha - v_0}{v_f \cos\alpha} \tag{4.48}$$

With
- Ω the rotation rate of the Earth, 7.2921159×10^{-5} rad/s
- R_e the mean radius of the Earth, 6371 km
- h the altitude above mean sea level at launch
- v_f the magnitude of the final velocity vector
- i the target inclination
- φ the latitude of the launch site

The control input vector to be optimised was the combination of payload mass, initial pitch angle, and the seven pitch rates. The optimisation was set up to maximise the payload mass, while constraining the trajectory with respect to the final values of the altitude above sea level and the vertical and horizontal velocities. These were calculated such, that the vehicle will insert into a parking orbit with the perigee at 200 km altitude, and the apogee at the height of the target orbit (eqs. (4.49) to (4.51)). It was assumed that the vehicle inserts itself and the payload into this orbit at perigee.

$$r_f = R_e + 200\,\text{km} \tag{4.49}$$

$$v_{h,f} = \sqrt{\mu_e \cdot \left(\frac{2}{r_p} - \frac{2}{r_p + r_a}\right)} \tag{4.50}$$

$$v_{v,f} = 0 \tag{4.51}$$

Table 4.16: Inputs to TSOT for the trajectory design of the ALTAR vehicle.

Stage	**1**	**2**	**3**
Dry mass (kg)	177.34	173.644	60.12[(a)]
Fuel mass (kg)	2360.4	931.2	433.7
Vacuum thrust (kN)	(b)	(c)	6.701
Specific impulse (s)	250	250	285
Drag coefficient	(d)	(d)	(d)
Reference area (m^2)	0.636	0.636	0.636
Initial conditions			
Latitude (°)	38.7		
Longitude (°)	−29.3		
Altitude (km)	40.0		
Target orbit			
Apogee altitude (km)	600		
Perigee altitude (km)	200		
Inclination (°)	98.6		

(a) Includes the dry mass of the third stage and the OMS fuel.
(b) See fig. 4.32a
(c) See fig. 4.32b
(d) See fig. 4.33

With μ_e the gravitational parameter of Earth, $3.986004418 \times 10^{14}\ m^3/s^2$
R_e the mean radius of the Earth, 6371 km
r_a the apogee radius, $r_a = R_e + h_{\text{target}}$
r_p the perigee radius, $r_p = R_e + 200\,\text{km}$

The most important result from the trajectory optimisation was the payload mass that can be placed into the design orbit. This was determined to be 46.4 kg. The optimised trajectory resulting from the TSOT for a target orbit of 600 km altitude at 98.6° inclination is plotted in fig. 4.34a. The separation points of the rocket can be clearly seen. The first stage separates 30 km downrange at an altitude of 54 km, and the second stage at 170 km downrange and 90 km altitude. They impact the ocean at 315 km and 1270 km downrange, respectively. Orbit insertion occurs 1060 km downrange of the launch site. fig. 4.34b shows that the impact locations of the first two stages are far from populated areas in the Atlantic ocean. After leaving the Azores, the flight path also does not go over any popu-

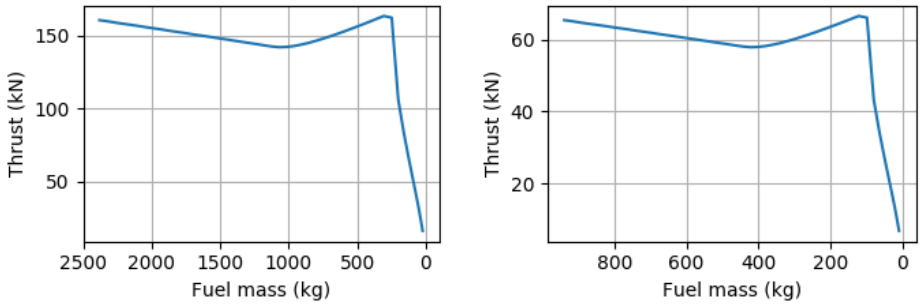

(a) Thrust curve for the first stage.

(b) Thrust curve for the second stage.

Figure 4.32: Inputs to the TSOT: thrust curves.

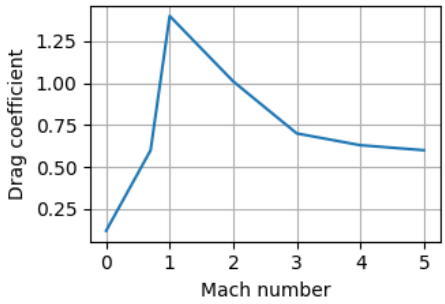

Figure 4.33: Inputs to the TSOT: drag coefficient versus Mach number.

lated areas. This means that even in the case of a launch failure, the stages do not have a significant risk of hitting a person. The resulting optimised pitch profile has an almost constant pitch rate of –0.20 °/s, as can be seen in fig. 4.34c. fig. 4.34d shows the thrust-to-weight ratio over time. The maximum TWR reached during launch is approximately 8.5, at burnout of the second stage. The hot-staging can also be seen: a stage is ignited when the previous stage's TWR falls below 1. It also shows that the third stage burns for approximately twice the time of the first two stages combined. From fig. 4.34e, it can be seen that the ΔV-loss due to drag is negligible (less than 10 m/s). The gravity and steering losses are approximately 500 m/s and 80 m/s, respectively. In fig. 4.34f can be seen that more than half of the orbital velocity is provided by the third stage. The maximum vertical velocity reached is just over 1000 m/s at burnout of the second stage.

4.7.2. NAVIGATION

The navigation subsystem is responsible for providing the guidance and control subsystems with reliable attitude, position and velocity information. To do this, it measures the acceleration on three axes using accelerometers and the attitude using gyroscopes. The measurements are done in the inertial measurement unit (IMU). This data is integrated in the flight computer to estimate the current position and velocity. This integrator is updated regularly with position and velocity information from a global navigation satellite system (GNSS) receiver.

Early launch vehicles used a stabilised platform on which the accelerometers were mounted. This platform keeps the accelerometers in a constant inertial attitude. Because gyroscopes of sufficient dynamic range and accuracy did not exist at the time, a strap-down (i.e. the accelerometers are fixed to the rocket structure) system, while mechanically much simpler, was not possible. Nowadays, due to the availability of fibre-optic and hemispherical resonator gyroscopes and more sophisticated digital electronics, a strap-down system is feasible at the required accuracy for space launch vehicles [27]. Because such a strap-down system is less complex and lighter, the launch vehicle will use a strap-down inertial navigation system.

Because the acceleration is integrated over time to generate position and velocity information, errors in the measurement are amplified. To correct for this, a secondary source of position and velocity information is required. This can either be done using range data transmitted by radar stations on the ground, or by GNSS data. Ground stations are not available all the way along the ground track, and are expensive to operate. For these reasons, the GNSS receiver will be used. The GNSS receiver can also act as primary position information, in case the IMU experiences a failure.

Commercial off-the-shelf inertial measurement units are available which are rated for ballistic mis-

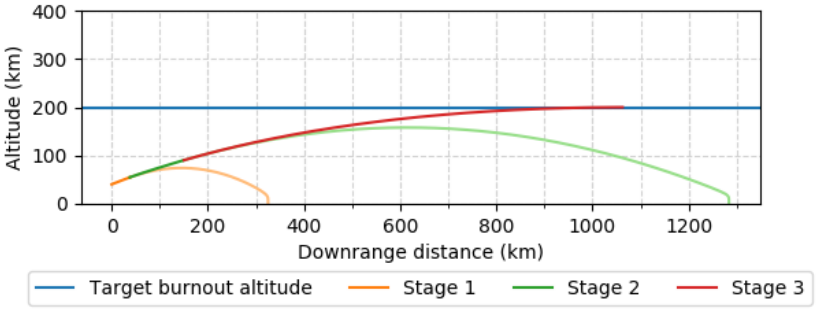

(a) Side view of the trajectory.

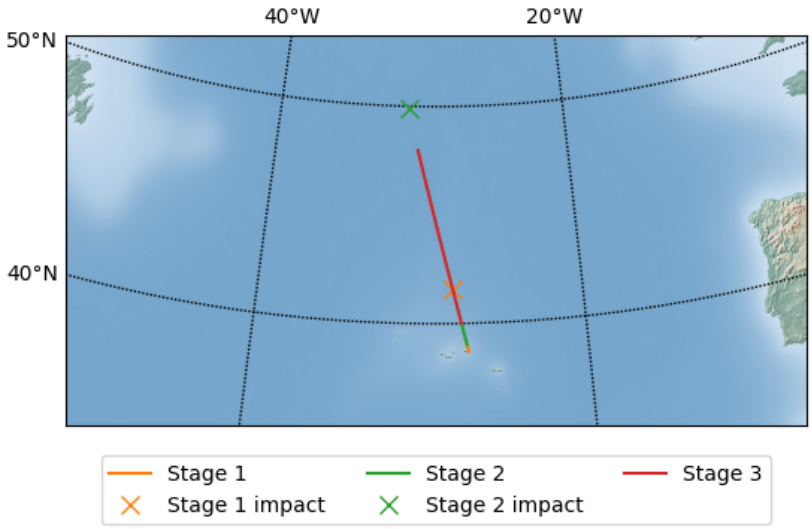

(b) Top-down view of the trajectory.

Figure 4.34: Launch trajectory of the ALTAR vehicle, optimised by the TSOT.

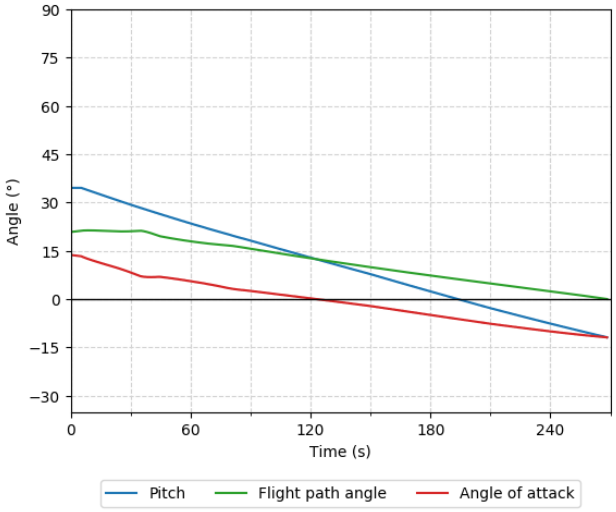

(c) Pitch, flight path angle and angle of attack over time.

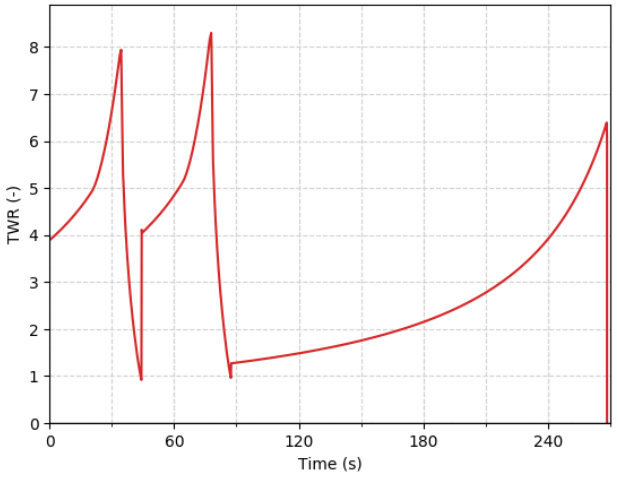

(d) Thrust-to-weight ratio over time.

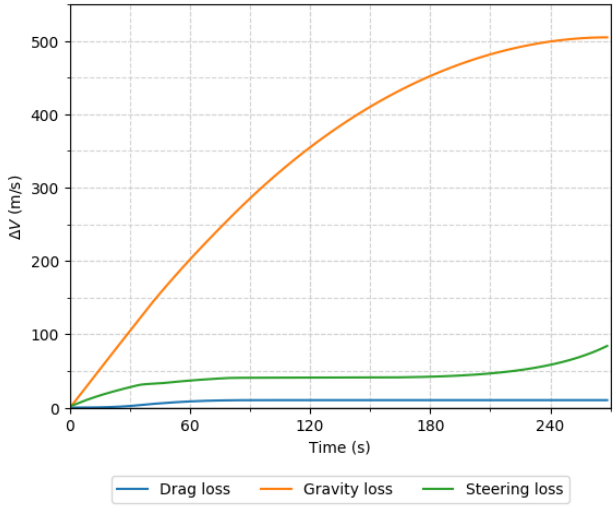

(e) Total gravity, drag and steering losses over time.

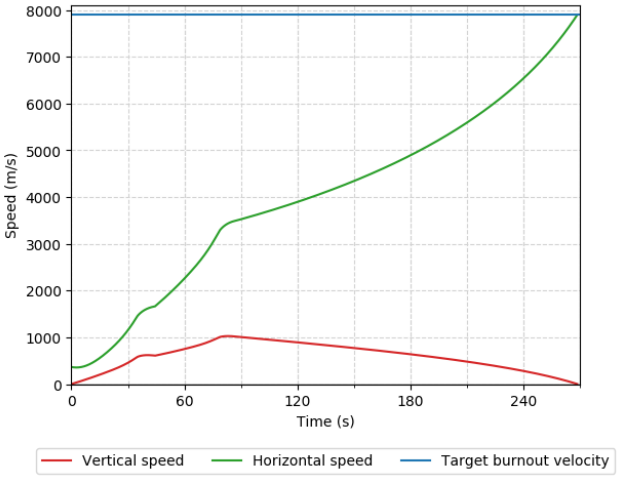

(f) Horizontal and vertical velocity over time.

Figure 4.34: *(cont.)* Launch trajectory of the ALTAR vehicle, optimised by the TSOT.

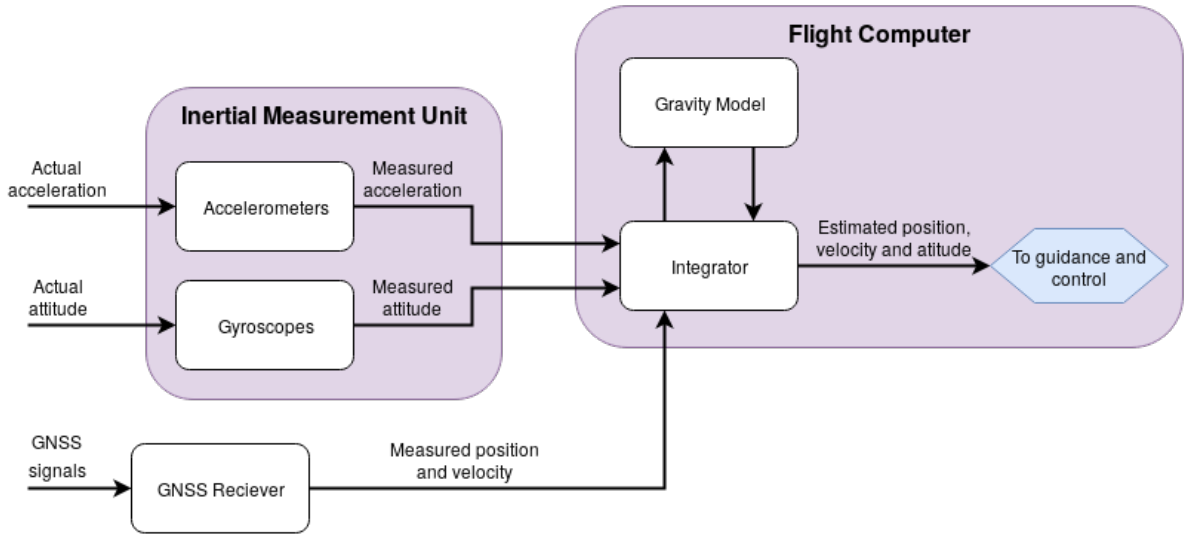

Figure 4.35: Architecture of the navigation component of the GNC subsystem.

siles [9]. Since these have a very similar mission profile to a launch vehicle, these can be used without modification for the ALTAR vehicle. Existing launch vehicles generally also use COTS navigation units [28, 29]. Based on a comparison of several IMU's of several commercial manufacturers, the power consumption and mass of a complete inertial navigation system, including GNSS receiver, are estimated to be on the order of 25 W and 1 kg, respectively.

4.7.3. ATTITUDE CONTROL

The attitude control section deals with the implementation of the the guidance trajectory by manipulating the attitude of the rocket. The implementation of an attitude control system is of utmost importance to correct for deviations from the intended trajectory. The attitude of a rocket can be changed by imposing a moment on it, which for most rockets is created by aerodynamic surfaces and/or by thrust vector control (TVC). The use of aerodynamic surfaces can directly be ruled out due to the fact that the rocket is launched above an altitude of 30 km at which it is past 99% of the atmosphere. Therefore, the only remaining feasible attitude control mechanism for the rocket is by means of TVC. The remaining part of this section will elaborate on the different TVC mechanisms and appoint one of these as the TVC mechanism for the rocket.

THRUST VECTOR CONTROL

In addition to providing thrust for the ascent of the rocket, the propulsion subsystem can also provide attitude control. This attitude control is achieved by triggering a change in the thrust vector, either by changing the direction and/or the magnitude of the thrust vector. Depending on the propulsion configuration, either one or both changes are applied. The different mechanisms that provide attitude control by means of TVC are shown in fig. 4.36.

The TVC mechanisms that can be applied make use of different working principles and actuators. As

[9] See for example
http://www.kvh.com/Commercial-and-OEM/Gyros-and-Inertial-Systems-and-Compasses/Gyros-and-IMUs-and-INS/IMUs.aspx,
http://www.northropgrumman.com/Capabilities/LN100GInertialNavigationSystem/Documents/ln100g.pdf,
https://www.safran-electronics-defense.com/aerospace/solutions-satellites/navigation-systems-satellites

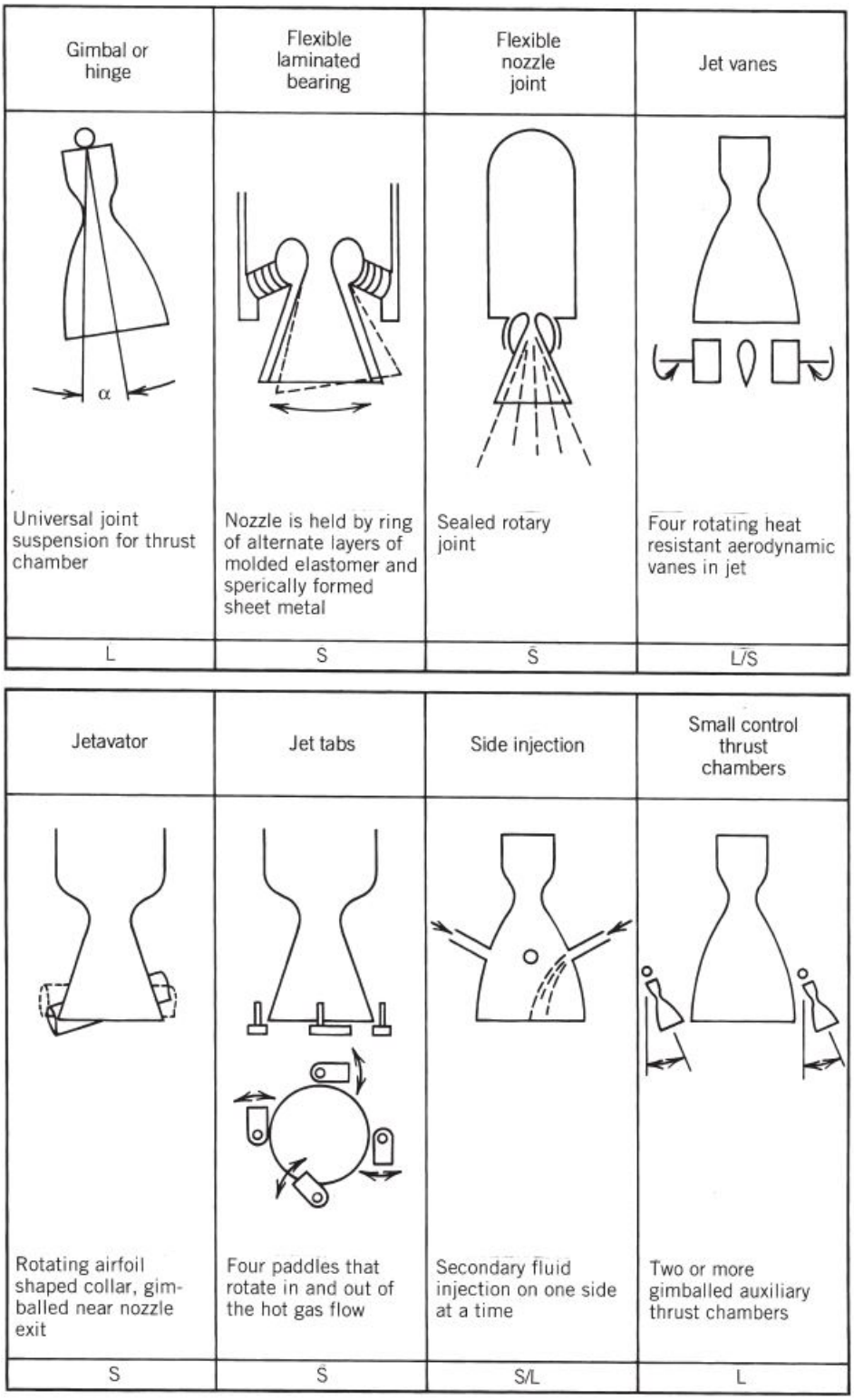

Figure 4.36: Simple schematic overview of eight different TVC mechanisms. The letter L means it is used with liquid propellant rocket engines and S means it is used with solid propellant rocket engines [18].

quantitative data of the mechanisms is limited, the elaboration of their main performance strengths and weaknesses will be done qualitatively in the list below.

- **Gimbal or hinge:** In this mechanism, the whole engine is pivoted on a bearing and hereby the direction of the thrust can be changed by moving the entire nozzle. This mechanism is only able to provide yaw and pitch control and thus another mechanism would have to be added for full attitude control, including roll control. However, this technology can only be applied on liquid rocket engines and since the rocket will use solid rocket propellant engines, (see section 4.7.3) the use of this technology is discarded.
- **Flexible laminated bearing:** The flexible bearing is a commonly used technology for solid rocket engines in which the entire nozzle is moved. This technology has proven itself to be thrustworthy. However, to move the entire nozzle, multiple mechanical or hydraulic actuators are used. These actuators increase the mass of the rocket as well as require a high actuation power, which increases the mass of the batteries that are carried on-board. On top of that, this technology is relatively complex due to the large amount of moving parts and therefore the development and production costs are high. Last but not least, this mechanism merely provides yaw and pitch control. This means that another roll control mechanism has to be added that adds mass and complexity.
- **Flexible nozzle joint:** This mechanism deflects the direction of the thrust vector by using a sealed rotary joint that allows movement of the entire nozzle. A major advantage of this technology is that no thrust is lost if the entire nozzle is moved. However, to deflect the rotary joint, high actuation power is required. This results in heavy batteries that have to be carried on-board. Besides that, this technology only provides yaw and pitch control. Therefore, another mechanism to control the roll behaviour of the rocket has to be added that adds mass and complexity to the system.
- **Jet vanes:** This mechanism deflects the thrust at the end of the nozzle by using small movable airfoils, or so called jet vanes. This mechanism allows full attitude control in all three axis with high slew rates. The jet vane technology also seems quite attractive due to the small actuation power, small mass and the relatively low complexity. A small drawback of this technology is the thrust loss, roughly 0.5-3% [18]. On top of that, erosion of the jet vanes occurs during operation of the rocket. This results in a reduced effectiveness of the jet vanes during operation.
- **Jetavator:** The jetavator has yet only been used on submarine-launched missiles. This mechanism uses a rotating airfoil shaped collar that deflects the direction of the thrust vector. This technology does not require high actuation power and can be relatively lightweight. A drawback of this mechanism is that erosion occurs as well as a thrust loss occurs. Additionally, this mechanism is only able to provide control for yaw and pitch. As explained before, this would require the addition of another mechanism for roll control which adds mass and complexity.
- **Jet tabs:** The jet tab technology uses paddles that are rotated in and out of the exhaust flow. By doing so, the direction of the thrust vector is changed. This mechanism does not require high actuation power and can be relatively compact. A drawback of these paddles however, is that this mechanism only provides control for yaw and pitch. For full attitude control, another mechanism must be added which will add more mass and complexity to the system.
- **Side injection:** This technology forms oblique shocks in the diverging section of the nozzle by injection of a secondary fluid. By doing so, an unsymmetrical distribution of the main gas flow is obtained which results in a side force. The major drawback of this technology is that it requires an external tank and feed system to injected the fluid and also that it is limited to

low vector angle applications. On top of that, this mechanism only allows for yaw and pitch control. All of this adds mass and complexity to the system.

- **Small control thrust chambers:** This technology makes use of small auxiliary gimballed control thrusters at the outside of the nozzle exit which can provide full attitude control. The mechanism has a high performance, low actuation power and can be relatively lightweight. Along with the jet vanes, this technology can solely provide full axis attitude control. However, the additional thrusters require an external tank and a feed system which add mass and complexity to the launch system.

To obtain the most suitable TVC mechanism, special attention is paid to the reliability, performance, cost effectiveness, compactness and integration ease, respectively, in decreasing significance, of each concept.
The reliability of the mechanisms is mainly determined by the number of possibly moving components and the amount of connections between them. The addition of such components adds complexity and mass to the rocket and therefore reduces the reliability. A reliable TVC mechanism is of utmost importance to the mission success and therefore the reliability has a relatively high significance.
The performance of the mechanisms is mainly determined by the attitude control capabilities. It is important that a mechanism is able to provide three axis control, and if so, that the slew rates are sufficiently high to provide precise orbit destination. The performance of the TVC mechanism is of absolute importance to the mission success, and therefore also has a relatively high significance.
The cost, compactness and integration ease of the mechanisms are mainly depending on the type of actuators used. It is important that the mechanisms are cost effective, lightweight and easy to integrate. As the cost effectiveness does not dominantly impede the mission success, the assigned significance is relatively low.

ASCENT TVC: JET VANES

If all the TVC mechanisms are compared relatively with the above mentioned criteria, it turns out that the jet vanes are the most suitable for the rocket during the ascent. There are several reasons for choosing the jet vanes for the ascent, the primary reason being the relative low complexity of this technology. The low complexity can be dedicated to the fact that the only moving components of this technology are two pairs of relatively small airfoils, whereas for the other mechanisms, much bigger components are moving such as the entire nozzle or an additional structure is needed such as an external tank and a feed system. On top of this, the jet vane technology is the only technology besides the auxiliary thrusters that is able to provide three axis attitude control without the addition of another mechanism. This avoids having to add more mass and complexity, as explained earlier. Last but not least, the jet vanes can be easily be pivoted at their center of pressure which results in low actuation power and prevents having to carry heavy batteries.
The drawback of jet vanes is that they are exposed to the extreme exhaust gas flow temperature during the entire burnout time, which requires the use of a suitable heat-resistant material. Additionally, the jet vanes cause a slight thrust loss due of roughly 0.5-3% due to the fact that they are emerged within the exhaust flow, causing a disruption in the expansion [18]. However, the low complexity, high performance and low mass outweighs the slight increase of cost and loss of thrust.

A similar result is obtained from a technical report done by Raytheon Missile Systems Company, who were assigned to research, develop, manufacture and service a guided missile system for several launchers [30]. They compared the technical performance, cost effectiveness and the risk of three TVC mechanisms: jet vanes, jet tabs and moveable nozzle. The company concluded that the

jet vanes have the lowest associated risk and cost. A comparison with this report is made to confirm the correctness of the qualitative trade-off that has been done whereas the report also includes quantitative analysis. The remaining part of this section will elaborate on the jet vane TVC mechanism in further detail.

Jet vanes are pairs of aerodynamic wing-shaped surfaces that are emerged within the exhaust flow of a fixed nozzle. Due to the fact that the jet vanes are emerged within the exhaust gas flow, the jet vanes experience aerodynamic forces from the exhaust gas flow and cause partial deflection of the exhaust gas flow. The jet vanes do not lie on the longitudinal axis of the rocket and therefore the aerodynamic forces, that are non-parallel to the longitudinal axis, are able to provide full attitude control around all three axis. The first (graphite) jet vanes were used by the Germans in the 1940s during the World War II in the V-2 missile. A simple view of jet vanes that are integrated in the exhaust of a rocket nozzle is shown in fig. 4.37.

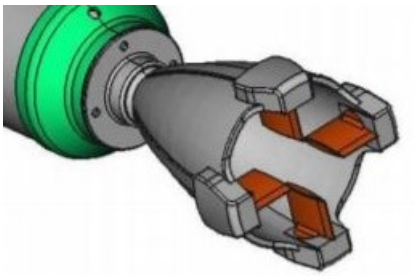

Figure 4.37: A simple view of jet vanes integrated in a rocket nozzle exit. The aerodynamic forces on the jet vanes cause moments on the rocket that provide attitude control around all axes [31].

The major advantage of using jet vanes is that the technology is trustworthy, the required actuation power is low, high slew rates can be achieved and unlike most other mechanisms, also roll control is provided. However, during the entire burnout time of the rocket, the jet vanes are exposed to the extreme temperature of the exhaust gas flow at the nozzle exit. This means that the jet vanes have to be made of heat-resistant materials. Additionally, the exhaust gas flow particles are expelled at extreme high velocities and therefore the jet vanes also must be impact resistant. A commonly used material for jet vanes is graphite. Graphite is known to be highly heat-resistant. However, graphite has a Mohs hardness of only 1-2 [10]. This causes the graphite jet vanes to be ablated away over time by the collision with the high velocity exhaust gas particles. This means that the use of graphite jet vanes is restricted to rockets and missiles that operate over short periods of time. Therefore, the use of graphite jet vanes is discarded for the rocket.

According to a technical paper by the Society of Automotive Engineers, if tungsten is alloyed with molybdenum, an alloy can be obtained which has a melting temperature that is above the stagnation temperature of the jet flame and also provides sufficient impact resistance against the high velocity particles [32]. The authors of this technical report measured the percentage jet vane area loss for different tungsten-molybdenum alloys during a burn time of 40 seconds. It turned out that the vane area loss is negligible if 65% of the alloy weight could be contributed to the tungsten. Other metals that have suitable properties are rhenium and tantalum. However, the availability of tungsten is much greater and the cost is much lower than that of rhenium or tantalum. Note that tungsten is almost twice as heavy as molybdenum. Therefore, a suitable alloy of tungsten and molybdenum will be used that uses as little tungsten as possible to keep the weight of the jet vanes as low as possible. This also increases the machinability of the tungsten-molybdenum alloy. As mentioned before, the weight percentage of tungsten in the alloy shall be at least 65%, preferably not more. The densities of tungsten and molybdenum at room temperature are 19 250 kg/m^3 [11] and 10 280 kg/m^3 [12], respectively. The density of the alloy (65% tungsten) can then calculated, resulting in a density of

[10] http://geology.com/minerals/mohs-hardness-scale.shtml
[11] https://en.wikipedia.org/wiki/Tungsten
[12] https://en.wikipedia.org/wiki/Molybdenum

16 110 kg/m^3.

It is hard to estimate the weight of the jet vanes because there are practically no estimation methods available that are within the scope of this design phase. Therefore, a weight estimation is performed by assuming the dimensions of the jet vanes with respect to the nozzle dimensions. These assumptions are based on visual observation of multiple jet vane images, for example the size of the Soviet Scud Missile jet vanes. For this particular missile, the jet vanes had a span of approximately 25%, a camber of approximately 15% and a thickness of approximately 2% with respect to the nozzle exit diameter, respectively [13]. Note that the volume of the jet vanes is assumed to have the shape of a rectangular box whereas in reality the jet vanes have the shape of a real wing. The estimated weight therefore contains a margin. A total number of four jet vanes will be used since this allows for simultaneous and sequential attitude changes around all three axes. The nozzle exit diameters have been calculated in and are 445 mm, 456 mm and 529 mm, respectively. With the above mentioned assumptions and using the largest diameter to assure an additional margin, the total weight per stage of the tungsten-molybdenum jet vanes turns out to be 6.8 kg.

The complete weight of the jet vane TVC mechanism can be obtained by adding to this the weight of actuator that will control the jet vanes. A suitable actuator that can provide the required control is the IRIS-T made by Sener Aerospace[14]. The IRIS-T is a jet vane control system with a mass and power consumption of 9.5 kg and 436 W, respectively, that allows rotation angles of the jet vanes up to around 38° [33].

ORBIT INSERTION TVC: RCS

The payload must be inserted in the intended orbit with the right attitude and therefore the rocket requires precise attitude control before releasing the payload. To provide this accurate attitude control, a reaction control system (RCS) will be used in the last stage.

The RCS will provide small amounts of thrust by using multiple thrusters, which will provide rotational movement around all three axes. The thrusters will be very small in size, so called vernier thrusters. To allow controlled rotational movement in both directions, each one of the three perpendicular axes needs 4 vernier thrusters. Therefore, a total number of 12 vernier thrusters have to be carried on-board by the last stage that performs the orbit circularisation. A suitable vernier rocket for this particular application is produced by a world-recognised rocket engine manufacturer, Aerojet Rocketdyne. They manufacture the MR-103M mono-propellant vernier rocket engine that can provide 1 N of thrust and which has a mass of 0.16 kg [34]. The MR-103M provides sufficient thrust to significantly change the attitude of the relatively light last stage and has an additional advantage of being lightweight.

For translational orbital manoeuvres however, a more powerful rocket engine is required as the MR-103M does not provide sufficient thrust for that purpose. Therefore, the MR-106E vernier rocket engine will be used which is also produced by Aerojet Rocketdyne. This engine can provide up to 22 N of thrust and weighs 0.52 kg [34]. As the last solid rocket booster will not be dumped, the longitudinal axis of the remaining vehicle is occupied. Therefore, to allow translational motion without rotating the last stage, two of these MR-106E engines will be used. The structural mass of RCS system is roughly obtained by summing up the masses of all rocket engines which gives a mass of 2.96 kg.

[13] https://en.wikipedia.org/wiki/Scud#/media/File:Wz8K14_RB3.jpg
[14] http://www.aerospace.sener/

4.8. TELEMETRY, COMMUNICATIONS, & DATA HANDLING CHARACTERISTICS

To successfully execute guidance, navigation and control and to acquire scientific data for future purposes, it is of utmost importance that the rocket possesses a telemetry and communications (TM&C) subsystem. The TM&C subsystem is responsible for transferring and receiving real time data (such as transferring radar tracking, performance data, stress levels, temperatures, operating environment, etc.) to and from the ground stations by means of antennas. To show that this is possible using particular antennas, this section will be dedicated on proving that the link budget is closed.

The ascent trajectory of the rocket launcher is characterised by extremely high velocities and large attitude changes. As the size and capability of the transmitter antenna that is carried on-board is limited, the use of an on-ground receiver antenna with high capabilities is required. In order to select a suitable receiver antenna, special attention has to be paid to the performance, such as the tracking velocity and the antenna gain-to-noise temperature, and to the applicability with the frequency band that will be used by the rocket. The rocket launcher will operate on the S-band (2 GHz to 4 GHz)[15] which is a commonly used band for commercial purposes. It is assumed that the transmitter used is identical to the one used by the Pegasus which also operates on the S-band and which has a transmitter power of 5 W, a power consumption of roughly 15 W using an efficiency of 30-40% [15] and a frequency of 2.27 MHz [14]. A suitable receiver antenna is the '2.4TSS3-3m S-Band TT&C Antenna System' [35] made by Orbital Systems[16], which has a relatively high tracking velocity of 7 °/s, an atenna gain-to-noise temperature of 14 dB and which operates on a suitable S-band frequency.

To make sure communication is possible at all times during the launch, the critical case is analysed. In the critical case the communication losses are the greatest, which for now is assumed to be the case in which the rocket launcher and the receiver have the greatest separation, i.e. during orbit insertion. In this case the rocket can be assumed to be in an orbit at an altitude of 600 km.

In order to perform the link budget calculation, several parameters have to be estimated. To show that the link budget does close, a MATLAB tool made by Stefano Speretta[17], researcher at the University of Delft, has been used. The tool takes as an input the orbit altitude, frequency of the signal, transmitter gain, transmitter output power, receiver antenna gain-to-noise temperature, bit error rate, required energy per bit to noise power spectral density ratio and finally a link budget margin. The output of the tool is a link budget margin versus the elevation of the vehicle. According to Stefano Speretta, during this phase of the design it can be assumed, that the transmitter gain equals 1 while the bit error rate can be assumed to be 10^{-6}. The assumed bit error rate can be translated to the energy per bit to noise power spectral density ratio (E_b/N_0) depending on the modulation scheme. It is assumed that binary phase shift keying (BPSK) modulation with a code rate (R) of 1/2 is applied (continuous red line in fig. 4.38), which is a commonly used modulation scheme. The relation between the bit error rate and the energy per bit to noise power spectral density ratio is shown in fig. 4.38, from which it can be seen that for a bit error rate of 10^{-6}, the (E_b/N_0) equals approximately 5. Last but not least, it is assumed that the margin on the link budget is 3 dB.

Now that all of the input values for the MATLAB link budget tool are known, the link budget margin can be computed for all elevation angles. The result is depicted in fig. 4.39.

As can be seen in fig. 4.39, the link budget has a positive margin at all elevation angles. This means that if the rocket launcher is within the point of view of the ground station, communication is possi-

[15] http://www.esa.int/Our_Activities/Telecommunications_Integrated_Applications/Satellite_frequency_bands
[16] http://www.orbitalsystems.com/
[17] https://www.tudelft.nl/staff/s.speretta/

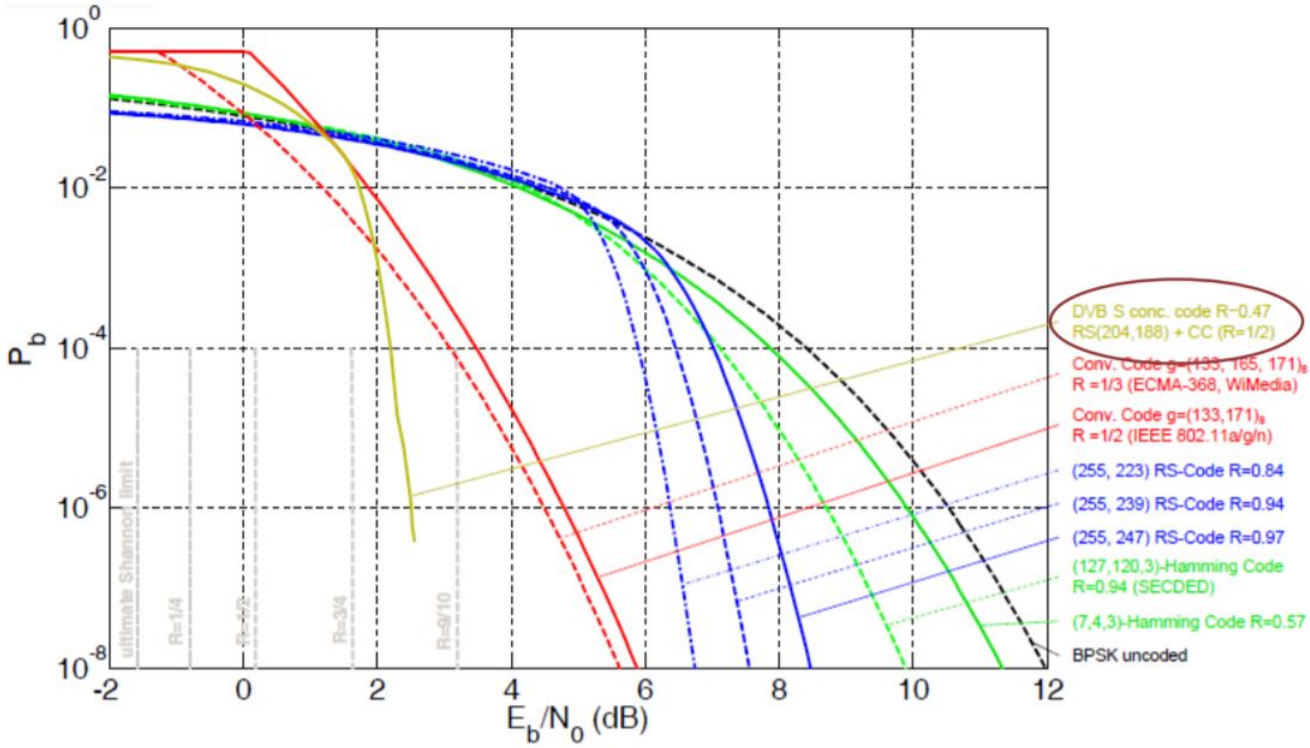

Figure 4.38: Bit error rate vs. the energy per bit to noise power spectral density for the binary phase shift keying modulation [36].

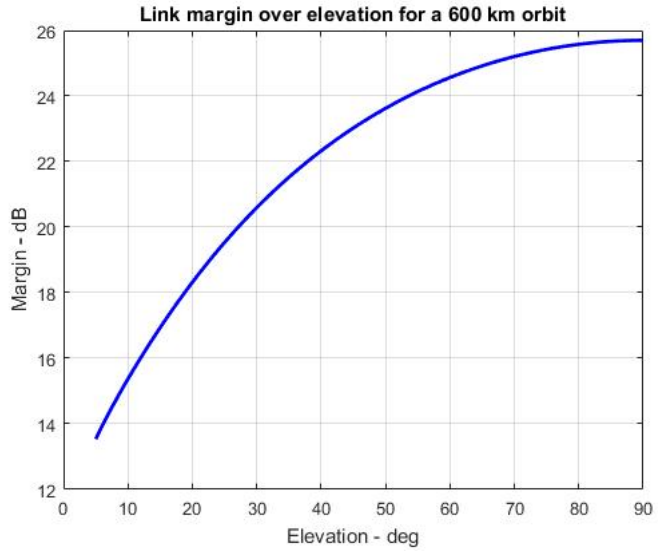

Figure 4.39: The estimated link budget for the launcher vehicle at different elevation angles.

ble at all elevation angles. Therefore, the use of this frequency, the transmitter and receiver antenna is suitable for this mission.

4.8.1. DATA HANDLING

The command and data handling architecture of the launch system is shown as a block diagram in fig. 4.40. It depicts the components of the data handling system as well as how the flow of data between these components.

It is clear that all information in the launch system flows through the avionics units of the Gondola and Rocket segments. It is responsible for processing all data into usable commands for the other subsystems to complete the mission. It is an entirely automated system, and so reliability of the avionics is paramount to mission success.

To increase reliability of the rocket avionics, a backup unit was incorporated into the design, making it a dual redundant system. As the gondola avionics are less critical to the success of the mission than the rocket avionics, no backup unit was included in the gondola segment. To increase simplicity, all of the avionics units are the same.

The avionics unit selected for the ALTAR launch system is the *C&DH Avionics Unit* from MOOG Incorporated. This unit is specifically design for space applications. Each unit has a mass of **3 kg**, a power consumption of **25 W**, and an input Voltage of **28 V**.[18]

4.9. ELECTRICAL POWER SUBSYSTEM CHARACTERISTICS

The design and architecture for the electrical power subsystem of the ALTAR launch system is discussed in this section. An overview of the power distribution and the interactions between the components is depicted in fig. 4.41. A power budget including all of the relevant components is presented in table 4.17. The power source for the launch system is explained and its specifications listed in table 4.18.

4.9.1. POWER DISTRIBUTION

The electrical power subsystem is separated into the Gondola and Rocket segments which are linked together through the Power & Data Umbilical. This umbilical runs down the length of the of the rocket connecting the first and second stages with the avionics and power supply housed in the third stage bus. Additionally it also connects with the interface attachment point linking the gondola and rocket power systems together.

More than a simple link, the umbilical serves as an auxiliary power supply line from the gondola up until separation at the interface where the Rocket transfers to internal power. The Rocket is powered in its nominal state with the Avionics, Telemetry Receiver/Transmitter (RX/TX), Flight Termination RX/TX, Navigation sensors, and Payload Power operating. This state is the peak power consumption of the Gondola segment power supply. It will be powered in this state for the initial ascent time of 121 min stated in section 4.2, and the loiter time before the launch window of 60 min. The Rocket segment experiences peak power consumption during operation of the TVC actuators for the first two stages, each with a burn time of 47.8 s.

During the initial ascent and loiter phases the Flight Termination subsystem will have redundancy

[18] Component specifications obtained from data sheet on the manufacturer website: http://www.moog.com/products/avionics-software-gnc.html

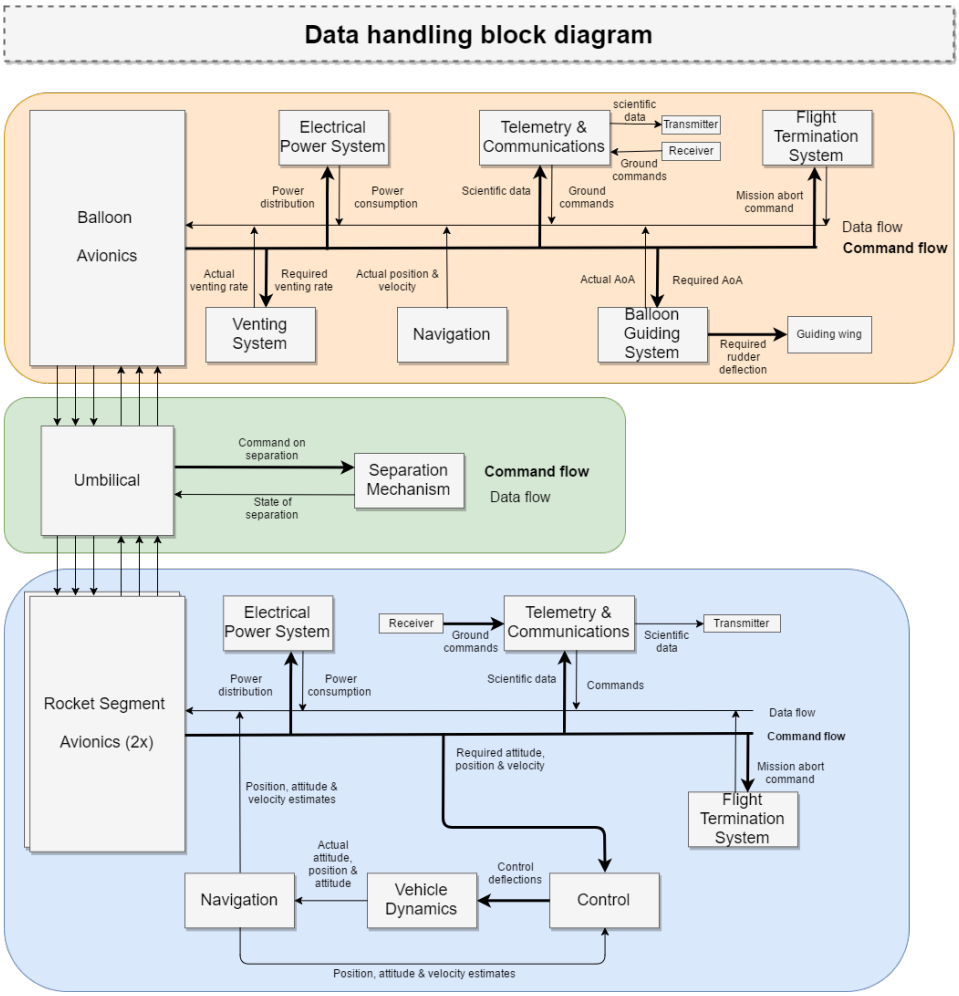

Figure 4.40: Data handling block diagram, which represents interconnection between the systems of the launcher.

with both the Gondola and Rocket segments operating the RX/TX units. The Gondola segment turns off the Flight Termination RX/TX unit after separation of the Rocket. Likewise, the Rocket segment turns off the Flight Termination RX/TX unit once making orbit after the third stage burn at 246.2 s post launch.

As an additional feature, a power line to the payload was added in the event a customer wishes to operate the satellite during the launch. The power load was determined by taking the nominal load of a 3U cube-sat of 7 W times the payload capacity of roughly 9 3U cube-sats [37]. This results in total power slightly over 50 W total power, however, it is unlikely these satellites will be operating in a nominal condition, thus 50 W seemed more than reasonable. The payload is supplied power all the way until separation from the stage 3 bus, it was assumed that this would occur at the worst case a full orbit after circularisation, approximately 2.5 hour after launch of the rocket.

The feed system of the rocket is only operational when propellant is needed, that is for the total burn times of the OMS and RCS thrusters which is 486.5 s and 519.6 s, respectively. The feed system of the gondola is operated only when its thrusters are operating which is in the worst case 6 min, as stated in section 4.3.2.

The other components on board the rocket operate continuously throughout the mission. These include the Avionics units, Telemetry RX/TX, Navigation Sensors, and miscellaneous components. It is assumed that the maximum expected operating time for the vehicle is to be 2 orbits plus launch and deorbit, in total 4.9 h. Similarly, the Gondola has it's Avionics, Telemetry RX/TX, Navigation Sensors, and miscellaneous components operating continuously throughout its mission. Additionally, in the descent phase, which takes approximately 120 min, it is assumed that the vent actuators operate the entire duration.

4.9.2. POWER BUDGET

The power budget for the ALTAR Launch system is presented in table 4.17. In this table, for each component, the peak power consumption, operational time, and total energy is shown. To calculate the required energy it was assumed that the component operated at peak consumption for the duration of its operation. This was done due of the lack of information available from the component manufacturers as they only specify a peak power consumption. It was thought that assuming a nominal value with no evidence was less valid than using the peak value, therefore the power sources are likely to be over estimated in this design.

In addition to the main components, there are smaller components which either have a low continuous power consumption like telemetry sensors placed throughout the vehicle, or a high finite power consumption like the igniters of the solid motors. Due to the lack of information available for these smaller miscellaneous components, it was assumed that collectively they contribute 5% of the nominal peak power and 5% of the nominal total energy for the gondola and rocket segments.

Furthermore, not all components run on the same type of power, some require different input voltage levels. This necessitates transformation in order to match the component requirements which causes a reduction in supplied power from conversion efficiency. Additionally, there is power lost from transmission efficiency due to the conductor resistance. The losses are difficult to predict without more detailed specification on the components and conducting wire resistances. Therefore, these factors are included into an overall contingency factor of 20% on the peak power, and 20% on the total energy.

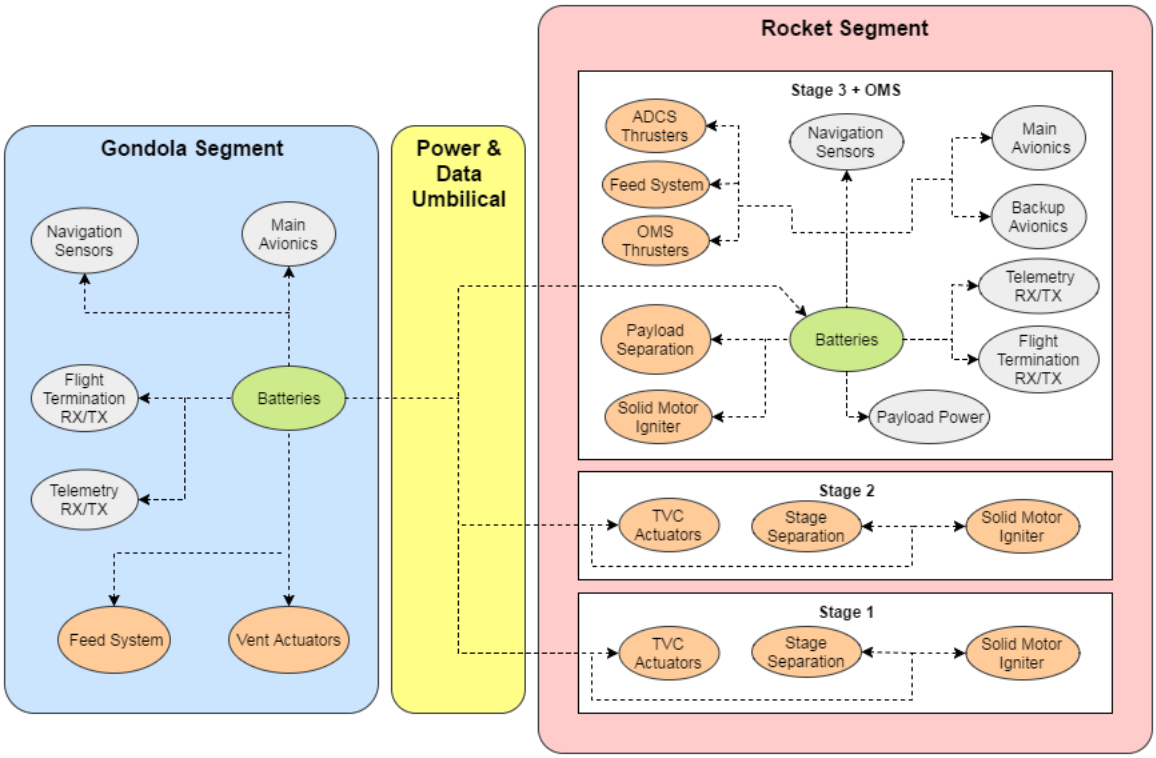

Figure 4.41: A Block Diagram Depicting the Flow of the Electrical Power in the System. Green blocks represent power sources, Orange blocks represent mechanical components, Grey blocks represent electrical components.

Table 4.17: Power Budget for the Electrical Power Subsystem

Component	Peak Power (W)	Operational Time	Total Energy (Wh)
Rocket Segment			
Main Avionics	25.0	4.9 h	123.0
Backup Avionics	25.0	4.9 h	123.0
Telemetry RX/TX	15.0	4.9 h	73.8
Flight Termination RX/TX	400.0	246.2 s	27.4
Navigation Sensors	25.0	4.9 h	123.0
Payload Power	50.0	2.5 h	124.7
Feed System	13.5	1006.1 s	3.8
OMS Thrusters	49.2	486.5 s	13.3
RCS Thrusters	10.9	519.6 s	3.1
TVC (Stage 2)	436.0	47.8 s	5.8
TVC (Stage 1)	436.0	47.8 s	5.8
Misc. (5%)	48.7	4.9 h	33.0
Contingency (20%)	243.7	*N/A*	164.9
Total Required	1218.4	*N/A*	824.3
Gondola Segment			
Rocket Power Umbilical	588.7	181 min	1778.0
Main Avionics	25.0	301 min	251.0
Telemetry RX/TX	2.0	301 min	9.5
Flight Termination RX/TX	400.0	121 min	1208.0
Navigation Sensors	0.3	121 min	1.5
Vent Actuators	0.7	120 min	1.4
Feed System	13.5	6 min	1.4
Misc. (5%)	54.2	181 min	171.1
Contingency (20%)	270.9	*N/A*	855.5
Total Required	1354.5	*N/A*	4277.3

Table 4.18: Power Source Specifications

Power Source	Power Available	Energy Available	Total Rails	Total Cells	Total Mass
Rocket	1736.6 W	881.3 Wh	9	72	3.492 kg
Gondola	8490.2 W	4304.5 Wh	44	352	17.072 kg

4.9.3. POWER SOURCE

The power source chosen for both the Gondola and the Rocket segments is a lithium ion battery system. This was chosen due to the greater energy density relative to fuel cells and other battery technologies. A lithium ion battery is composed of smaller individual cells configured to meet the voltage and current requirements. The cell used for the battery systems of the gondola and rocket segments is the Panasonic NCR18650B lithium-ion cell. It has an operating voltage of 3.6 V, a maximum current of 6.7 A, a rated capacity of 12.6 W·h, and a per unit mass of 48.5 g.[19].

The configuration of batteries is derived from the maximum power consumption, total required energy, and operating voltage. The operating voltage of the battery was selected to be same as the Avionics unit for increased reliability, that is 28.8 V. This means that one 28.8 V rail of the battery requires 8 cells placed in series. The number of rails is determined by both the power throughput requirement or the total energy requirement, fro both segments the limiting factor was energy storage. A summary of the battery specification for the Rocket and Gondola segments is presented in table 4.18.

4.10. RECOVERY SUBSYSTEM CHARACTERISTICS

The recovery subsystem is one of the essential parts of the design because it allows the safe recovery of the balloon and the components which are connected to it. Therefore, parts such as the balloon film, load tapes, ropes, gondola, communication system and other electronics can be used for multiple missions. Not only it will lead to the reduction in cost, but it will also improve sustainability of the launch.

This section describes methods used to recover the balloon and the on-board equipment after the rocket has been released. The recovery system composition is reported in section 4.10.1. The discussion on the balloon guidance system performance can be found in section 4.10.2 and the recovery strategies are described in section 4.10.3.

4.10.1. RECOVERY SUBSYSTEM DESCRIPTION

In order to avoid the balloon descending in a densely populated area and to allow for the choice of the landing location, there should be a method to steer the balloon in the desired direction. Therefore, there is a need for a control system which can increase the flexibility of balloon operations.

At the floating altitude of 40 km air density is low $\left(0.0038\,\mathrm{kg/m^3}\right)$ and thus it is not effective to use aerodynamic forces at this altitude to control the balloon. As a solution to the controllability of a stratospheric balloon, Knock et Al. propose a balloon guidance system (*BGS*), which exploits the natural wind-field variation with the altitude in order to generate control forces on a balloon [38]. This is done by using a tether-deployed lifting body below the balloon.

[19] Obtained from Data sheet found at http://www.panasonic.com/industrial/batteries-oem

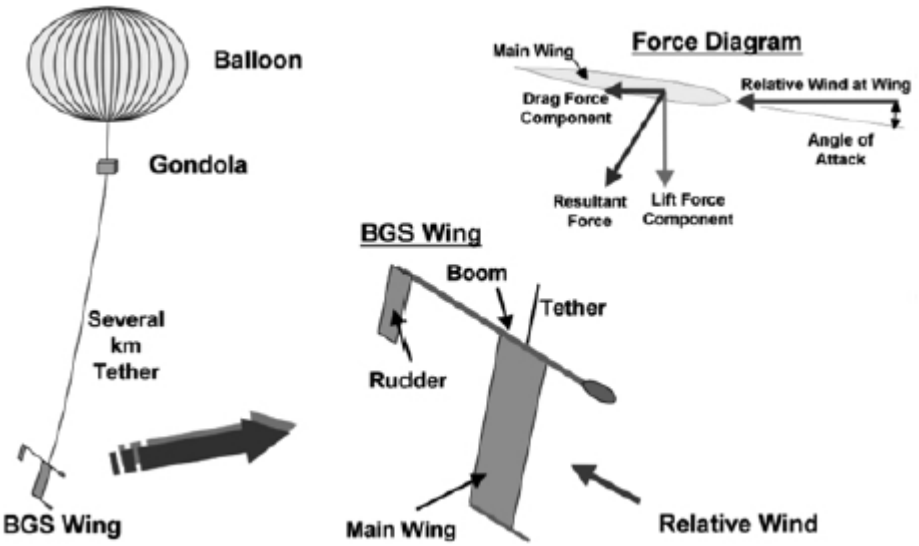

Figure 4.42: Principle of operation of single-wing balloon guidance system [38].

The main components of the balloon guidance system are a controller, mechanical devices for deployment and termination, the main-wing, the rudder and rudder actuator, the boom and the tether. A compete overview of the BGS is shown in fig. 4.42. The wing is attached to the balloon by a 20 km light-weight tether and hangs vertically beneath the balloon at the 20 km altitude. Due to the higher-density air at 20 km, the horizontal lift force generated by the wing can alter the balloon flight path and its velocity. Moreover, the rudder controls its angle of attack and is able to keep the wing at its maximum lift coefficient.

The NACA0015 airfoil is used for the BGS wing and has a $C_{L_{max}}$ value of 1.4. The other characteristic parameters are an Oswald efficiency factor of $e = 0.6$, a drag coefficient at zero AOA of $C_{D_0} = 0.08$, a wing span ($b = 5.5$ m), a chord ($c = 1.1$ m) and a wing aspect ratio ($A = 5$). A tether is made out of Zylon, has diameter (d_{tet}) of 1 mm, sufficient to withstand weight of the BGS system, length (l_{tet}) of 20 km and tether drag coefficient($C_{D_{thether}}$) of 1 [38]. The material properties of Zylon are given in table 4.5. These properties are used to estimate the mass of the tether. The total mass of BGS is estimated as 142 kg, including the mass of all the sub-components.

Furthermore, the production cost has been estimated for the BGS system. The average production price per kilo, as stated by Markish [39], has been used for price estimation of the wing and rudder. The price of zylon[20] has been used to estimate price of the tether. Assuming that rest of the components cost 1285 €, the total BGS system cost is 200 000 €. The power required to move the rudder is 0.71 W. This value has been estimated using the power formula $P = F \cdot V$.

4.10.2. RECOVERY SUBSYSTEM PERFORMANCE

The recovery subsystem performance is determined for the worst-case scenario, or the situation when the direction of the winds at the balloon float altitude and at the guidance system float altitude are blowing in the same direction. Such condition would lead to the smallest possible change in the direction of the balloon flight path under the action of BGS. Therefore, this analysis aims to enable the launch system recovery under any unexpected circumstances.

First of all, the resultant force acting on the BGS has been determined. It is assumed that this force

[20] http://www.mse.mtu.edu/~drjohn/my4150/compositesdesign/props.html

Table 4.19: The value of the atmospheric parameters

	Symbol	Value	Unit
Air density at balloon float altitude	ρ_{40}	0.00385	kg/m^3
Air density at BGS float altitude	ρ_{20}	0.0889	kg/m^3
Wind speed at balloon float altitude	V_{40}	30	m/s
Wind speed at BGS float altitude	V_{20}	5	m/s

is translated from the wing and tether directly to the balloon. As it can be seen from eq. (4.52), the resultant force is calculated as combination of the systems lift and drag force components. The total drag is determined as $D_{sys} = D_{wing} + D_{tether}$. All of the parameters that are used in the eqs. (4.53) to (4.55) can be found in section 4.10.1. The atmospheric parameters are shown in table 4.19.

$$F_{control} = \sqrt{L_{wing}^2 + D_{sys}^2} \tag{4.52}$$

The lift and drag forces of the BGS wing are calculated using eq. (4.53). The velocity applied to the wing is relative, and therefore is computed as $V_{rel} = V_{40} - V_{20}$. The maximum value of the lift coefficient is used to determine the biggest achievable control force. The drag coefficient of the wing is calculated using eq. (4.54).

$$L_{wing} = C_{L_{max}} \cdot \frac{1}{2} \cdot \rho_{20} \cdot V_{rel}^2 \cdot S \qquad D_{wing} = C_{D_{wing}} \cdot \frac{1}{2} \cdot \rho_{20} \cdot V_{rel}^2 \cdot S \tag{4.53}$$

$$C_{D_{wing}} = C_{D_0} + \frac{C_{L_{max}}^2}{\pi \cdot A \cdot e} \tag{4.54}$$

As the tether is spread over 20 km, an average value is taken for the air density and the relative velocity in order to approximate the drag force. The tether drag is calculated using eq. (4.55).

$$D_{tether} = C_{D_{tether}} \cdot \frac{1}{2} \cdot \frac{\rho_{40} + \rho_{20}}{2} \cdot \frac{V_{rel}}{2}^2 \cdot l_{tether} \cdot d_{tether} \tag{4.55}$$

Now that all of the parameters have been estimated, the total control force acting on the balloon due to the guidance system is calculated to be equal to 264.5 N. The control velocity of the balloon due to BGS is determined using eq. (4.57), as suggested by Knock et Al. [38]. In this equation A_B is the cross-sectional area of the balloon calculated as shown in eq. (4.56) and $C_{D_B} = 0.2$ is the balloon drag coefficient.

$$A_B = \pi \cdot R_B^2 \tag{4.56}$$

$$V_{control} = \sqrt{\frac{2 \cdot F_{control}}{\rho_{40} \cdot A_B \cdot C_{D_B}}} \tag{4.57}$$

From eq. (4.57), the control velocity results to be equal to 8.52 m/s. In order to check feasibility of BGS, the time needed to reach equilibrium of the full system is calculated. Acceleration due to the force is calculated as shown in the first equation of eq. (4.58) and equals to 2.9 m/s^2. Therefore, the time needed to reach the control velocity is calculated using the second equation in eq. (4.58) and

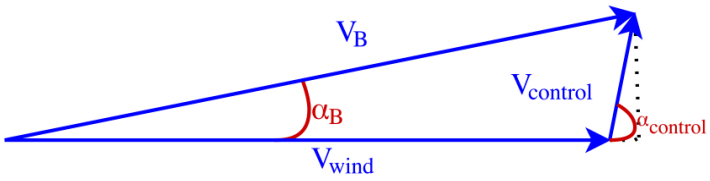

Figure 4.43: The figure shows the velocity vector components that are acting on the balloon.

equals to 2.4 min. This value is quite small in comparison with the overall mission duration, and therefore can be neglected.

$$a = \frac{F_{control}}{m_B} \qquad t_{control} = \frac{V_{control}}{a} \tag{4.58}$$

The next step is to compute the maximum change of the balloon flight path direction. The velocity vectors and angles in between them can be found in fig. 4.43. Angle of the control velocity acting on the balloon is calculated using eq. (4.59). It is assumed that initially the balloon is moving with the wind velocity. The deviation of balloon from original trajectory is calculated using the geometry, as shown in eq. (4.60).

$$\alpha_{control} = \arctan \frac{L}{D_{sys}} \tag{4.59}$$

$$\alpha_B = \arctan\left(\frac{V_{control} \cdot \sin(\alpha_{control})}{V_{38.7} + V_{control} \cdot \cos(\alpha_{control})}\right) \tag{4.60}$$

The calculation results in α_B of 12.6°. Furthermore, the velocity of the balloon under action of the guidance system is determined with eq. (4.61) and equals to 34.7 m/s.

$$V_B = \frac{V_{control} \cdot \sin(\alpha_{control})}{\sin(\alpha_B)} \tag{4.61}$$

4.10.3. RECOVERY STRATEGY

Since the control system of balloon is highly dependent on the wind, all possible landing locations must be found. Mainly, it can be divided into two main landing conditions: landing on the sea and on the ground. While landing at the sea would not require a specific landing location, it is not the case for the ground landing. As it is not possible to accurately predict the wind direction, it has to be ensured that there are going to be enough clean spots or "platforms" to land the balloon after the mission accomplishment.

From the ALTAR-BAL-01 requirement which can be found in section 5.9, it follows that the maximum distance from the balloon launch site to the landing spot should not exceed 200 km. This total distance (d_{total}) can be separated into two sections: uncontrolled drift until the rocket launch (d_{drift}) and controlled descent ($d_{control}$).

Illustration of the angles and lengths used for the recovery strategy calculations can be found in fig. 4.44. The maximum angle in between the landing platforms is calculated using eq. (4.62). Furthermore, eq. (4.63) is used in order to determine the minimal number of the landing platforms.

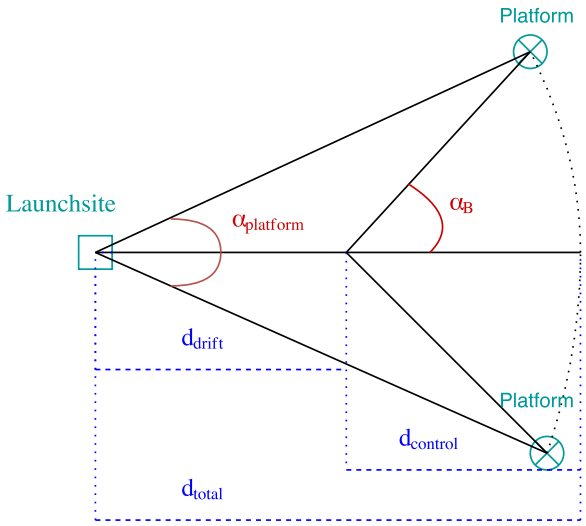

Figure 4.44: Illustration of the recovery strategy of the ground landing

$$\alpha_{platform} = 2 \cdot \left[\alpha_B - \arcsin\left(\frac{d_{drift} \cdot \sin(\pi - \alpha_B)}{d_{total}} \right) \right] \tag{4.62}$$

$$N_{platform} = \frac{2\pi}{\alpha_{platform}} \tag{4.63}$$

The analysis has resulted in a minimum amount of 29 possible landing spots spread out at a equal distance of 43.25 km from each other, and at the equal distance of 200 km from the balloon launch site. If this condition is satisfied, it is possible to safely land and recover the balloon under any weather condition. It has to be noted that even though the amount of platforms is quite high, they can be as simple as a small empty field.

The maximum distance the balloon will cover from the rocket launch to the landing and the time it will take are calculated with eq. (4.64) and eq. (4.65), respectively.

$$d_{platform} = \frac{\sin\left(\frac{\alpha_{platform}}{2}\right) \cdot d_{total}}{\sin(\alpha_B)} \tag{4.64}$$

$$t_{control} = \frac{d_{platform}}{V_B} \tag{4.65}$$

It was determined, that it will take 48.6 min for the balloon to arrive at one of the platforms. Even though the descent process is going to be initiated before balloon is going to reach the landing spot, some additional time is going to be required to complete the landing. This is due to the reason that wind velocity will start to drop with the descent. Additionally, the balloon is not going to be fully inflated anymore and therefore wind will not accelerate it as much as previously. Due to mentioned reasons the total descend time is going to be approximately 2 h.

Exhaust vent is an important structural part of the zero-pressure balloon. After the balloon has reached its maximum volume, any further expansion of the lifting gas will lead to the opening of the venting hole. This will cause overflow of the additional gas and therefore prevent the build up

of pressure inside of the balloon film. The venting duct is going to be attached along the envelope, with the opening valve located at the bottom of the balloon. In this way, whenever pressure at the base will exceed the outside pressure, the duct is going to be pushed from inside allowing for smooth flow of the lifting gas through it. Six exhaust vents are going to be used for the mission. Such configuration would enable efficient control of the internal pressure and prevent the structural failure after the payload release. Additionally, an exhaust valve is going to be installed on upper part of the balloon in order to begin the descent by controllable release of the lifting gas.

A shock-absorbing device is going to be installed on the bottom of gondola to protect the equipment from the landing shock. A lightweight honeycomb construction would perform well for this purpose.

4.11. FLIGHT TERMINATION SUBSYSTEM CHARACTERISTICS

Complex space-related engineering designs always bring along the possibility of having one or multiple sub-system failures, which might impose danger to the environment. To prevent such event, a flight termination system (FTS) must be designed that is able to terminate the flight to prevent any harm to anyone at any moment. The flight termination strategies in case of the rocket or balloon failure are described in section 4.11.1 and section 4.11.2, respectively.

4.11.1. ROCKET FAILURE

A rocket failure can occur at different times during the launch: after the rocket engines has been ignited or prior to igniting of the rocket engine. In the first scenario, the rocket would have to be exploded on command in order to prevent serious damage to anyone. The rocket launcher will be equipped with a FTS that continuously receives and sends a high power signal from and to the ground station through the uplink and downlink, respectively. In the same fashion as most rocket launchers, including the Falcon 9 and the Pegasus, the FTS includes a tracking transmitter and receiver [14, 40]. It is assumed that the tracking transmitter is identical to the one used by the Pegasus which operates on the C-band (4 GHz to 8 GHz)[21], has a power output of 400 W and a frequency of 5765 MHz. The tracking receiver also operates on the C-band and has a slightly lower frequency of 5690 MHz. As the tracking receiver is only receiving a high power signal, the power consumed is negligible. A possible ground station antenna for the tracking is the high-performance AL-1100-LSC [41], made by Orbit[22], that can operate on the C-band. The ground station and the launch vehicle will continuously communicate back and forth, and if they succeed to do so, the FTS will not terminate the flight. If one of these communication links fails for a small predetermined time window, the automated FTS will terminate the ascent by shutting down the propulsion system and by setting off charges that combust all the propellant carried on-board. Active termination of the ascent is achieved by the range safety officer in case it is observed that the rocket is (going to be) outside the safety zone. Lastly, the FTS will be operating independently of the avionics system to assure that it can terminate the ascent in case of an avionics failure.

If the rocket has not yet been launched and is still hanging under the balloon, it is still possible to safely retrieve the payload. As landing the rocket itself would be too dangerous for the surrounding environment due to the risk of explosion, the payload would be separated from the rocket and attached to the gondola. Meanwhile, the rocket would be released and manually commanded to self-explode by a signal from the ground. Afterwards, the stratospheric balloon would descend and bring the payload to the ground with the methods described in section 4.10.

[21] http://www.esa.int/Our_Activities/Telecommunications_Integrated_Applications/Satellite_frequency_bands
[22] http://orbit-cs.com/

Table 4.20: Input of eq. (4.66).

Input	Symbol	Value	Unit
Surface area of the canopy	S_0	440	m^2
Specific mass of the canopy	w_c	0.056	kg/m^2
Number of suspension lines	N_{SL}	68	-
Length of suspension lines	L_S	19.3	m
Specific mass of suspension lines	w_{SL}	0.049	m^{-1}
Strength of suspension lines	F_{SL}	130 [42]	kg

4.11.2. BALLOON FAILURE

In case of a balloon failure, the gondola and payload are to be recovered with a use of parachute. The preliminary size of the parachute has to be estimated in order to make sure that it is capable of lifting an extra 827.3 kg that have to account for the mass of the recovery system, gondola and suspending ropes. The material used for the parachute is Kevlar and the mass of the parachute can be calculated using eq. (4.66), all of the inputs to which can be seen in table 4.20 [42]. The production cost of the parachute is estimated as €11333 based on the National 360 Back Parachute model [23].

$$M_{para} = S_0 \cdot w_c + N_{SL} \cdot L_S \cdot w_{SL} \cdot \frac{F_{SL}}{1000} = 27.7\,\text{kg} \tag{4.66}$$

4.12. STRUCTURES & MATERIALS CHARACTERISTICS

In this section, the structural analysis and design of the rocket is presented. In section 4.12.1 the design of the various structural components is performed, making use of basic structural sizing equations which are governed by the mission critical loads. Then, in section 4.12.2, a FEM analysis is performed on the preliminary design to validate the obtained analytical results. Next, in order to chose an appropriate material, a brief analysis is performed in section 4.12.3. At this point, the structure's response to the vibration loads occurring during flight is studied in section 4.12.4.

4.12.1. PRELIMINARY SIZING

For the preliminary sizing, three static failure modes will be analysed: Buckling failure due to inertial loads, hoop failure due to internal pressure of the component and thermal failure. This will allow to size the structure and to calculate the structural mass of each component and of the thermal coating needed. Also, Aluminium 7075-T6 will be used as a first approximation for the sizing of all structural load components (everything except the payload fairing, since the drag loads are almost negligible). A more detailed material analysis will be explained in section 4.12.3. This aluminium has a yield stress of 503 MPa, an ultimate stress of 572 MPa, a modulus of elasticity of 71.7 GPa, a density of 2810 kg/m^3 and a melting temperature of 477 °C.

PROPELLANT TANKS

For the solid propellant tanks of the three stages, a pill-shape without the bottom spherical cap will be assumed. These tanks will be subjected to a internal pressure of 3.5 MPa, an assumed outside pressure of 0 MPa and to a vertical acceleration of 6.9g's. Therefore, they will not only take the loads

[23] http://www.nationalparachute.com/page8.html

due to the pressure difference, but also they will maintain structural integrity for the rest of the loads the rocket will be exposed to. Also, a thermal liner capable of maintaining the temperature of Aluminium down and therefore its structural integrity will be integrated. This coating will be sized in section 4.12.1. The following formulae will be used to calculate the required thickness for the cylindrical part [43].

$$\sigma_{hoop} = \frac{\sigma_{yield}}{2} = p_c \frac{R}{t} \tag{4.67}$$

$$\sigma_{actual} < \sigma_{critical}\ ; \qquad \frac{P_{actual}}{A} = \frac{a_{max} M_{top}}{2\pi R t} < 9E\left(\frac{t}{R}\right)^{1.6} + 0.16E\left(\frac{t}{L}\right)^{1.3} \tag{4.68}$$

The hoop stress in the cylinder is represented by eq. (4.67). In this equation, p_c is the combustion chamber pressure, R the radius and L the height of each stage. For this loading case, the selected safety factor will be 2 [43].

Equation 4.68 represents the critical buckling stress of a hollow cylinder. The critical buckling stress $\sigma_{critical}$ has to be higher than the actual axial stress σ_{actual}, dependant on the maximum acceleration of the launcher (6.9g´s), the mass lumped on top of the cylinder and the radius and thickness.

In order to calculate the required thickness due to the applied loads, eq. (4.67) will be directly applied with the aforementioned safety factor of 2 and eq. (4.68) will be iterated, increasing the thickness in each iteration , until this calculated critical buckling stress becomes bigger than the applied stress times the selected safety factor for buckling of 1.5 [43]. The required thickness of each tank´s casing cylindrical part will be the highest of the required either due to buckling or to pressure, since an isotropic material was chosen.

For the spherical end caps, the hoop stress is half the hoop stress for the cylindrical part [43]. Since these components will not take any longitudinal loads that might cause buckling, the hoop stress will dictate the thickness of the cap, which will be half of the cylinder as shown in table 4.21

The required thickness for both the top spherical end and the cylindrical part are shown in table 4.21 with the smallest one being that of the spherical end.

To calculate the total mass of each tank, the following relationship will be used and the results can be found in table 4.21.

$$M_{tank} = M_{cylinder} + M_{sphericalend} = 2\pi R t \rho L + 2\pi R^2 \frac{t}{2} \rho \tag{4.69}$$

After calculating the thicknesses and masses analytically, the parts could be designed in CATIA, paying attention to the merges between the cylindrical and spherical parts. These models allowed production of a more accurate weight estimation of the structure. An example of the CAD drawing of the first stage propellant tank is shown in fig. 4.45.

INTERSTAGES

A similar procedure will be used to analyse the interstages. The interstages will be assumed to be hollow cylinders. Also, it will be assumed that they will not be pressurised and therefore, the critical load case will be buckling. As explained before, the maximum acceleration and mass lumped on top of each interstage will dictate the applied load which might cause buckling failure. Using eq. (4.68), with an L calculated with the required length of the nozzle plus the spherical end of the

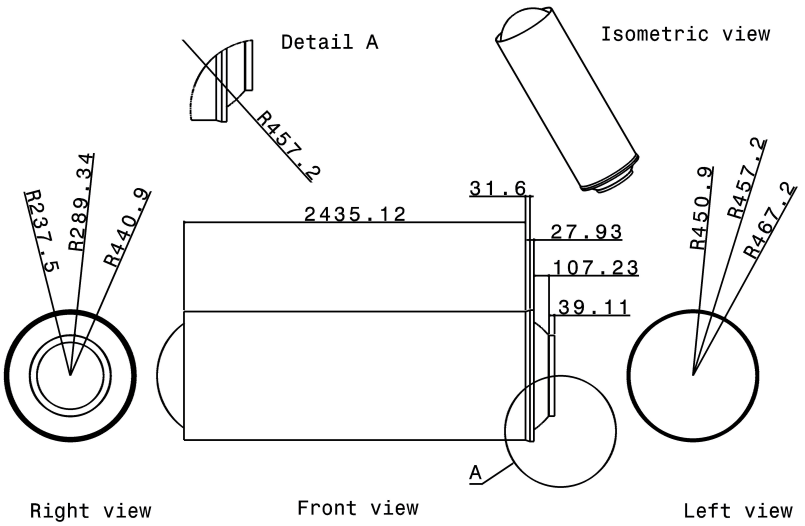

Figure 4.45: CAD drawing of the first stage

propellant tank of the previous stage and R being the same radius of the cylinder and the first term of eq. (4.69), the required thickness and mass of each interstage can be calculated. These are shown in table 4.21.

INSULATOR MASSES

The thermal liner of a solid motor is what separates the grain (propellant) from the engine casing and it works based on the principle of ablation. Hot gases, product of the combustion of the propellant, react with the insulating material which ablates and forms a layer of char on its surface. This way, the material below the char is prevented from burning due to its very low heat conductivity [17].

For the preliminary sizing of the insulating material, a correlation derived from data of solid motors, which use silica-loaded EPDM (ethylene propylene diene monomer) insulation, is used as taken from a space propulsion design book [17].

$$m_{insul} = 1.778 \cdot 10^{-9} \cdot m_{prop}^{-1.33} \cdot t_b^{0.965} \cdot \frac{L}{D}^{0.144} \cdot L_{sub}^{0.058} \cdot A_w^{2.69} [\text{kg}] \tag{4.70}$$

In eq. (4.70), m_{insul} is the mass of the insulating material, m_{prop} is the propellant mass per stage, t_b is the burn time, L is the length of the motor, D is its diameter, L_{sub} is the length of the submerged part of the nozzle into the combustion chamber and A_w is the surface of the motor exposed to the hot gases. Assuming L_w to be equal to 0.05, A_w to be equal to the total surface of the combustion chamber (top spherical cap and cylindrical section), eq. (4.70) is used to calculate the mass of the insulating material of each stage. The results are presented in table 4.21, where the thickness of the insulator is assumed to be constant in the whole motor. This mass estimation is verified by looking at comparable sized solid engines for space application taken from an extensive data sheet found in Space Propulsion Analysis and Design [17]. From there, it can be seen that solid engines with a propellant mass between 2010 kg and 3250 kg have insulator masses ranging from 27.1 kg to 75.6 kg. The insulator mass estimated for the first stage of the launcher (propellant mass of 2221.0 kg) is

equal to 36.4 kg and it then falls between the aforementioned range. To conclude, a margin of 15% is applied to the insulator masses, according to the uncertainties associated with eq. (4.70) [17].

PAYLOAD FAIRING

Finally, for the fairing, due to the high release altitude, the aerodynamic forces acting on the fairing will be almost negligible (approx 600N). This allows for a lighter and less constrained design of the fairing. As shown in fig. 4.46, the shape will consist of three parts: The first, increasing the radius of the rocket to accommodate the payload, the second one, cylindrical, which increases the allowed payload volume and the third one, conical, which encloses the payload to prevent damaging it and reduces the already low drag. The fairing will be made of High-density polyethylene (HDPE), a material with a high strength-to-density ratio. HDPE has a density of 958 kg/m^3, a yield strength of 26 MPa and a modulus of elasticity of 0.9 GPa. The disadvantage of using this material is the low yield stress that might cause some deformations, for which some reinforcement might need to be added. Following the same procedure as for the interstages and applying a point load of 600N on the tip, the required thickness and mass were calculated by designing it in CATIA. The results are shown in table 4.21.

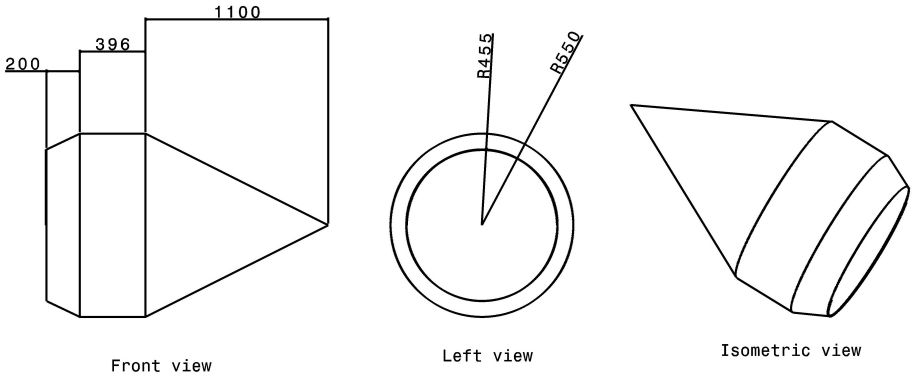

Figure 4.46: CAD drawing of the fairing

STAGE SEPARATION

For the stage separation there are three options: Use of pyrotechnics, spring based separation or hot staging. Spring based was deemed inefficient as these systems can get rather heavy relative to the other two options. Furthermore, spring based separations main advantage is that it gives a much "smoother" shock. Using pyrotechnic charges to push away the stages after burn-out would increase the weight with respect to hot staging and thus hot staging is deemed the best option. This would however require a way for the exhaust gases to escape while the inter-stage is still in place. A possible option would be open inter-stages as used by the Soyuz. The mechanical link between the burnt-out stages and the inter-stages is separated using frangible nuts and NASA Standard Detonators (NSDs), which both have been used in many rockets and are deemed very reliable.

4.12.2. FEM ANALYSIS

Once the preliminary sizing of each component was performed, it was possible to design the components in CATIA and perform a Finite Element Method (FEM) analysis using ANSYS. This FEM analysis was performed with the purpose of verifying the results obtained with the analytical method

Table 4.21: Analytically calculated structure and coating masses for each component of the rocket

Nº Stage	**Radius (m)**	**Length (m)**	**Thickness req. (mm)**	**Structure mass (kg)**	**Insulator avg. thickness (mm)**	**Insulator mass (kg)**
1st stage	0.46	1.19	3.13–6.27	70.46	0.96	7.55
1st interstage	0.46	1.275	1.17	11.83	–	–
2nd stage	0.46	0.61	3.13–6.27	41.85	1.44	7.367
2nd interstage	0.46–0.28	0.625	0.75	3.70	–	–
3rd stage	0.28	0.895	1.94–3.9	19.73	8.61	28.94
3rd interstage	0.28–0.4	1.12	0.46	3.67	–	–
Fairing	0.4–0.55	1.695	5.0	20.03	–	–
Total	**–**		**–**	**171.27**	**–**	**43.87**

and to obtain more accurate results on the joints between the different thicknesses, such as the joint between the cylindrical part of the propellant stages and the end spherical cap. With the results obtained from the FEM analysis, these discrepancies will be checked and an iteration on the preliminary design will be performed, if necessary. An example of the results of the FEM analysis is shown in fig. 4.47. FEM analysis was performed on the stages, interstages and the payload fairing. It was not performed on the OMS due to the complexity to model this geometry.

For the FEM analysis, the mesh size to be adaptive due to the complexity of the parts which would create inconsistencies and non convergent solutions otherwise. Each part that was analysed was assumed to be clamped at the bottom face. Each propellant casing will be assumed to be loaded with the aforementioned inside pressure of 3.5 MPa and with a distributed load equal to the mass lumped on top of each stage times the maximum acceleration of 6.9g´s. Each interstage was assumed to have a distributed load equal to the mass lumped on top times the maximum acceleration of 6.9g´s.

DISCREPANCIES ANALYSIS

As shown in table 4.22, there are substantial discrepancies between the analytical results and the numerical results obtained with ANSYS that need to be addressed. As shown, while the pressure stage loads seem to be underestimated, the buckling loads in the interstages seem to be overestimated. Some of the causes that might cause these discrepancies are:

1. The difference between the geometry of the simplified analytical model and the CATIA model that allows to perform the FEM. Even though the general geometry is similar, the edges and transitions between components are not taken into account when calculating it analytically.

2. A second possible source of discrepancies are the inputs selected during the FEM analysis. These are the mesh size and the clamped edge. The mesh size was chosen to be adaptive with a low resolution due to the computational budget available. A more detailed mesh convergence study should be performed in the future. As mentioned before, the clamped edge was always selected to be the bottom edge of each component for simplification purposes, which might cause the results close to the clamped edge to be inaccurate.

3. More possible sources of errors can be the assumptions used in the analytical expressions, explained in [43], which might have caused to underestimate the loads for the case of the pressure loads in the propellant tanks, and overestimate them for the buckling of the interstages.

Table 4.22: Maximum allowed analytical stresses and simulated stresses. For each stage, yield stress over the safety factor of 2. For the interstages, the critical buckling stress times the safety factor of 1.5

Part	Maximum allowed analytical stress (MPa)	Maximum ANSYS calculated stress (MPa)	Error (%)
1st stage	250	311.4	24.56
1st interstage	74.34	62.134	16.48
2nd stage	250	294.9	17.96
2nd interstage	38.31	35.1	8.37
3rd stage	250	273.3	9.32
3rd interstage	17.23	16.3	5.32
Payload fairing	13	15.9	22.3

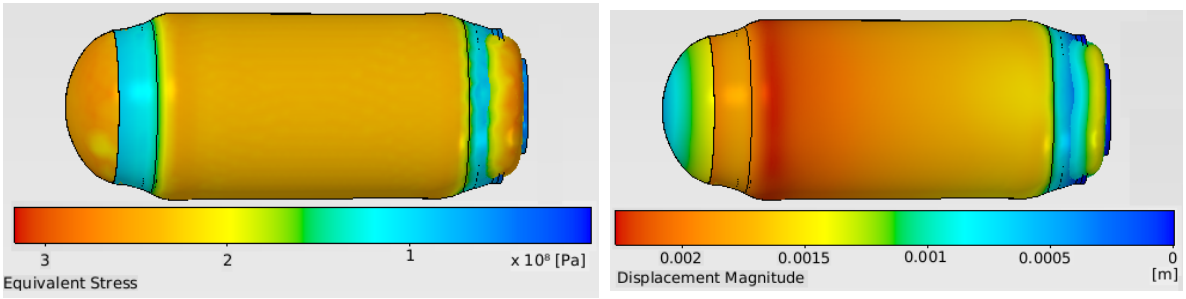

(a) Equivalent stress heat map

(b) Displacement magnitude heat map

Figure 4.47: Example of the FEM analysis results for the 1st stage. Performed using Ansys .

Concluding, for the case of the propellant tanks, even though some these discrepancies were above 20%, through a visual inspection of the FEM analysis, it was shown that they happened either close to the clamped edge or to a transition between parts. Over 90% of the surface area stresses were within the expected limits, especially the areas where there were specific analytical equations to use (e.g. the cylindrical and spherical cap of the propellant tanks). These results, which can be appreciated in fig. 4.47, emphasises the importance of the 1st named possible cause for discrepancies. These edges and transitions should be looked into more detail in future stages of the design.

Also, it seems like the analytical expression used to calculate the critical buckling load of a hollow cylinder, eq. (4.68), overestimates the required thickness, resulting in an over designed structure which should be looked into in future stages of the project.

4.12.3. MATERIAL ANALYSIS

The next step was to perform a material analysis. The choice of material can severely affect the weight of the structure and the cost of it. In table 4.23, the different materials considered for the solid motor casings and interstages are shown. These are: Al-7075 T6, the one considered in the first iteration due to its good material properties but that might have a high cost, Al-6061, a more common, less expensive aluminium alloy and two composite prepegs; Carbon fiber and glass fiber, both with a fiber volume of 60 % and 2D isotropic behaviour. The materials shown have different properties which will alter the required thickness of the structure and therefore the weight and cost. For the aluminium alloys, the yield strength will be used, for the composites, the tensile strength

will be used since a 2D isotropic behaviour was assumed. It is also important to note that since these composite prepeg do not have 3D isotropic behaviour, only 2D , the thickness of the tanks will not be selected in the same way as for the aluminium alloys, instead the thickness required for buckling and for the internal pressure will be assumed to be independent and therefore, summed. This assumption allows to obtain a first order estimation of the weight and cost of the structure but should be researched in more depth in later stages of the design.

To calculate the costs, only the raw material cost will be considered in this comparison. It will be assumed that the manufacturing costs are included within the development costs and production costs of the launch system and that will be calculated in later sections.

Table 4.23: Different materials considered for the analysis. The data shown was obtained from Callister and Rethwisch's book of Material Science and Engineering [13].

Material	E-Modulus (GPa)	Yield strength Tensile strength (MPa)	Cost of material ($/kg)	Total weight (kg)	Total cost($)
Al-7075	71	505	11.30–14.70	151.24	2219.994
Al-6061	69	276	6.60–8.50	251.37	2136.64
Glass fiber	45	1020	24-50	92.65	4632.5
HS Carbon	220	760	250	60.54	15135

As shown in table 4.23, even though composite materials produce the lowest weight, their material cost is higher when comparing it with the aluminium alloys. This produces a need for a trade-off between weight and cost that shall be performed in future design stages. For now, Al-7075 proves to be a good solution, and will be used during the current design phase.

4.12.4. VIBRATION ANALYSIS

Following the static analysis of the rocket, a vibration analysis was performed for the thrust profile of the first stage. This analysis allowed the calculation of the eigenfrequencies of the rocket, which gives information about the forcing frequencies that must be avoided. For this analysis, each stage was simplified to a spring/damper system with the mass lumped on top as shown in fig. 4.48. Each mass will consist of the propellant, structure and nozzle mass of the considered stage, except the last mass, M_3, which will consist of the orbital manoeuvre system lumped together with the payload, the fairing and the third stage. This resulted in a 3 degrees of freedom spring-damper system in which three masses are connected in series. The analysis will be performed by introducing the equations of motion into a state space representation and simulating it with Python. The equations of motion of such a system are:

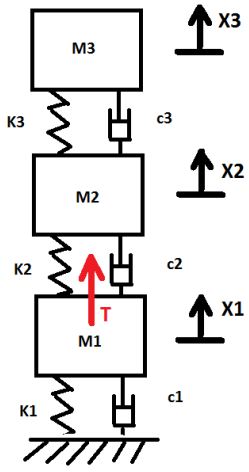

Figure 4.48: Spring-damper representation of the rocket.

$$\begin{cases} \ddot{x}_1 = -\frac{(c_1+c_2)}{m_1}\dot{x}_1 - \frac{(K_1+K_2)}{m_1}x_1 + \frac{c_2}{m_1}\dot{x}_2 + \frac{K_2}{m_1}x_2 + \frac{T}{m_1} \\ \ddot{x}_2 = \frac{c_2}{m_2}\dot{x}_1 + \frac{K_2}{m_2}x_1 - \frac{(c_2+c_3)}{m_2}\dot{x}_2 - \frac{(K_2+K_3)}{m_2}x_2 + \frac{c_3}{m_2}\dot{x}_3 + \frac{K_3}{m_2}x_3 \\ \ddot{x}_3 = \frac{c_3}{m_3}\dot{x}_2 + \frac{K_3}{m_3}x_2 - \frac{c_3}{m_3}\dot{x}_3 - \frac{K_3}{m_3}x_3 \end{cases} \tag{4.71}$$

In order to simulate the response of the system to the first stage thrust, the state space system will look like:

$$\dot{x} = Ax + Bu \qquad y = Cx + Du \tag{4.72}$$

Next, the state space variables are introduced to reduce the second order differential equation into a first order one. This reduction produces three more equations. The state space variable vector is:

$$x = \begin{bmatrix} x_1 \\ x_2 \\ x_3 \\ \dot{x}_1 \\ \dot{x}_2 \\ \dot{x}_3 \end{bmatrix} = \begin{bmatrix} x_1 \\ x_2 \\ x_3 \\ v_1 \\ v_2 \\ v_3 \end{bmatrix} \tag{4.73}$$

With the following relationships:

$$v_1 = \dot{x}_1 \qquad v_2 = \dot{x}_2 \qquad v_3 = \dot{x}_3 \tag{4.74}$$

The matrices A, B, C and D determine the relationships between the state and input and output variables. A is the state (or system) matrix, B is the input matrix, C is the output matrix"and D is the feedthrough (or feedforward) matrix. They look like:

$$A = \begin{bmatrix} 0 & 0 & 0 & 1 & 0 & 0 \\ 0 & 0 & 0 & 0 & 1 & 0 \\ 0 & 0 & 0 & 0 & 0 & 1 \\ -\frac{(K_1+K_2)}{m_1} & -\frac{(c_1+c_2)}{m_1} & \frac{K_2}{m_1} & \frac{c_2}{m_1} & 0 & 0 \\ \frac{K_2}{m_2} & \frac{c_2}{m_2} & -\frac{(K_2+K_3)}{m_2} & -\frac{(c_2+c_3)}{m_2} & +\frac{K_3}{m_2} & \frac{c_3}{m_2} \\ 0 & 0 & \frac{K_3}{m_3} & \frac{c_3}{m_3} & -\frac{K_3}{m_3} & -\frac{c_3}{m_3} \end{bmatrix} \tag{4.75}$$

$$B = \begin{bmatrix} 0 \\ 0 \\ 0 \\ \frac{T}{m_1} \\ 0 \\ 0 \end{bmatrix} \qquad C = \begin{bmatrix} 1 \\ 1 \\ 1 \\ 1 \\ 1 \\ 1 \end{bmatrix} \qquad D = \begin{bmatrix} 0 \\ 0 \\ 0 \\ 0 \\ 0 \\ 0 \end{bmatrix} \tag{4.76}$$

Next, the axial stiffness of each spring will be determined using beam theory with the following relations:

$$F = K \cdot \delta = \frac{\delta \cdot E \cdot A}{L} \qquad K_i = \frac{E_i \cdot A_i}{L_i} \tag{4.77}$$

Where F is the force of the spring, δ is the displacement of the beam, E is the modulus of elasticity, A is the cross sectional area and L the length of the beam. Finally, the damping coefficient will follow:

$$c_i = \zeta 2\sqrt{K_i \cdot m_i} \tag{4.78}$$

Where ζ is the damping ratio. According to Dr. Sergio Turteltaub, lecturer and researcher at the Delft University of Technology, ζ will be assumed to be around 0.02 for all stages [44]. An example of the response of the system to a step input is shown in fig. 4.49. In order to calculate the natural frequencies of the system, the eigenvalues of matrix A will be obtained with Python. The linear

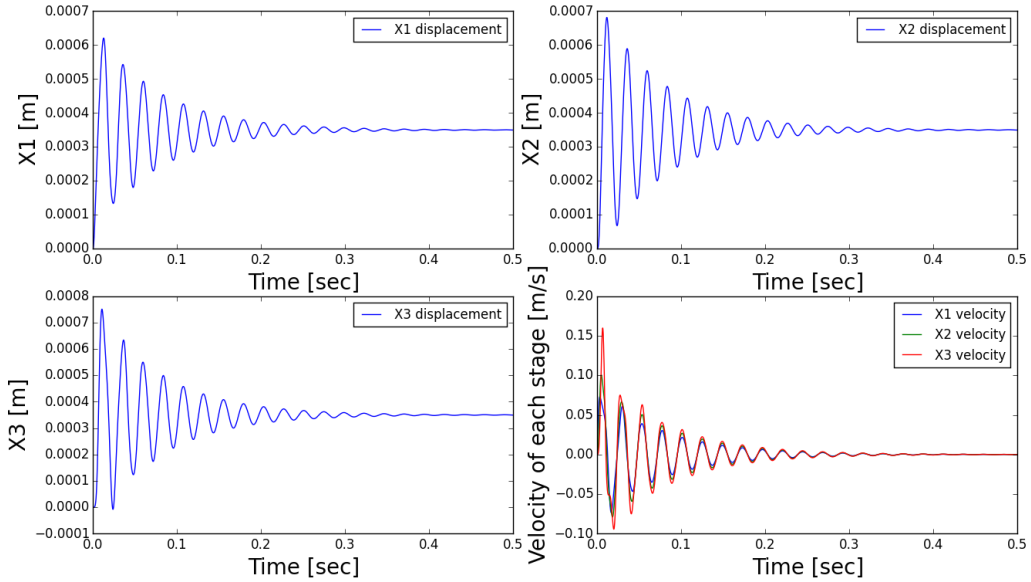

Figure 4.49: Response of the spring damper system for a step input with an initial thrust of 109.65 kN and a damping coefficient of 0.02

algebra solver gives three pairs of complex conjugates: $-31.924 \pm 1076.12\,j, -13.50 \pm 667.68\,j, -3.73 \pm 263.2\,j$. By being complex, the periodic behaviour of the system is proven. With these eigenvalues, the natural frequencies can be calculated:

$$f_{n_i} = \frac{1}{2\pi}\sqrt{\alpha_i^2 + \beta_i^2} \tag{4.79}$$

This gives three natural frequencies: 171.35, 106.29 and 41.89 Hz. These frequencies need to be avoided in order to prevent resonance from happening.

Finally, to calculate the maximum vibration loads, the maximum acceleration of each stage will be calculated using the velocity outputs of the Python vibration tool and differentiating it with respect to the time vector. Once done, the acceleration due to the thrust force will be subtracted.

4.13. SYSTEM CONFIGURATION & LAYOUT

Once all the systems parts have been integrated, an exploded view of the rocket is shown in fig. 4.50. Moreover, a rendering of the complete system is presented in fig. 4.51

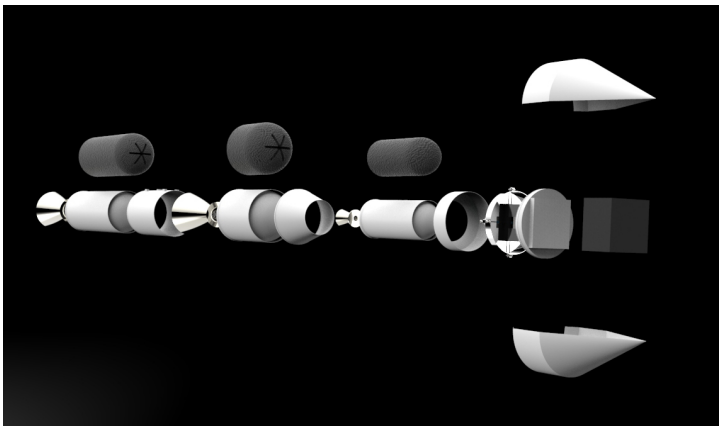

Figure 4.50: An exploded view of the ALTAR and its main components.

Figure 4.51: A render of the ALTAR complete system at high altitude.

5

System Design Analysis

This chapter starts with a performance test of the final design. Hereafter, this performance will be tested again with varying parameters, a so called sensitivity analysis. Afterwards, a RAMS analysis is performed and a sustainability strategy will be proposed. Next, a risk assessment and a risk mitigation strategy will be elaborated. To conclude, a requirements compliance check is performed to see whether the design performs as intended.

5.1. Performance Analysis: payload mass vs. target orbit

An important relation to investigate is the amount of payload that can be brought to different orbits. This investigation can be seen as an overall view on the performance capabilities of the launch service. This gives the customers a clear view on the performance capabilities of the launcher system in case a customer would like to bring a payload to an orbit other than the 600 km sun-synchronous orbit.

To analyse the performance to different orbits, the TSOT was used to optimise the trajectory to a range of different orbit altitudes and inclinations. The inputs are the same as in section 4.7.1, except for the target orbit. The results can be found in fig. 5.1. It has to be noted that this does not include the orbit raising manoeuvre by the OMS. Enough OMS fuel is included to provide a payload of 35 kg with 118 m/s of ΔV.

5.2. Sensitivity Analysis

In this section, the robustness of the launch system design will be tested by means of a sensitivity analysis. This will be done by investigating the sensitivity of the design to changes in major system parameters. By doing so, the degree of feasibility of the design for such changes can be established. This section will perform a sensitivity analysis on the payload mass that can be carried to a sun-synchronous orbit at an altitude of 600 km (design orbit) with respect to changes in the specific impulse of the different stages, the structural mass and finally the maximum altitude that the stratospheric balloon can reach.

5.2.1. Payload mass vs. specific impulse

An important subsystem of the launch system is the propulsion subsystem. A parameter that accounts for the propulsion subsystem as a whole is the specific impulse of the different stages, which is a measure for the efficiency of a rocket engines. To test the robustness of the design to the specific impulse, it is important to test the capabilities of the launch service for such changes. Therefore, the payload mass that can be brought to a sun-synchronous at an altitude of 600 km will be sequentially investigated for different specific impulses of the different stages. Note that when the sensitivity analysis is performed on one stage, the other stages are assumed to have their nominal specific impulse of 250 s, 250 s and 285 s for the first, second and third stage, respectively.

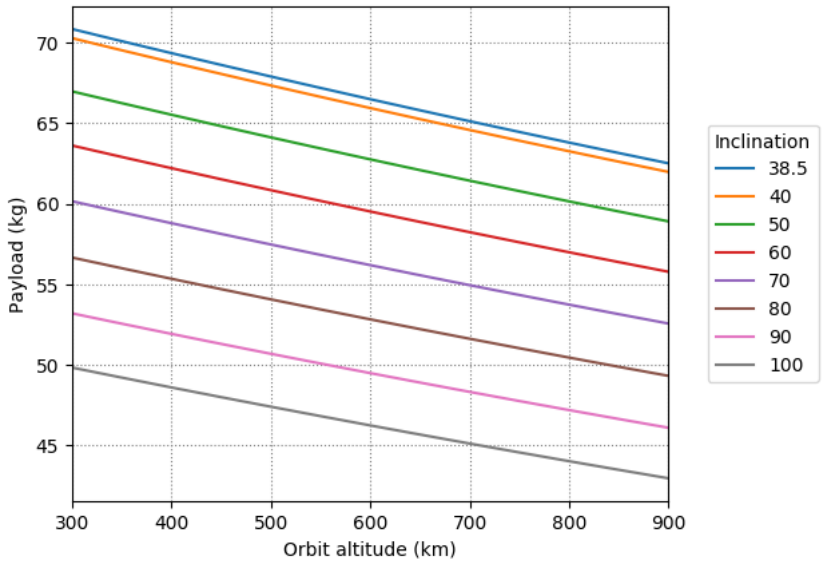

Figure 5.1: Payload versus target orbit.

As can be seen in figs. 5.2a to 5.2c, the payload mass that can be brought in to a sun-synchronous orbit at an altitude of 600 km varies from approximately 24 kg to 63 kg with changes in the specific impulse for the different rocket engines within the range of 220 s to 310 s. The three graphs can be assumed to be roughly linear with a gradient of 0.36 kg/s, 0.36 kg/s and 0.67 kg/s for the first, second and third stage, respectively. From the different gradients it can be seen that the payload mass that can be brought in to the design orbit is the most sensitive to changes within the specific impulse of the third solid stage.

5.2.2. Payload mass vs. maximum balloon altitude

As the main objective of the balloon is to carry the rocket launcher to a certain altitude, a sensitivity analysis will be done on this performance parameter. Progress in the field of stratospheric ballooning could possibly lead to higher altitudes. On the other hand, unfavourable weather conditions or unforeseen risks could possibly decrease the maximum altitude that the balloon can reach. Therefore, the different payload masses that can be brought to an sun-synchronous orbit at an altitude of 600 km will be investigated for different maximum balloon altitudes.

As can be seen in fig. 5.2d, the payload mass that can be brought to a sun-synchronous orbit at an altitude of 600 km varies from approximately 44.6 kg to 46.7 kg for the maximum balloon altitude changes within the range of 30 km to 45 km. Within this altitude range, the graph can be assumed to be roughly linear with a gradient of 0.2 kg/km. It can be seen that it takes a significant change in the maximum balloon altitude to carry slightly more payload to orbit. Varying the maximum altitude of the balloon within a feasible range does not allow for large variations in the payload mass.

5.2.3. Payload mass vs. structural mass

Another important parameter of the rocket launcher is the overall structural mass. The structural mass of the rocket launcher is highly variable due to the complexity of systems engineering design. Small changes in the rocket design could lead to significant changes in the overall mass, including the structural mass. Therefore, it is important to check how robust the design is to such changes. For this, the different payload masses that can reach an sun-synchronous orbit at an altitude of 600 km

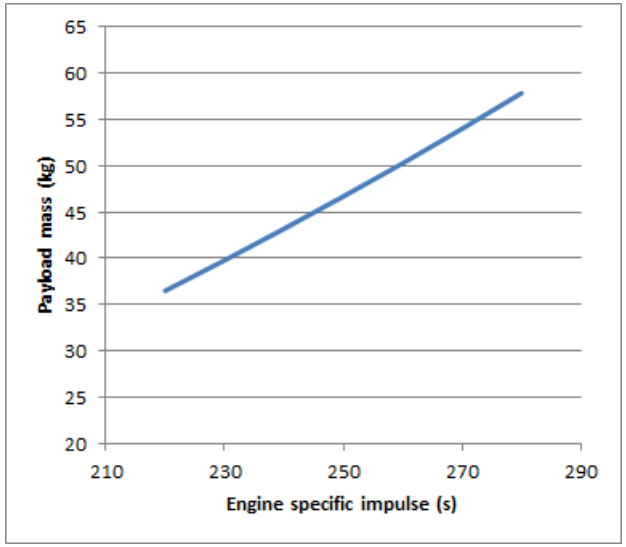

(a) Payload mass variations to design orbit with respect to changes in the first stage specific impulse.

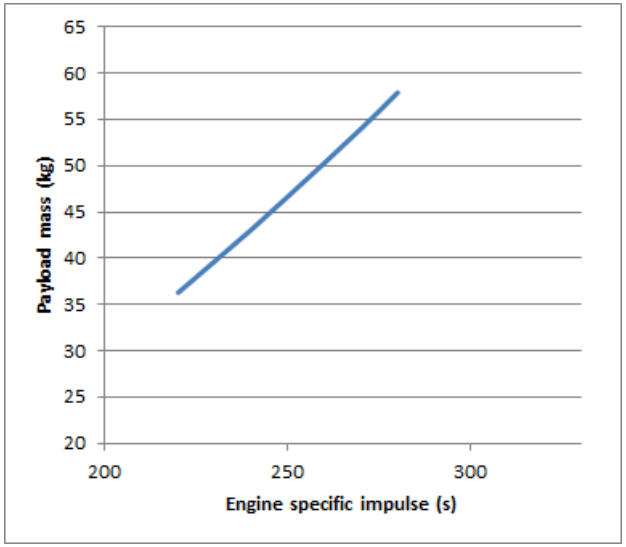

(b) Payload mass variations to design orbit with respect to changes in the second stage specific impulse.

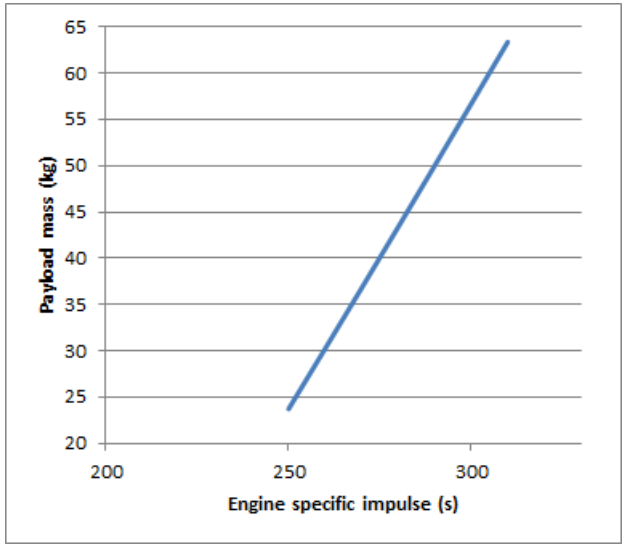

(c) Payload mass variations to design orbit with respect to changes in the third stage specific impulse.

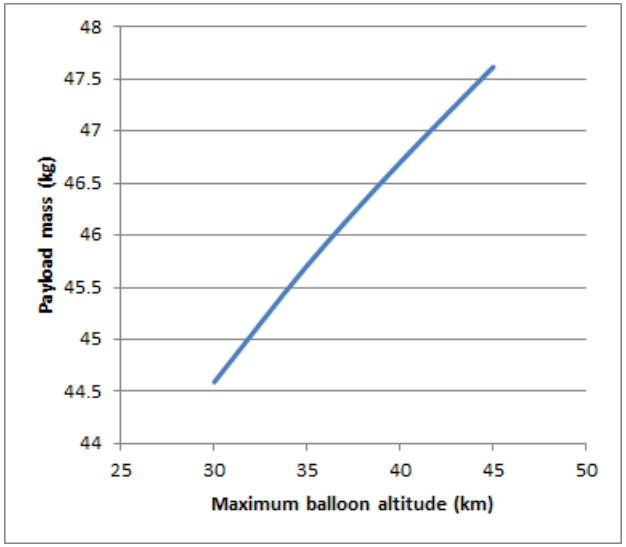

(d) Payload mass variations to design orbit with respect to changes maximum balloon altitude.

Figure 5.2: Sensitivity analysis of the payload mass to design orbit with respect to changes within the specific impulse and the maximum balloon altitude.

will be investigated.

As can be seen in figs. 5.3a to 5.3c, the payload mass that can be carried to a sun-synchronous orbit at an altitude of 600 km varies from 42 kg to 64 kg with respect to changes in the structural mass of the different stages within the range of 150 kg to 200 kg for the first and second stage and 40 kg to 65 kg for the third stage. The three graphs can be assumed to be roughly linear with a gradient of –0.034 kg/kg, –0.086 kg/kg and –0.88 kg/kg for the first, second and third stage, respectively. From the gradients it can be concluded that the payload mass is the most sensitive to the structural mass of the third stage.

5.3. RELIABILITY

In order to assure reliability and mission success, a suitable redundancy philosophy is or has to be applied to each subsystem. The redundancy philosophies that are applicable for a launch system are the fail-safe design and safe-life design.

The fail-safe design makes sure that there are redundant components in a subsystem, such that it is safe for a component to fail. This means that the subsystem and the whole system will not be jeopardised by a single component failure. A component will be designed such that fatigue cracks may occur. Also, structures are arranged so that cracks will not lead to failure of the structure before they are detected and repaired.

The safe-life philosophy is the way of designing such that no redundant components are used to cope with failure. The component will be designed such that the component will not fail during a specified life time. The safe-life technique is employed when in critical systems it is difficult to perform repairs or difficult to inspect. For a safe-life design, a general safety factor of 1.5 is applied for the ALTAR launch system, which is conventional for the aerospace industry. In some cases a more specific safety factor is defined. As for more critical components in a subsystem, the safety factors are higher than the general safety factor.

Something is a critical aspect when it has the ability to jeopardise the mission success. In this case, mission success is accomplished when the payload has reached its target orbit without any damage. To map the reliability of the launch system, the critical aspects of the subsystems or possible single points of failure are analysed. This is followed by assigning a suitable redundancy philosophy. An overview of the redundancy philosophies that are or should be applied to the subsystems are given below.

- **Balloon structure**: The balloon structure has three cables which are attached to the gondola, these three cables are the minimum amount needed to ascent the gondola in a stable manner. To increase mission success, a safe-life design was applied to the balloon cables to prevent stress failure. A safety factor of 1.5 was applied to assure safe-life design. Also for the balloon load tapes, a general safety factor was applied to cope with uncertainty in shear stresses acting on the balloon.
- **Gondola system**: The gondola structure consists of a upper and a lower half. The two halves are connected by a rotation mechanism. This mechanism is then part of the pointing system of the gondola. A safety factor of 3.0 is used for this, since these are primary structural members and reusability of this structure is desired. In the lower half of the gondola structure, the separation and pointing mechanisms are present. The separation mechanism is the most critical of the two, since in case of emergency the rocket can still point itself when it is detached. Though this will burn more fuel and the probability of missing target orbit might increase. The separation mechanism will be designed with a fail-safe philosophy. So when

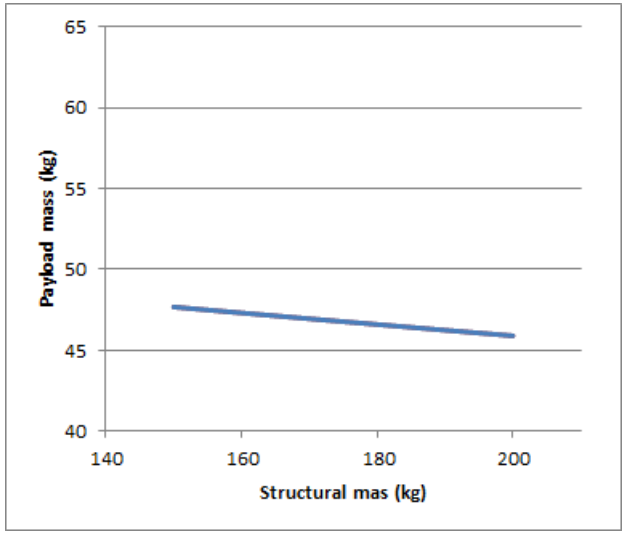

(a) Payload mass variations to design orbit with respect to changes in the first stage structural mass

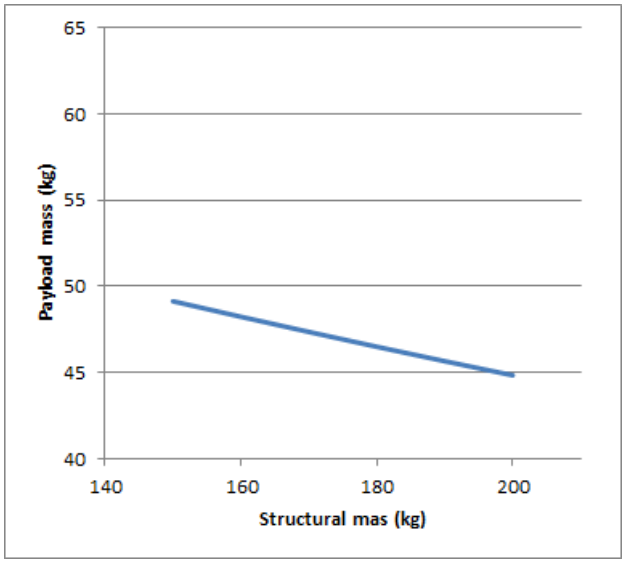

(b) Payload mass variations to design orbit with respect to changes in the second stage structural mass

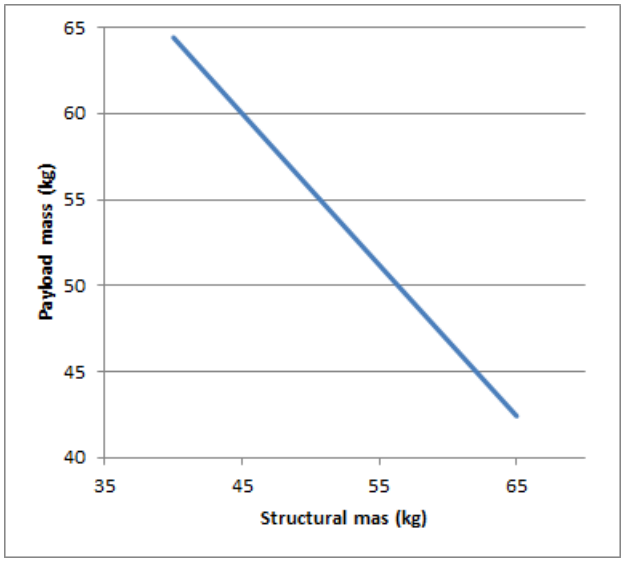

(c) Payload mass variations to design orbit with respect to changes in the third stage structural mass

several pyrotechnic fastener are not working a set of redundant pyrotechnic fasteners should still be able to separate the rocket from the gondola.

- **Propulsion system**: The most critical spot where failure must not occur, is the intersection between the nozzle and combustion chamber of the solid rocket. A safe-life design has been applied for this failure. To prevent this, a safety factor should be applied on the thickness of the thermal liner at that intersection. Also, the proper functioning of the OMS is critical for mission. Especially the propellant feed system of the OMS must be reliable to prevent any unexpected combustion. To assure this, the feed system of MOOG, see section 4.4, use has been made of COTS technology with at least three sigma reliability.
- **Payload separation**: This system is the last step for mission success. The payload separation system will be bought from renowned manufacturers who provide COTS technology. In this case, the Lightband Mark II of Planetary Systems Corporation was chosen. This separation system has a reliability of 100 % and the mechanism within was designed with a fail-safe philosophy.
- **Guidance, navigation & control system**: When the rocket becomes unguided, it can endanger people. In that case, if control cannot be regained, it must be destroyed, thus causing a mission failure. To avoid this, a fail-safe design is used for the position and attitude determination. The fail-safe component of the inertial measurement unit is the global navigation satellite system. The jet vanes of the TVC are designed according to the safe-life principle. When the rocket is in space, the Vernier thrusters which are meant for more precise attitude control, can be used as a fail-safe component for the jet vanes.
- **Telemetry, communication & data handling system**: This system must have a fail-safe design. Since it is standard procedure in industry to explode the rocket when the communication link has been lost for a specified time. A redundant telemetry, communication & data handling system minus the on-board antenna, will be added on the rocket to make sure that a permanent communication link will be maintained.
- **Electrical power system**: To prevent losing the communication link as previously mentioned, this system must also be designed according to the fail-safe philosophy. An extra power supply system is added to support the telemetry, communication & data handling system.
- **Balloon recovery system**: This system is has no impact on the defined mission success, since the balloon recovery system will kick in when the rocket has been launched and separated from the balloon. So an analysis on this system is not applicable.
- **Flight termination system**: This system in itself is redundant to coping with mission failure and it follows the fail-safe principle. An analysis on this system is not applicable.
- **Rocket structure**: The interstage is a critical component in the separation. The interstages should be designed for restraining large deflections imposed by the inertial loads. These deflections can cause improper functioning of the rocket engine. When the stage above will collapse on the stage underneath. A safe-life philosophy was applied and a safety factor of 2.0 is used to prevent this failure.

The expected reliability of the launch system will mostly depend on the gondola and rocket. To compare the reliability of this rocket the reliability of a selection of existing solid rockets are gathered in table 5.1, these rockets all have three or four stages. From the table, it can be concluded that there are not many launches for these rockets and that the reliability is on average 91.5 % with a standard deviation of 6.2 %. It is assumed that the rocket for the ALTAR launch system will have this reliability.

Table 5.1: Reliability rate of solid rocket launches. The first two rockets are air launched from an aircraft. The remaining rockets are launched from the ground. The first four launch vehicles are still active. The

Launch vehicle	Company	Total No. of launches}	No. of successes	Reliability [%]
Pegasus	Orbital ATK	11	10	90.9
Pegasus XL	Orbital ATK	32	29	90.6
Minotaur I	Orbital ATK	11	11	100.0
Start-1	MITT	7	6	85.7
M-V	ISAS	7	6	85.7
M-3SII	Tokyo University	8	7	87.5
M-3S	Tokyo University	4	4	100.0

5.4. AVAILABILITY

Availability is defined as the degree, percent, or probability that a system will be ready or available when required for use [45]. According to an internal survey performed to several cube-sat manufacturers, the minimum waiting time from the moment a launch slot is obtained up until the actual launch is 6 months. Therefore, ALTAR must be available within 6 months of notice. To be ready, the balloon subsystem, together with the gondola shall be refurbished, the rocket shall be manufactured, shipped to the launch site and assembled together with the payload. Other aspects that need to be taken into account are: the supply of the propellants for both the balloon and rocket, the testing of each component alone, the system testing once integrated. Each of this aspects might cause delays but will be taken into account when designing the operational and logistics of the launch system in section 7.3. There is no reason to think that the system will not be available when required unless external factors such as weather or natural catastrophes occur, for which the operational and logistics characteristics will be designed with enough redundancy to account for these remote occurrences. The launch system will be ready to launch in less than 6 months, the minimum time it takes for the customer to make the payload ready for launch after they have obtained a slot.

5.5. MAINTAINABILITY

As explained in section 4.10.3, the balloon and the gondola will be recovered. Therefore, only in the design of these parts the concept of maintainability plays an important role. First of all, a maintenance diagram, which has the basic structure suggested by the system engineering book [45] is determined and presented in fig. 5.4. Preventive maintenance includes all the actions that can be planned and scheduled, corrective maintenance the ones that occur after a singular unexpected event. Periodic maintenance shall be performed after each launch, conditional maintenance only after certain launches. As it can be seen in fig. 5.4, preventive periodic maintenance is scheduled after every launch, this was chosen because the system will always have a "turnaround time" sufficiently long to allow the system to be thoroughly checked.

Periodic maintenance includes, beside the other maintenance actions, lubrication of all the moving parts of the mechanisms present in the gondola and also nominal load tests of the primary structure, which includes suspending ropes, the attachment rod and the components presented in section 4.12, section 4.3.2 and section 4.2.3. Moreover, every 5 launches the balloon film will be substituted entirely and its material recycled as mentioned in section 5.7. This was determined based on the hypothetical lifetime of the film that composes the balloon. According to a scientific arti-

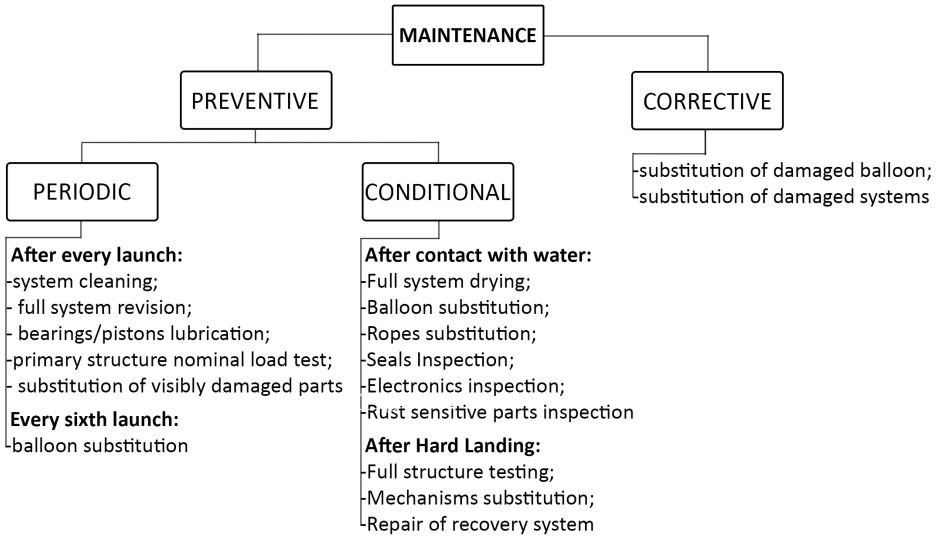

Figure 5.4: The maintenance chart of the balloon and gondola system which shows the periodic, conditional and corrective actions to keep the system functional and reliable during its expected lifetime.

cle [46], thin HDPE films are affected by UV radiation negatively and if they are exposed to it their properties rapidly degrade. Particularly for the balloon, this could lead to excessive leakage of Helium during the mission, a more brittle film and a easier propagation of holes and cracks, due to the chains breakage and formation of cross-links in the polymers and to the formation of carbonyl and vinyl groups [46]. If a thin film of HDPE is exposed to a UV-B continuous radiation, after five days its properties start changing rapidly, according to test performed and reported in [46], which extended in duration to sixty days. For the balloon, it is assumed that during a single mission of the duration of few hours, its exposure time to solar radiation at such a high altitude could be compared to a day long exposure at sea level. Therefore, the balloon film was decided to be substituted after five launches in order not to compromise its properties that could determine a mission failure.

Under conditional maintenance in fig. 5.4, it can be seen that in case of the balloon and gondola systems getting in contact with water (rain or sea landing), the balloon will be substituted entirely. This is because the materials used for the construction of this system are permeable to water and would absorb some of it [1]. Moreover, particular attention would be paid to the electronics and seals in the gondola and all the parts which are sensitive to water damage. In the case of a hard landing, the structure and mechanisms of the gondola would need to be repaired or substituted as well as the mechanism in charge or recovering the balloon.

In order to estimate important parameters such as Mean Time To Mantain (MTTM), Mean Down Time (MDT), Maintenance Labor Hours (MLH), Mean Time Between Maintenance (MTBM), some assumptions need to be made:

- The system has a reliability in compliance with the requirements, that is equal to 0.915, as calculated in section 5.3;
- Periodic and conditional maintenance can be associated with a type A-check for aircrafts, which requires 70 man-hours according to [47];

[1] http://polymerdatabase.com/polymer%20physics/Permeability.html

- Corrective maintenance can be associated with a type B-check for aircrafts, which requires 180 man-hours according to [47];
- A total number of 384 successfull launches is assumed to take place within 15 years as explained in chapter 8;
- A total number of 7 engineers are assumed to be working on maintenance with a working day of 8 hours;

Now, MTTM, MTBM, MLH and MCPF can be calculated with the following equations:

$$MTTM = (1-0.915)\cdot 180 + 0.915\cdot 70 = 79.35\,\text{h} \tag{5.1}$$

$$MDT = 24 + \frac{MTTM}{7} - 8 = 27.34\,\text{h} \tag{5.2}$$

$$MTBM = \frac{15\cdot 365.25\cdot 24}{384} = 342.42\,\text{h} \tag{5.3}$$

$$MLH = MTTM\cdot 384 = 30\,470.4\,\text{h} \tag{5.4}$$

5.6. SAFETY

To insure the safety of people and equipment it will be necessary to identify the most crucial functions that need to be carried out to minimise the likelihood and impact of possible failures. Redundancy in these crucial functions is favoured as this lowers the chance of catastrophic failures. The most important functions that need to be fulfilled and have been identified are listed below:

- **Leak Checks**: Both before and after the balloon is filled with helium it should be checked for possible tears and places it might leak. Leakage of the balloon can be catastrophic for the performance as the target altitude will definitely not be attained. Luckily the leaked helium does not pose a huge threat to the ground personnel.
- **Rocket Separation**: Both failing to release the rocket and releasing the rocket too early can have a detrimental effect on the performance on the mission. The payload and might be salvaged as the parachute system could be deployed if the rocket was released too early, but if the engine would start while the rocket is still attached the effect would be disastrous. Thus to insure safety the separation system should be fail safe while also clearly communicating with the rocket to insure the engines aren't started if separation has not (yet) been completed.
- **Stage Separation**: Stage separation failure will directly mean mission failure as well as loss of payload. Therefore this component should be completely redundant to make sure that even when one part fails the stage can still be separated.
- **Payload Separation**: Very similar too the stage separation, with the exception that CubeSat Dispensers might still be used even if separation from the final stage fails. Furthermore, COTS technologies for payload separation are available with 100% success rate and flight heritage, which might lessen the need for redundancy.
- **Ignition System**: Obviously if the engine is not started the mission will fail. This is most easily mitigated by making sure redundancy is implemented. Reliability of the ignition system should be very high as well.
- **Abortion System**: If the rocket or balloon deviate too much from their expected trajectories they might pose a risk to the personnel or uninvolved population. To prevent that they are harmed by a crashing rocket or balloon an abortion system should be present to explode the

rocket in mid air. Within this system it is favourable to integrate a system that saves the payload.

- **Parachute Deployment**: As mentioned in the point before, the rocket or balloon might fail or the rocket is exploded through mission abortion. To prevent harm to the payload, a parachute system is connected to the payload and balloon control gondola. Thus, both possibly can be preserved even in the case of mission abortion.
- **Propellants**: Cryogenic liquids and hypergolic propellants are dangerous to humans, most often toxic and it takes only a slight spark to ignite. Solids have less potential to be harmful to handling personnel and often require stronger stimuli to ignite, however once they are ignited there is almost no way of stopping it [48]. Thus, to minimise possible human errors with catastrophic consequences very strict regulations should be in place and followed to make sure the propellants are handled with due care.

The above mentioned crucial safety points might often seem like they warn for something rather obvious, but the possible consequences of neglecting one of these points can be enormous. Therefore, it is necessary to identify and track even the most obvious risks to safety to be sure mitigation is incorporated in the design.

5.7. SUSTAINABILITY STRATEGY

The use and reuse stratospheric balloons will have a beneficial impact on the environment, conservation of resources and cost with respect to the ground based multi-stage rockets. The stratospheric balloon is used to bring the rocket to 38 km altitude and reduces the required propellant mass of the vehicle. In addition, during the ascent of the balloon, no propellant fuel is emitted into the atmosphere and it does not harm the environment through air pollution. Moreover, landing the balloon close to the launch site will decrease operational costs (namely, transportation costs). Furthermore, the balloon and balloon guidance system can be reused for a few more launches. To be able to reuse the balloon and BGS, it needs to land in a safe zone. Two strategies for landing the balloon are described in section 4.10.3. If the balloon is damaged, the film of the balloon (HDPE) can be recycled. Many new products can be manufactured using recycled high-density polyethylene; rope, toys, piping, recycling bins and trash cans.

Solid propellants are less harmful and dangerous than hypergolic propellants and mono-propellants to the personnel handling them. During the first iteration phase, a hypergolic propellant (nitrogen tetroxide) was to be used in the upper stage of the rocket. However, the liquid form of this propellant is very toxic and can damage body tissue. In addition, one of the biggest risks when handling nitrogen tetroxide is inhalation of its toxic vapors [49]. Due to this propellant's high toxicity, after the first iteration phase, a mono-propellant (hydrogen) that is less hazardous than nitrogen tetroxide, was chosen to replace it for the upper stage of the rocket. An ascending route is planned in the Atlantic ocean near the Azores, in order to avoid accidents in the event of mission failure or mission abortion and termination.

Jet vanes are made of tungsten and their potential to cause harm to animals and humans is low. In addition, it has a recycle rate of 35% [50]. Aluminium composites are used for the payload adaptor and most of the structural components. They have a high recyclability, thereby allowing a large reduction in waste; moreover, they have lower energy costs and carbon emissions [51]. Complementing these benefits, composites do not need surface finish processes like metals, which often lead to a lot of toxic waste. Finally, their shipping costs are reduced due to their light weight. The energy required to produce new aluminium is down more than a quarter since 1995 [51]. To reduce operational costs, test facilities as well as the launch site should be in Europe because it will be

manufactured in Europe. Throughout the manufacturing and testing process, pollution and waste of resources will be reduced by optimising manufacturing processes.

The space debris created by launch vehicles can be hazardous because it can collide with satellites or cause a liability when it falls back to earth. As an example, fragments as small as a centimetre have the potential to destroy whole satellites due to high relative speeds[2]. In order to avoid catastrophic collisions of future payloads and launchers from space debris. A re-entry method that brings the upper stage of launch vehicle down in a safe ocean area will be used. According to section 4.6.5, during the re-entry, the upper stage components will completely burn through the atmosphere. Other options for sustainability include the reduction of the number of test fires and decreasing the use of qualification models to the minimum.

The just-in-time chain, which has also been widely applied in the aircraft industry, can be used to improve sustainability for the production of a launch vehicle. This procedure ensures all production steps that can be done in parallel are done so, while minimising waiting time. Margins need to be carefully considered as one missed deadline should not halt the complete process. Another process applied in the aerospace industry, which can be applied to most production processes, is the involvement and training of employees, both for safety and the importance of environmental sustainability. This can have drastic effects on the effectiveness of the workers, while decreasing workplace accidents.

5.8. TECHNICAL RISK ASSESSMENT

Technical performance, cost resources and time resources are the components of the systems engineering universe which are interconnected via risks. The risk of an event can be described as the product of the probability that the event occurs with the impact of occurrence. Project risk management is to be continuously applied throughout the design process in order to ensure that the product meets all requirements in time and within budget. This includes cost, time and technical risk management activities. Technical risks pertain to the possibility that the product cannot fulfil a technical performance, cost or scheduling requirement in the system life cycle [52].

Main risk events which could affect the capability of the product to satisfy the requirements described in section 5.9, are identified and evaluated in section 5.8.1. Methods used to mitigate the highest magnitude risk events are described in section 5.8.2.

5.8.1. RISK IDENTIFICATION

The ordinal scale for the probability of occurrence is shown in table 5.2. The probability of occurrence of a risk event increases with an increase in the 'scaled number'. The ordinal scale used for the risk event consequence can be seen in table 5.3. As explained in the *Systems Engineering & Technical Management Techniques, Part I* reader, a negligible impact would create an inconvenience or a non-operational impact. A risk event with a negligible consequence does not result in a reduction in technical performance. A marginal impact results in a degradation of the secondary mission and a minimal reduction in technical performance. A critical consequence results in a degradation of system performance to the extent that mission success is questionable with some reduction in technical performance. A catastrophic impact will result in a mission failure, with significant reduction of technical performance [52].

Technical risks that may hinder compliance to requirements of the ALTAR system are identified and assessed in table 5.4. Here, risks are divided into groups, such as balloon system related risks (B),

[2]https://www.theguardian.com/science/across-the-universe/2012/oct/04/astronomy-space

Table 5.2: Risk probability scales.

Scaled Number	Probability of Occurrence
1	Unlikely
2	Somewhat Likely
3	Likely
4	Very Likely

Table 5.3: Risk impact scales.

Scaled Number	Impact
1	Negligible
2	Marginal
3	Critical
4	Catastrophic

rocket system related risks (R), and general risks (GEN). Assessing the risks include assigning an estimated probability of occurrence and impact of occurrence to each identified risk. The likelihood of the risk events has been based on past data where possible, and otherwise assigned with engineering judgement. The identified risks are plotted in the pre-mitigation risk map shown in fig. 5.5. Events in the upper right corner of the risk map pose the highest risks and must be mitigated.

Table 5.4: Risk identification and analysis.

Risk #	Risk Event	Likelihood	Impact	Risk Description
B-STRUCT-01	Balloon envelope failure	1	4	As there is no pressure difference and no objects surrounding the envelope during the mission, the likelihood of such event is low. Envelope failure would lead to the lifting gas leak, and therefore the mission would have to be aborted.
B-STRUCT-02	Unexpected loads on balloon	2	3	If the balloon enters a turbulent flow, the wind force is going to act on the film from different directions. Shear out of the film might occur due to this phenomenon.
B-GNC-01	Balloon control system failure	4	2	The balloon control system has a comparatively low TRL of 6, and therefore is likely to perform not as expected. However, it is used only for recovery and does not put main mission into danger.
B-COMM-01	Balloon communication system failure	1	4	The balloon is going to drift not more than 200 km from the ground station, which is not a large distance considering the technology level. If the connection is lost, no commands can be sent during the rocket launch and descent procedures.
B-REC-01	Parachute deployment failure	1	4	The parachute is used only when a mission abort is needed. Failure to open the parachute would lead to a critical damage on the payload during landing. It's catastrophic, because the payloads are going to be damaged.
B-REC-02	Landing on unsuitable surface	2	2	There is a risk that the landing might lead to the structural damage of the gondola and mechanisms inside it. This will affect the reusability of the gondola and increase recovery costs.
R-STRUCT-01	Rocket structural failure	1	4	This event can be caused by a change in operating conditions or an improper design. It will cause a complete mission failure.
R-STRUCT-02	Unexpected loads on rocket	2	3	This can be caused by inadequate analysis of the design. It will lead to a critical impact because it can cause a complete failure or reduction in performance.
R-PROP-01	Solid rocket inadvertent ignition	2	4	The solid rocket motor is ignited in the incorrect setting. This can happen from induced currents activating the igniter, sparks or discharges, impacts, mechanical energy absorption or nuclear radiation. It will cause a critical safety concern.
R-PROP-02	The SRM chamber over-pressure	2	4	This will cause a mission failure because it could lead to the combustion chamber rupture, which will result in a loss of thrust. This can happen from chemical changes in propellant, incorrect chamber manufacturing and nozzle obstruction.

Risk #	Risk Event	Likelihood	Impact	Risk Description
R-GNC-02	Rocket GNC failure	2	4	Impact is catastrophic, as clients need would not be satisfied. The probability of this event is somewhat likely, as avionic subsystems fail infrequently.
R-COMM-01	Rocket communication system failure	2	3	This risk event is somewhat likely, due to uncertainties in the atmosphere. The impact is critical because it severs communication with the range safety officers and could hinder a needed control input from the ground.
GEN-COST-01	Project cost goes over budget	3	3	This event is likely due to the nature of designing complex aerospace systems. Its impact is critical because the project could fail, unless more investment is obtained.
GEN-COST-02	Project BEP is delayed	3	2	This can be caused by overrun development costs and time frames or reduction in the small satellite market. This event is critical as it will put at risk the overall success of the project.
GEN-TIME-01	Launch gets delayed	3	1	This event is likely to occur because the balloon launch system is sensitive to the weather conditions and might require additional time to get allowance for the launch.
GEN-TIME-02	Development goes over time budget	4	2	This can mainly happen from inadequate systems engineering procedures. This risk is common to complex aerospace projects hence it has a high probability. It will delay the BEP and causes a risk to the success of the project.
GEN-TIME-03	Missing the launch window	3	3	This event can be caused by multiple reasons: high winds causing the balloon to drift out of it's window, a failed first stage ignition of the rocket, or too long rise time. If the launch window is missed, payload would have to be returned to the ground.
GEN-MASS-01	Individual subsystem masses are over-budget	4	3	This event is very likely due to the nature of designing complex aerospace systems. Its impact is critical because it has the potential to snowball and drive the designs of subsystems to an unacceptable extent.
GEN-SEP-01	Separation failure	2	4	The mission profile encompasses multiple separations. If separation fails, the mission would have to be terminated and requirements will not be met.
GEN-EPS-01	EPS system failure	1	4	The electrical subsystem failures are unlikely. Its impact is catastrophic because it could sever the telemetry link and leave the on-board GNC computer without power.

5.8.2. Risk Mitigation

After the risks have been identified, approaches have been determined to mitigate them. The process can be seen in table 5.6. After the proposed mitigation efforts have been applied to the risk events, risks have been plotted in the post-mitigation risk map shown in fig. 5.6.

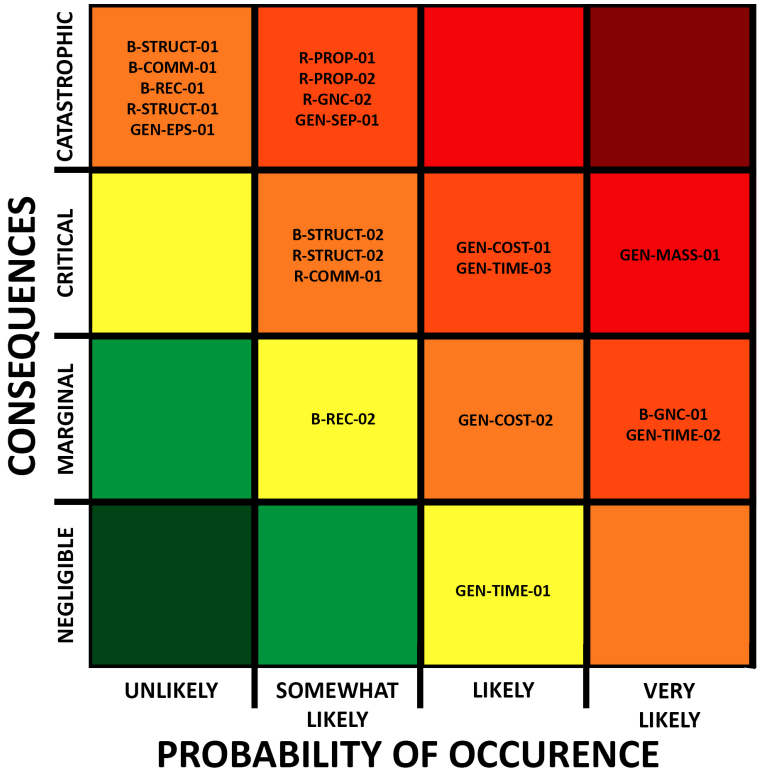

Figure 5.5: Pre-Mitigation Risk Map.

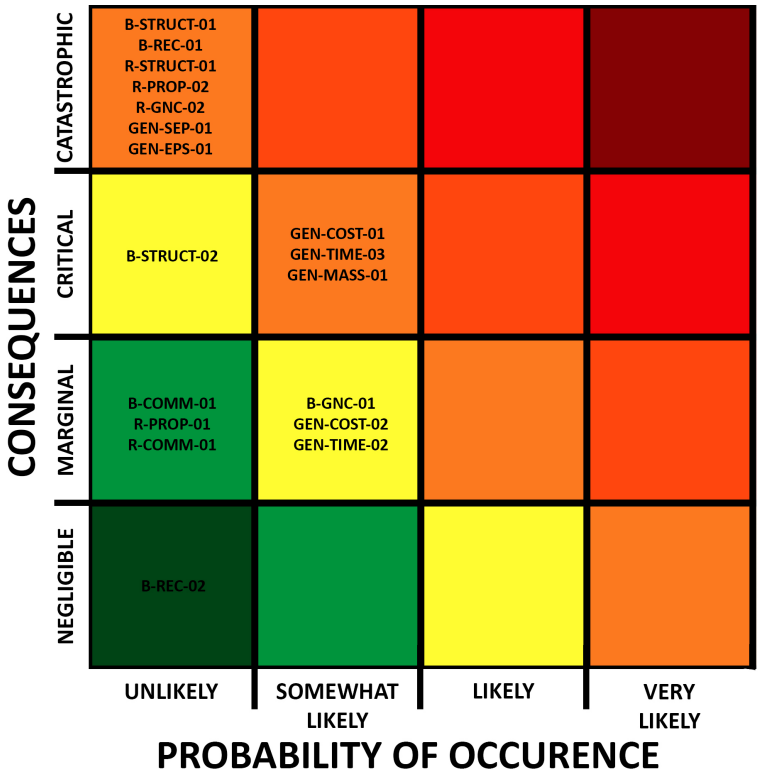

Figure 5.6: Post-Mitigation Risk Map.

Table 5.6: Risk mitigation strategy.

Risk #	Risk Event	Mitigation Strategy	New Likelihood	New Impact
Test in a related environment; Model creation				
B-STRUCT-02	Unexpected loads on balloon	Test should be done on the balloon loads during the windy day. Safety factor can be applied on the largest expected gust.	1	-
B-GNC-01	Balloon control system failure	Detailed analysis and test is going to be performed on the BGS.	2	-
R-PROP-02	The SRM chamber overpressure	Likelihood of this event is going to be reduced by proper inspection of grains before the use and limits on storage life.	1	-
R-GNC-02	Rocket GNC failure	Mitigation is done by detailed simulations and flight test of the complete system.	1	-
GEN-SEP-01	Separation failure	Probability of the event is reduced by lab testing all separation mechanisms.	1	-
GEN-TIME-03	Missing the launch window	Flight test of the balloon will allow for the better prediction of ascend trajectory and velocity.	2	-
Modification in design				
R-STRUCT-02	Unexpected loads on rocket	This event is mitigated by application of the safety factors.	1	-
B-COMM-01	Balloon communication system failure	The on-board computer capable of performing actions by itself is going to be implemented on board of the balloon. Therefore, the impact of communication system failure is reduced.	-	2
B-REC-02	Landing on unsuitable surface	Likelihood can be decreased by choice and preparation of suitable landing platforms. The shock absorbers will smoothen shock during landing.	1	1
R-COMM-01	Rocket communication system failure	Mitigation is done by creation of model and implementation of the on-board computer.	1	2
Utilisation of the system engineering tools				
R-PROP-01	Solid rocket inadvertent ignition	Likelihood is reduced due to safety procedures. Impact could be less critical, if loaded rockets are stored in secured location.	1	2

Risk #	Risk Event	Mitigation Strategy	New Likelihood	New Impact
GEN-COST-01	Project cost goes over budget	Mitigation is done by using proper budget management and contingencies.	2	-
GEN-COST-02	Project BEP is delayed	Mitigation is done by utilising systems engineering tools.	2	-
GEN-TIME-02	Development goes over time budget	Mitigation is done by using proper time-budget management and contingencies.	2	-
GEN-MASS-01	Individual subsystem masses are over-budget	Mitigation is done by using proper technical-budget management and contingencies.	2	-

5.9. REQUIREMENTS COMPLIANCE

During the previous phase of the project, system requirements have been derived based on the stakeholders, the environment and other matters, which could have an impact on the project. In this section, the system compliance with the requirements is analysed and presented in table 5.8. It should be noted, that compliance with some of the requirements, such as ALTAR-SH-05 or ALTAR-SH-06, would only be proven after a certain amount of performed missions or only after some years. At this stage of the project, compliance represents whether the designed system complies with a certain requirement.

Table 5.8: All of the requirements and compliance of the design with them.

Identifier	Requirements	Compliance
ALTAR-SH-01	The launcher shall put the payload into a circular orbit at up to 600 km altitude.	✓
ALTAR-SH-02	The launcher shall launch the payload into an orbit with an inclination up to 100 °C.	✓
ALTAR-SH-03	The launcher shall be able to accommodate payloads up to 35 kg.	✓
ALTAR-SH-04	The launch costs shall not exceed 50 k$/kg.	✓
ALTAR-SH-05	The launcher shall be ready for operational use by year 2022.	✓
ALTAR-SH-06	The launcher shall have a launch success rate greater than 0.9.	✓
ALTAR-SYS-01	The launcher shall provide a velocity increase of at least 8500 m/s.	✓
ALTAR-SYS-02	The launcher vehicle shall be controllable at all times.	✓
ALTAR-SYS-03	The launcher shall be available within 6 months of notice.	✓
ALTAR-SYS-04	The total cost per launch shall not exceed 1 750 000 $.	✓
ALTAR-SYS-05	The launcher system shall have a technology readiness level (TRL) of at least 6.	✓
ALTAR-SYS-06	The break-even launch shall take place by year 2028.	✓
ALTAR-SYS-07	The launcher shall support the release of multiple satellites in one launch.	✓
ALTAR-SYS-08	The launcher shall separate from the payload in orbit.	✓
ALTAR-SYS-09	The launcher shall integrate sustainability.	✓
ALTAR-SYS-10	The launcher shall be inspectable before the launch.	✓
ALTAR-SYS-11	The launcher shall be able to terminate at any point in the launch sequence.	✓
ALTAR-SYS-12	The upper stage shall be able to have a controllable reentry.	✓
ALTAR-GNC-01	The retrieval of the launcher components shall not impose any danger to the payload.	✓
ALTAR-GNC-02	The retrieval of the launcher components shall not impose any danger to anyone.	✓
ALTAR-PROP-01	The launcher shall have a maximum thrust to weight ratio of 9.	✓
ALTAR-PROP-02	The first stage of the launcher shall provide a total impulse of at least 5.78 MN · s.	✓
ALTAR-PROP-03	The second stage of the launcher shall provide a total impulse of at least 2.29 MN · s.	✓
ALTAR-PROP-04	The third stage main engine of the launcher shall provide a total impulse of at least 1.01 MN · s.	✓
ALTAR-PROP-05	The third stage orbit manoeuvring system shall provide a total impulse of at least 22.6 kN · s.	✓

Identifier	Requirements	Compliance
ALTAR-PROP-06	The launcher shall have a maximum chamber pressure of 3.5 MPa.	✓
ALTAR-PROP-07	The launcher shall posses an active thrust vectoring control system.	✓
ALTAR-PROP-08	The propulsion subsystem shall be able to terminate on command at any time.	✓
ALTAR-STR-01	The payload fairing shall withstand the maximum dynamic pressure loads of 140 N encountered during launch.	✓
ALTAR-STR-02	The launcher shall withstand the maximum vibrational loads of 0.6 g encountered during launch.	✓
ALTAR-STR-03	The launcher shall withstand the maximum thermal loads encountered during launch.	✓
ALTAR-STR-04	The launcher shall withstand the maximum axial acceleration loads of 9 g encountered during launch.	✓
ALTAR-STR-05	The launcher shall withstand loads encountered during the ascent phase of the balloon.	✓
ALTAR-STR-06	The launcher shall prevent any damage to the payload during launch.	✓
ALTAR-STR-07	The stratospheric balloon shall withstand the maximum shear loads encountered during the ascend.	✓
ALTAR-STR-08	The launcher shall encompass a multiple payload dispenser mechanism.	✓
ALTAR-STR-09	The launcher payload bay shall be able to store multiple payloads.	✓
ALTAR-STR-10	The launcher payload bay shall be able to accommodate payloads up to 250 dm^3.	✓
ALTAR-BAL-01	The maximum distance from the launch site to the landing spot shall not exceed 200 km.	✓
ALTAR-BAL-02	The stratospheric balloon shall be re-usable.	✓
ALTAR-BAL-03	No damage should be imposed to equipment during landing.	✓
ALTAR-BAL-04	Balloon shall be able to reach the altitude of 40 km.	✓
ALTAR-TT&C-01	The launcher shall be capable of sending telemetry data to the ground stations.	✓
ALTAR-TT&C-02	The launcher shall be capable of receiving command data from ground stations.	✓
ALTAR-TT&C-03	The launcher shall have on-board data storing capabilities.	✓
ALTAR-EPS-01	The launcher power supply shall be able to provide the expected peak power of 1736.6 W to the gondola segment subsystems.	✓
ALTAR-EPS-02	The launcher power supply shall be able to provide the total energy of 881.3 $W \cdot h$ to the gondola segment subsystems.	✓
ALTAR-EPS-03	The launcher power supply shall be able to provide the expected peak power of 8490.2 W to the rocket segment subsystems.	✓
ALTAR-EPS-04	The launcher power supply shall be able to provide the total energy of 4304.5 $W \cdot h$ to the rocket segment subsystems.	✓

This page is intentionally left blank.

6

VERIFICATION & VALIDATION

The design needs meet the requirements and accomplish it's intended purpose; launching one or multiple satellites with a combined mass of 35 kg into a prespecified orbit, with high certainty. To insure this, the launch system, models and requirements need to be verified and validated. Usually the validation and verification process is divided into five parts as mention in lectures by professor E. Gill and A. Cervone [53], which will be followed throughout this chapter. These five parts are:

1. Requirements Validation
2. Model Validation
3. Product Verification
4. Product Validation
5. Certification

The validation of the requirements has been established in the Midterm Report where all requirements have been checked on validity and careful wording [5]. Furthermore, certification can only be achieved after the launch system is produced, thus, both certification and requirment validaiton are not discussed further within this chapter. Furthermore, whether the product adheres to the requirements formulated will be checked within the chapter 5. So, only two parts of the verification and validation process remain; model and product validation, which both will be discussed in the following sections.

6.1. PRODUCT VERIFICATION

Production verification can be done in four ways, which are listed below:

- **Test**: Components and (sub)systems are tested under relevant environment to comply with requirements
- **Analysis**: Components and (sub)systems are verified through a mathematical
- **Demonstration**: Operation of test and qualification models shows compliance with requirements.
- **Inspection**: Components and (sub)systems are inspected and shown to conform to requirements.

6.2. MODEL VALIDATION

All models that have been used to estimate or predict the behaviour of necessary systems need to be validated to insure they estimate the reality to the degree that is necessary for this conceptual design.

Models can be validated through either experience, comparison or analysis. One of these three methods should be applied to each model that has been used throughout the analyses for this design. Although most models are discussed extensively in their respective chapter or section as well as their validation and verification, a short summary of all models used and the verification and validation efforts for them will now follow.

Trajectory Simulation & Optimisation Tool
Verification: By comparison with the TUDAT library simulation model using the same assumptions as made in the trajectory tool.
Validation: By comparison with the TUDAT library simulation model using the least amount of assumptions possible (so reality is simulated as closely as possible).

Structural Analysis Program:
Verification: By comparison with hand calculated results of simple geometries.
Validated: By comparison to the results of an ansys FEM analysis.

Vibration Analysis Program:
Verification: By comparison to hand calculated results for a step input.
Validation: By comparison to results attained for a simplified model.

ISA Model:
Verification: By comparison to results of existing ISA tools.
Validation: By comparison to acquired atmospheric data.

Drag Model:
Verification: By comparison to trajectory model.
Validation: By comparison to TUDAT Model and comparison with trajectory model results

Recovery Model:
Verification: By doing a sensitivity analysis and engineering judgement (do the changes make theoretical sense?)
Validation: By analysis to show correct integration of different validated parts.

Parachute Mass Estimation:
Verification: By entering dimensions of known parachute with known mass and comparing that to the result.
Validation:By analysis; correct integration of different mass estimations.

Propellant Grain:
Verification: By comparison to hand calculated results of simple grain geometries.
Validation: By comparison to a validated tool or real engine characteristics (both are unfortunately not available to us currently).

Re-entry Aerodynamics:
Verification: By comparison to hand calculated values for one stage.
Validation: By experience of Hankey [26]. Following his proposed model.

Total Mass Estimation
Verification: By careful inspection of program and mathematics used by multiple people.
Validation: By careful analysis as all mass estimation parts have been validated on their own, only their correct integration needs to be validated.

6.3. PRODUCT VALIDATION

To make sure all components of the design will fulfil their tasks once the launch system will be operated, each component will need to be tested for its respective performance. Data streams need to be established, ground operations need to be tested to be able to follow the launch time-line and structural components need to be demonstrated to be able to handle the maximum expected loads. There are four stages within the product validation process. All of which should be executed for each component of the launch system and are listed below:

- Interface Compatibility

- Mission Scenario Test
- Operation Readiness Test
- Fault Condition Testing

These procedures should be executed in this order; from the most basic to the most detailed of testing. Interface compatibility is the most basic and is there to ensure that, for example, data is sent in the right manner such that it can be handled by other software within the design or that the same diameter is used such that stages can be mounted to each other. Then, the mission scenario tests make sure the components can operate under the required conditions, which are followed by operation readiness test that ensure that all components can work together within the time intervals mandated by the mission timeline. Lastly, the whole system is tested within in mission relevant environment as to how it reacts to faults and incidents that might occur within the system (what happens if the system only receives half the data it expects etc.). A few important tests specific to this design are listed below:

- Tank pressure test
- Engine static fire test
- Balloon leak test
- Structural load test
- Ignition redundancy test

Furthermore, for almost all hardware, there should be qualification models that can be (destructively) tested to withstand the maximal thermal, mechanical and vibration loads.

6.3.1. BALLOON & ROCKET TESTS

There shouldn't be any loss of life associated with a failure if everything is done within the safety protocols. Subsequently the testing of the balloon, gondola and rocket can be kept significantly lower than, for example, the testing timeline for the Stratospheric Balloon and Cabin used by Felix Baumgartner, which in total had ten manned and unmanned tests with full sized balloons before the final jump. This would be very excessive for the current design, as too much Helium would be wasted in the process which, in the volumes necessary, would be very expensive. Therefore, the balloon and it's materials, as well as the cables connecting it to the gondola and rocket are tested in small scale. This will be followed by full scale tests, which do not reach full altitude. The first full scale balloon will reach 10 km as a test. After this, a full scale balloon, complete with gondola and rocket, is tested at 25 km, followed by a last full scale test at the target altitude of 40 km. If successful, the second full scale test should also include a test of the termination system.

This page is intentionally left blank.

7

Development & Operational Characteristics

7.1. Post-DSE Activities

After the preliminary design phase of the project has been finished, the next steps to be performed to get the launcher ready for operation by the year 2022 have to be considered. The first big phase would be preparing the more detailed final design. Afterwards, each system and subsystem would have to perform well in tests, or be redesigned. Finally, the launcher would be produced and be ready to deliver the payload to the orbit. Project design & development (PD&D) logic shows logical order of actions which are going to be executed in the post-DSE phase of the project. The PD&D logic can be seen in fig. 7.1. The Project Gantt Chart showing an estimated start and end date of each post-DSE action can be seen in fig. 7.2.

7.2. Production Plan

There are three main lines in fig. 7.3 and fig. 7.4. The middle line is the assembly line where all subsystems and large parts are integrated. The lines above or underneath the assembly line are the sub-assembly lines. The rounded rectangle blocks are components that are manufactured and assembled in-house. The ellipse blocks are components that are manufactured or assembled at original equipment manufacturers (O.E.M.), but that component is installed in-house. The first number in the blocks indicate the launch system element. The second number indicates to which integration process it belongs. The third number indicates the subsystem that belongs to that integration process. The fourth number gives the component that belongs to the subsystem. The letters are appointed to processes that are very similar. The numbering does not define the sequence in which the activities occur. The order from left to right gives the chronological order of activities.

Points of interest in this diagram are; firstly, in the beginning there are lot of work forces on the rocket work floor. After the first rocket manufacturing phase, they will move to balloon or gondola. Since the rocket consists of more parts and more larger parts, more resources should be put there such that the production rates increase. Secondly, as can be seen in fig. 7.3, the payload fairing shell is manufactured, but not integrated. This is done on purpose, since the payload still has to be integrated. The payload integration is not part of the production plan. It is part of the mission functional flow block diagram seen in fig. 2.3. Thirdly, in the balloon assembly, it can be seen that the length of the arrow is longer than the average arrow length. This indicates that the balloon manufacturing process takes longer than the other processes in the gondola manufacturing procedure. So it is relative only relative to the gondola manufacturing procedure.

The logic where employers work faster and more efficient over time, thus reducing the production costs, can be described by the learning curve. The learning curve effect is maximal when the amount of identical component that are used in a system are maximal. In this case, the propellant mixture is identical for all three stages. Also, the grain pattern for stage 1 and 2 are the same. Furthermore, the nozzle of stage 1 and 2 are almost identical. This makes the aforementioned components more cost

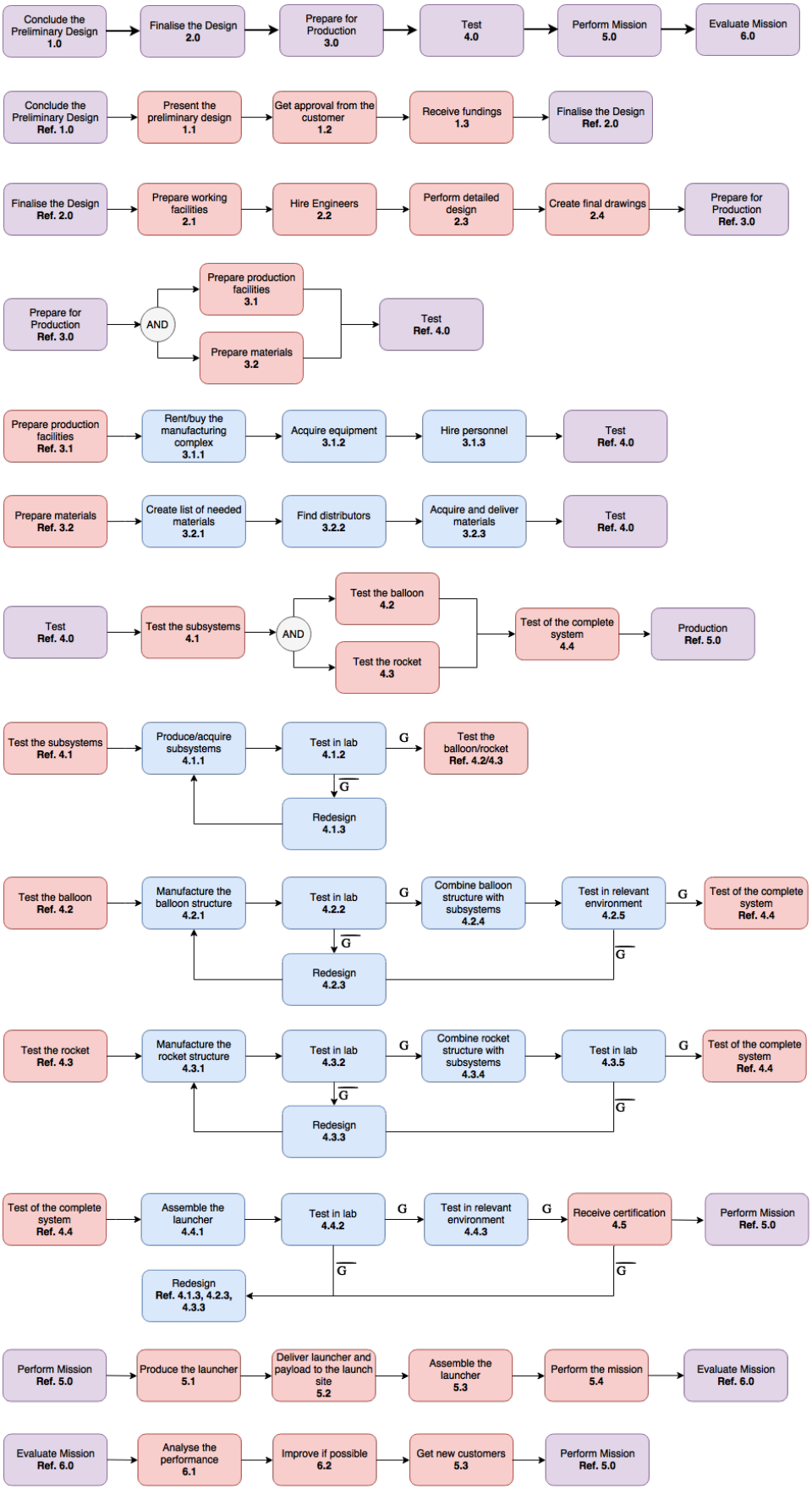

Figure 7.1: Project Design & Development Logic representing the post-DSE actions.

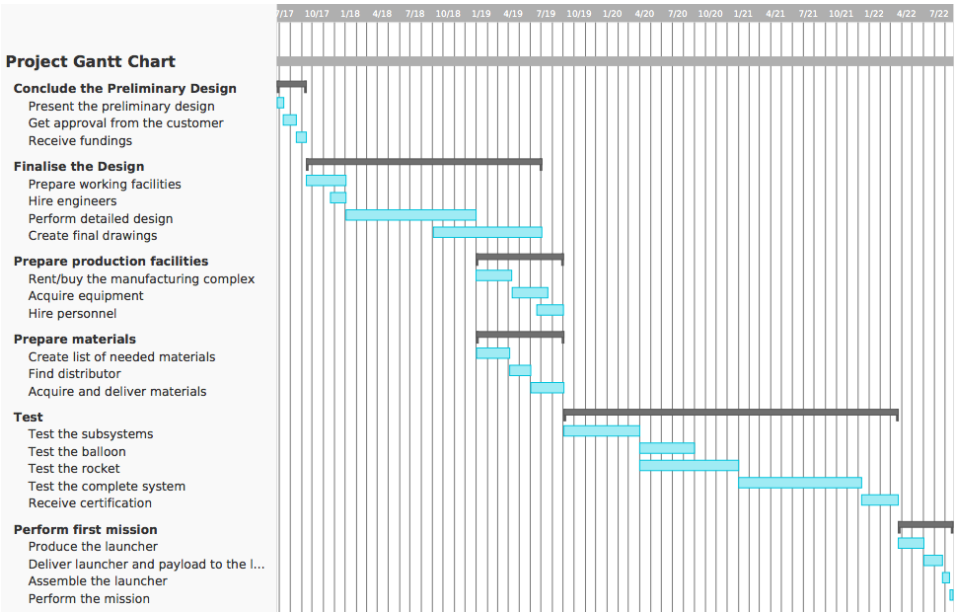

Figure 7.2: Project Gantt Chart.

effective in a shorter time frame than for other components. This production plan is designed for a nominal production rate of 40 to 50 launches per year, which is the desired nominal production rate. In the beginning of the company, it will not have enough capital to start with large production facilities which can facilitate this production rate. Many operations will be executed in series instead of parallel, increasing the production time. This is not a problem according to the forecast table 8.2 from the business plan. There it can be seen that 44 launches per year will be reached in 15 years. In this time, more capital and investments can be gained for production facilities. This production strategy will assure that the production facilities will not overproduce such that overcapacity of this product will be avoided.

7.3. OPERATIONS & LOGISTICS

The viability of a project is not only dictated by the technical feasibility, but also by the operations and logistics required for the launcher to perform its mission. In this section, the operations and logistics of transportation, assembly and launch were investigated. Concluding, these logistics, even though need to be further considered, do not impose an impossibility on the project.

7.3.1. TRANSPORT AND ASSEMBLY LOGISTICS

Once the launcher is produced, it needs to be packed, transported to and assembled in the selected launch location. First, the launch location needs to be chosen. Since the balloon has a drift radius of 200 km, a remote launch location needs to be chosen. The pre-selected launch locations were: Esrange Space Center in Sweden, widely used for balloon launches, Kourou Space Center in French Guinea, common launch location for European Launchers, and a launch site from international waters. Based on the drift radius, Korou was discarded since there are populated villages in range. From the simulation tool, Esrange could not be chosen, since the trajectory of the rocket puts it above populated areas before reaching space and the first stage could potentially fall in these zones. Therefore, a launch from a ship in international waters in the Atlantic Ocean was chosen.

Due to the remoteness of the launch location selected, the logistics of transporting the required

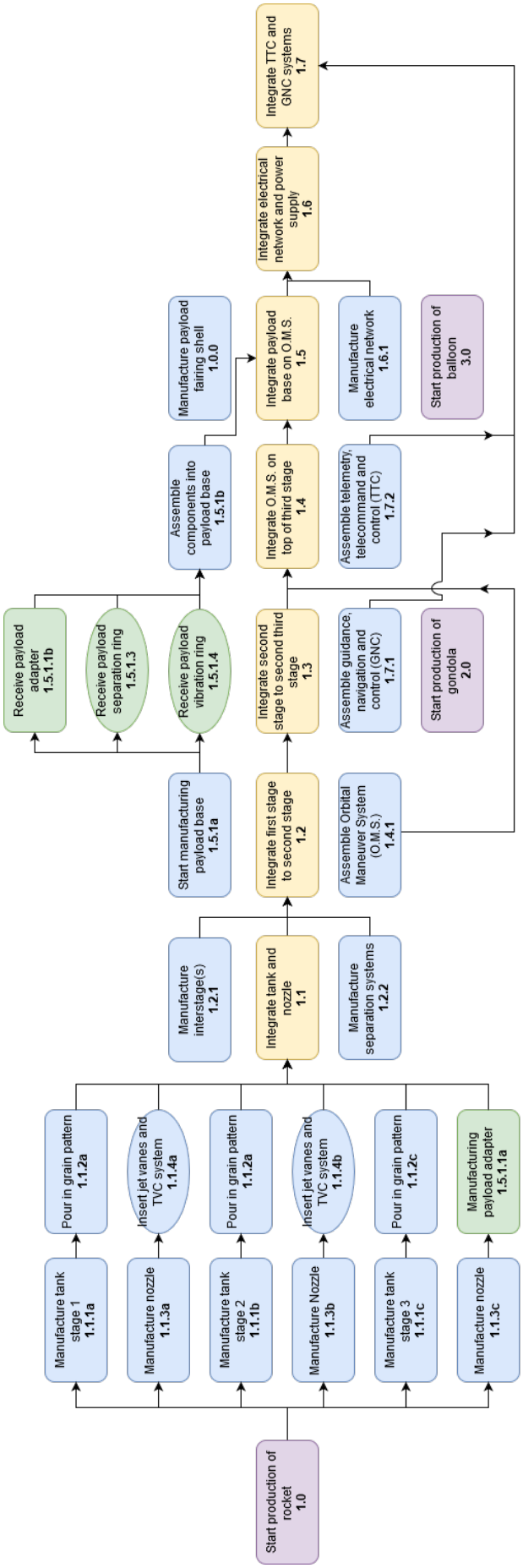

Figure 7.3: A flow diagram of the production plan. Blocks that are aligned on the vertical axis are processes that are executed in parallel. On the horizontal axis are processes that are executed in series.

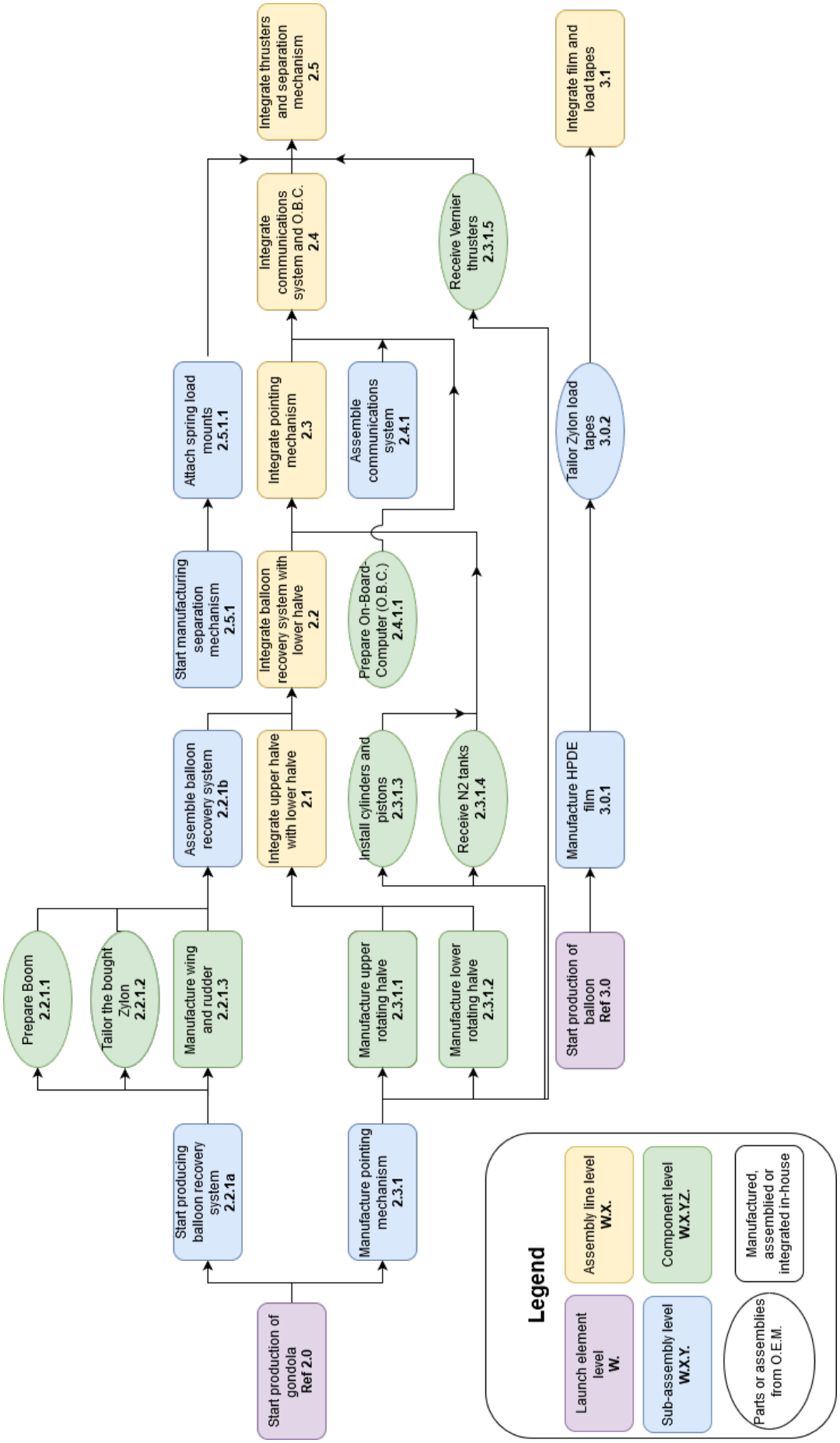

Figure 7.4: The second part of production plan flow diagram.

hardware and personnel to such a location need to be checked. In order to do so, it was assumed that the rocket would be manufactured at the production facility established in Delft, assembled in the Portuguese archipelago of Azores and launched from a barge sufficiently away from the archipelago. By assembling it in this archipelago, it allows the vehicle to reach every orbit without crossing any populated areas. Also, it was assumed that the gross mass of the components to be transported from Delft to Azores does not exceed 28.300 kg. This weight estimation, which is around 6 times the take-off mass of the rocket, allows to use the ISO standard 12.192 m shipping container and check for the logistics of transportation of these containers instead of each component independently. These containers are widely used for a variety of products ranging from food to dangerous and fragile components and reduce the complexity of the logistics.

First, the price of these containers need to be checked. Market values put the cost per unit of a 12.192 m container to be at €3578 for a used one and no more than €7156 for a new one [1], which is preferable over the rental of these due to the required long rental time.

Secondly, the route to be taken needs to be chosen taking into account two main factors: Transportation time and cost. Transportation time is important due to the unpredictability of the travel conditions which might damage the components. Also, the faster the transportation, the more time the team has to react in case of encountering problems. Multiple transportation methods were investigated. A combination of ground and sea travel was chosen to be the best one, and within this category, the following route was chosen. The route would start with a transportation from Delft to Rotterdam's port by truck, which would take around 30-60 minutes to complete. This road haulage has an approximate cost of €277. Next, the container would be shipped by cargo ship to Horta´s port, with a transshipment in Leixoes port and an estimated travel time of 10 days. This trip has an approximate cost of €250 for Terminal Handling Services of Rotterdam´s port, €110 for the Rotterdam Port fee, € 1798.51 for the port to port trip and additional charges of €120 for the Terminal Handling Services of Horta´s port. [2]. Summarising, the total cost for transporting a 12.12 m container of under 28 300 kg from Delft to the assembly location of Faial Island will take 10 days and € 2,555.51 to complete and is shown in fig. 7.5 [3].

Next, once the components reach the island, they need to be assembled, so an assembly facility needs to be created. Faial Island is approximately 173 km^2 and has approximately 15000 inhabitants. Thanks to the availability of terrain for sale in this location, an assembly factory in this island is assumed not to be a problem. The assembly process will consist of introducing the solid fuel into the rocket stages and assemble each stage together. At the same time, the gondola will be assembled, ready to be connected to the balloon. Next, the payload will be introduced into the fairing and attached on top of the rocket. Three main components will be present ready to be loaded in the barge: The rocket with the payload integrated, the gondola and the deflated balloon.

Figure 7.5: Transportation from Delft to the Portuguese island of Faial

[1] http://www.containeralliance.com/informative-articles/shipping-container-prices/used-shipping-container-prices-and-costs/
[2] https://www.icontainers.com/quotes/FCL/NLRTM/PORT/NL/PTHOR/PORT/PT/
[3] https://www.searates.com/reference/portdistance/

7.3.2. LAUNCH LOGISTICS AND OPERATIONS

After the aforementioned components have been assembled, they need to be transported back to the port, set into a boat, and shipped to the launch zone. During the transportation to the launch area, the rest of the components need to be attached together, and once the barge is stationary, the balloon will start to be inflated. This inflation, which would take around 45-60 minutes, is a critical part of the mission. While most of the risks have been minimised by choosing Helium as the gas, there is still the risk of damaging the balloon while inflating which would abort the mission.

When the balloon is fully inflated and generating enough lift, the balloon will be released, the final step will be releasing the gondola and the rocket. Once the launch system has been fully released, the barge will set a course to the expected landing zone of the balloon and gondola in order to retrieve them. When this mission is performed, the barge will go back to Faial Island, where the balloon and gondola will be checked and prepared for the next mission.

This page is intentionally left blank.

8

BUSINESS PLAN

A business plan is a road-map in which the project financials are explained. In this chapter, a business plan for the ALTAR launch system will be developed. First, a market analysis that will allow to position the product will be explained. Afterwards, the business goals for the system will be developed. To conclude, a cost analysis in which the costs for the whole project will be investigated and the financing, income forecast and project profitability will be calculated.

8.1. MARKET ANALYSIS

The market, as defined in the *Systems Engineering & Technical Management Techniques, Part I* reader, is a pocket of latent demand [52]. Through a thorough market analysis, this demand was identified. The growth of the small satellites market defines a demand for a flexible and affordable launcher for small payloads. For the purpose of this project, the market can be seen as the Earth-orbiting, under 50 kg satellite launchers. In this section, the market dynamics, the possible customers and the competition will be discussed.

8.1.1. MARKET DYNAMICS

The historical development of the small satellites market, together with future predictions, will be explained in this section.

The growth of the small satellite sector was made possible by technological progress, both in hardware and software components. These advances are allowing a progressive miniaturisation of the payload, which becomes more dense in scientific capabilities and computing power. An example of this when applied to electronics is Moore's Law.

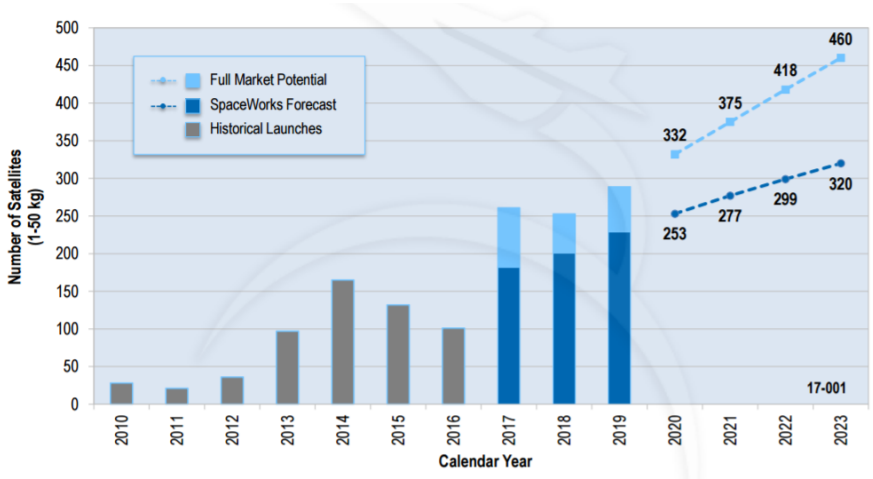

Figure 8.1: Small-satellites market historic data and predictions 2010-2023 [2]. It is possible to see the expected growth.

Figure 8.1 indicates that during the 2011-2014 period, the small satellite market grew considerably. This is due to two main reasons: firstly, the boom of universities interested in launching their own satellites. Secondly, due to the first launched satellite constellations by companies such as Planet Labs, which sent 98 nanosatellites in the period 2012-2014. Planet Labs' fast deployment accounted for approximately one third of the total number of small satellites launched during that period [1].

During the last two years, the number of small satellites launched decreased from approximately 155 in 2014 to 100 in 2016. This was mainly due to three launch failures in this period: Antares, Falcon 9 and Super Strypi, which resulted in the combined loss of 51 small satellites [2]. These failures produced launch delays which decreased the number of ride-share opportunities for small satellites, and consequently the launched ones in the 2015-2016 period.

The aforementioned delays grounded many, already built, small satellites that justify the predictions of a significant increase of demand in the next couple of years.

According to the Euroconsult firm, around 3600 small satellites will be launched in the next ten years, with a corresponding market value of 22 Billion USD (manufacturing and launch) [54]. In addition, the 2017 Nano/Microsatellite Market Forecast projects a market potential of 2390 small satellites in the 2017-2023 period [2]. This gives a growth rate of 226.53 % in the next 5 years. This rapid growth in the next years is also in compliance with the expectations of the Satellite Industry Association [3].

8.1.2. THE CUSTOMERS

In this section, a closer look was taken at the customer characteristics. This allowed a better understanding of the customer´s needs and wishes which affected the design strategy.

The first type of customers are universities. These are testing their satellite hardware and software mainly as proof of concepts. They are generally characterised by a low budget, which might affect their launcher choice.

These customers are followed by research institutions such as the Netherlands Aerospace Centre NLR and the German Aerospace Centre DLR, which in general have the same goal for their satellites as universities, but they have a somewhat larger budget.

Space agencies such as ESA and NASA, are customers that mostly have satellites equipped with proof-of-concept technology to be tested. These technologies are of a broader field than the ones from universities and research institutions. For example NASA has life sciences experiments carried aboard nanosatellites. These agencies have the largest budget of all customers. They might also be interested in taking part of funding this project.

The next type are already existent private companies and start-ups, such as PlanetLabs and Astrocast. These companies are creating constellations of small satellites with diverse applications such as: Imaging Earth at a high resolution or providing global internet access in the near future.

Finally, other customers can be lower level educational facilities as schools, which currently rely on free launches offered in programs by space agencies and private citizens with high acquisitive power interested in accessing space.

One thing that characterises all these customers is that they are dependent on either piggyback launches or rideshare launches, since there are no dedicated nanosatellite or microsatellite launchers yet. Even though these systems might reduce costs with respect to dedicated launchers, they have important disadvantages that the customers would like to see changed: First, their flexibility

in scheduling is very limited, which makes them have to book a flight well in advance (more than 6 months). Secondly, this makes them dependant on more important third parties, which might subject them to delays. Finally, flexibility of orbits, which requires the customers to design for non-optimal conditions.

8.1.3. THE COMPETITORS

While the small payload to orbit launchers form a highly competitive market, most of the companies currently involved have not yet finalised the development of the necessary technology. In this section, a current overview of the companies competing to gain market share will be given. As shown in section 8.1.3, the diversity of companies involved, represented by the different types of concepts proposed, will affect the marketing strategy. Also, the most important field of play will be the price per launch, which needs to be reduced as much as possible to be able to gather as much market share as possible. The average cost per kilo calculated from section 8.1.3 is $44k/kg. ALTAR will aim to have a 20% lower price, bringing the cost down to $39k/kg in order to obtain price leadership in the market.

Table 8.1: A selection of competitors that indicates the diversity of the sector and its potential.

Organisation	Vehicle Name	Concept	First Launch	Payload [kg]	Launch Cost [M$]	Cost/mass [k$/kg]	Altitude [km]
ARCA Space Corporation	Haas 2CA	SSTO aerospike	2018	100	1	10	LEO
Interorbital Systems	NEPTUNE N5	SSTO/modular	2015	40	0,25	13	310
Nanoracks	Platform-3	Stationary Rack on ISS	2013	8	0.28	35	370
Swiss Space Systems	SOAR	Air Launch/Spaceplane	2017	250	10	44	400
Rocket Lab	Electron	MSTO	2016	150	4,9	45	500
Virgin Galactic	LauncherOne	Air Launch with MSTO	2017	225	10	45	LEO
Aerojet Rocketdyne	Super Strypi	MSTO	2015	250	12	48	400
CubeCab	CubeCab	Air Launch	2017	5	0,25	50	400
Generation Orbit	GOLauncher 2	Air Launch	2018	44	2.5	57	LEO
Lin Industrial	TAYMIR	MSTO	2020	180	0,6	60	LEO
Orbital ATK	Minotaur I	MSTO	2000	460	28	61	400
Zero2Infinity	Bloostar	Balloon Assisted	2018	75	4.5	60	600

8.2. BUSINESS GOAL

The next step in developing a business model is to establish a market share goal. As decided, the launch system shall have an approximate break even point in 15 years time. In this time, the number of launches has to increase from 0 % to the decided market goal of 20% by the end of 2038. In order to do so, a rapid growth logistic function will be chosen to represent the yearly goals [55]. This function will be defined by:

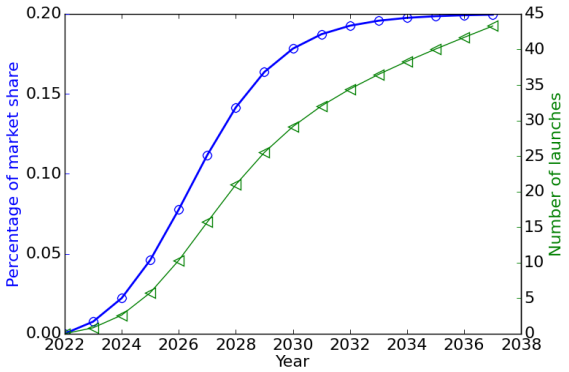

Figure 8.2: Percentage of market share and number of launches required per year

$$y = \frac{0.2x}{x + e^{1-7x}} \tag{8.1}$$

This equation represents the percent-

Table 8.2: Projected number of small satellites built, expected percentage of market share and number of commercial launches per year.

Year	Projected number of small satellites	Percent of market share	Number of launches
2022	299	0	0
2023	320	0.7	1
2024	343	2.21	3
2025	365	4.59	6
2026	388	7.77	11
2027	410	11.16	16
2028	433	14.15	21
2029	454	16.36	26
2030	477	17.82	30
2031	499	18.72	32
2032	522	19.26	35
2033	544	19.57	37
2034	566	19.75	39
2035	689	19.85	40
2036	691	19.99	42
2037	693	20	44
Total	**7693**	**-**	**383**

age of market share per year from 2022 until 2037 and is shown in fig. 8.2. As shown, starting slow, it has a rapid growth between the 3rd and 10th year, typical in the tech sector, to reach an equilibrium of the aforementioned 20% market share by the end of 2038. After 2038 another business model of sustainable growth should be implemented. The same figure also represents the number of launches expected every year. The number of launches was calculated assuming an average mass per satellite of 12 kg, since the market expects this mass class to grow significantly during the next 20-30 years [8].

As the market of small satellites is expected to continue growing during the next 20-25 years, a constant market share means a growth in the number of launches. The projected number of small satellites to be launched was linearly extrapolated from the data presented in fig. 8.1 and is summarised in table 8.2, together with the yearly percentage of market share and number of launches required to put these satellites into orbit.

8.3. COST ANALYSIS

To ensure that the cost requirement is met, cost analysis of the ALTAR system must be performed. This includes estimating the development, production, operation costs and salaries of the system. The cost analysis is broken down into the costs for the rocket in section 8.3.1, the balloon in section 8.3.2 and the interface in section 8.3.3. Moreover, in section 8.3.4, the operational costs are calculated for the full system. Next, the cost of salaries for the company is estimated in section 8.3.5 and then, in section 8.3.6 an overview of the total system costs are presented in the form of a cost breakdown. In addition, a financing plan and the predicted income statement per year are presented in section 8.3.7 and section 8.3.8, respectively. Finally, the profitability of the project is described in section 8.3.9, by calculating the return on investment (ROI).

8.3.1. ROCKET COSTS

The development cost is determined by one CER in eq. (8.2) [56]. The f_{tvc} equals 1.15 for stages with thrust vector control. The system engineering factor, f_0, corrects for the overall system development cost and the development of the interfaces between stages. This factor $f_0 = 1.4$ for an air-launched, 3 stage rocket. The development standard factor, f_1, takes the nature of the project into account. For air-launched vehicles, $f_1 = 0.9$. It is assumed that the development costs for the three stages are not separate, but lumped into one development cost using the combined stages propellant mass. This assumption is made because the engines are similar to each other. They all have the same propellant composition and chamber pressure. The first two stages have the exact same propellant grain geometry (internal stars), burn time and radius. The first and second stages only have a different length and thrust. The differences between the first, second and third stages is that the third stage is an end burning grain with a different thrust and size. This will slightly change the required thermal liner and the design of the combustion chamber structure.

$$DC_{Small\,SRM} = f_0 \cdot f_1 \cdot f_{tvc} \cdot 16.8 \cdot \left(\frac{M_p}{1000}\right)^{0.32} = 1.4 \cdot 0.9 \cdot 1.15 \cdot 16.8 \cdot \left(\frac{3732}{1000}\right)^{0.32} = €37.1M \quad (8.2)$$

To estimate the first unit production cost for the rocket stages, the CER in eq. (8.3) is used [57]. In this equation, f_8 is the country productivity factor. This value is equal to 0.73 for Germany, and this value is used for this cost estimation for production in The Netherlands. f_{10} is the cost engineering reduction factor, and this is equal to 0.5, because extensive cost engineering will be applied throughout the program. f_{11} is the commercial cost reduction factor and is equal to 0.45, due to the lack of governmental contract requirements and interference. With the inert masses of stages one, two and three equal to 177 kg, 173 kg and 50.2 kg, respectively, the total first unit production cost for the rocket stages is €3.3M.

$$PC_{ESS} = 2.75 \cdot M_{inert}^{0.412} \cdot f_8 \cdot f_{10} \cdot f_{11} \quad (8.3)$$

8.3.2. BALLOON COSTS

The development costs of the balloon have to be estimated. The mission development costs for typical high volume stratospheric balloon related mission range from €5M to €10M [1]. Therefore it is estimated that the development costs are €7.5M.

To estimate the first unit production cost of the balloon, the Stratos mission financed by Redbull was used as the starting point. The total cost of this balloon was declared to be equal to $250000[2] and, knowing its radius to be of 64.6 m as specified by the Stratos Mission website [3], it results to have a total cost per meter of radius of $3483. Now, eq. (8.4) is used to compute the first unit production cost of the balloon.

$$C_{B_P} = C_{STRATOS} \cdot R_B \cdot ER \cdot PP = 3483 \cdot 78.2 \cdot 0.9 \cdot 0.3 = €81,711 \quad (8.4)$$

[1] http://bopps.jhuapl.edu/ballooncraft/index.php
[2] http://www.theaustralian.com.au/news/world/felix-baumgartners-plunge-from-stratosphere-breaks-broadcast-records/news-story/204e359cb84e66cc215b9fce5b28f074
[3] http://www.redbullstratos.com/technology/high-altitude-balloon/

Where $C_{STRATOS}$ is the unit production cost of the Stratos balloon, R_B is the radius of the balloon as taken from table 4.4, ER is the exchange rate between US Dollar and Euro [4] and PP is the percentage of the production cost over the total cost of a classic aerospace product as taken from the systems engineering reader of TU Delft [45].

8.3.3. INTERFACE COSTS

To estimate the development costs of the interface, it is assumed that it should not be more than 30% of the development cost of the balloon. In fact, the gondola is mainly composed by components that could be bought directly from retailers (cold gas thrusters, pneumatic pistons, on board computers) or by relatively simple ones (N2 tank, batteries). Therefore, this number is taken and the development cost of the interface results to be of €2.25M.

To predict the production cost of the interface, it is assumed that this should not exceed 1.33 times the cost of the recovery system estimated in section 4.10.2 based on engineering judgement. Therefore, the production cost of the interface is calculated to be equal to €300,000.

8.3.4. OPERATING COSTS

The operating costs of the entire system are divided into maintenance, balloon gas, transportation and launchpad (LP). In section 5.5, it is calculated that, on average after each launch, 79.35 h of maintenance are needed. According to Erwin Mooij, Professor at TU Delft, the cost of an engineering hour (EH) in 2017 can be assumed to be equal to €150, a number that is used for cost budgeting at ESA. Correcting this number for inflation, as taken from forecasts of market analysts [5], this cost should become of €168.7 in 2023, the year of the first launch. Therefore, in 2023 the cost per launch for maintenance (MC) can be calculated using eq. (8.5).

$$MC = EH \cdot MTTM = 168.7 \cdot 79.35 = €13383 \tag{8.5}$$

The balloon gas costs are calculated by determining the amount of Helium that is spent on each mission. According to the results of the Python ascent simulation program, it is necessary to release around 70% of the gas contained in the balloon in order to get it back on the ground. Taking a margin on this number, it is estimated that 20% of the gas contained in the balloon could be recovered. That means that for each launch, 942.6 kg of Helium will be expended. The price of Helium (PHe) is approximately of 52 \$/kg [6]. Using eq. (8.6), the cost of Helium per launch (C_{He}) can be calculated.

$$C_{He} = M_{He} \cdot 0.8 \cdot PHe \cdot ER = 1178.2 \cdot 0.8 \cdot 52 \cdot 0.9 = €44112 \tag{8.6}$$

Transportation cost per launch is calculated in section 7.3 and it is equal to €2658, assuming that one container can only carry the parts and the material needed for one launch. The cost associate with the rental of the launchpad per mission is estimated to be equal to €10000 based on engineering judgement, keeping in mind that this cost should be comparable to the one of large balloon launches.

8.3.5. SALARIES

First of all, it has to be specified that salaries that the company has to pay for development, production and maintenance are already accounted for in the previous parts of section 8.3 because of the

[4] Data taken on the 23.06.2017 from https://www.bloomberg.com/quote/EURUSD:CUR
[5] https://knoema.com/zobdrl/euro-area-inflation-forecast-2015-2020-and-up-to-2060-data-and-charts
[6] http://www.chemicool.com/elements/helium.html

nature of the equations used in order to obtain those cost estimates. Therefore, salaries have only to account for administration, organisation and operations that will occur during the years after the first launch.

Rocket Lab, which is estimated to be a company that could have a number of employees comparable to the ALTAR company, had 100 employees in June 2016[7]. Then, it is predicted that at least half of these employees will have a role in producing and maintaining the launcher system. Therefore, an average of 50 full-time employees still needs to be accounted for when estimating the cost of salaries. To account for the different annual salaries for the employees of the company (e.g. manager and janitor) it is chosen to use EH as the average cost of one work hour of the company. Then, using eq. (8.7), the cost of salaries in year 2023 can be calculated.

$$C_{sal} = HPY \cdot EH \cdot n_{employees} = 1674 \cdot 168.7 \cdot 50 = €14.1M \tag{8.7}$$

Where HPY is the amount of hours worked in a year, which was assumed to be equal to the amount of hours that an employee works on average in Germany, as taken from the "Handbook of Cost Engineering and Design of Space Transportation systems" [57].

8.3.6. COST BREAKDOWN

First of all, it has to be decided how many rockets, balloons and interfaces need to be produced every year. With a reliability equal to 0.915 as estimated in section 5.3, every 10 launches there is going to be a failure. That means that no parts of the launch system can neither be recovered nor reused. In addition, it is known that one rocket needs to be produced every launch, one balloon needs to be produced every 5 launches (lifetime of the balloon is 5 missions, see section 5.5) and that the interface needs to be produced only after an unsuccessful launch. Moreover, at all times there must be an extra rocket, a balloon and an interface to serve as backup in case of a mission failure. Considering these facts and using the number of launches per year as estimated in section 8.1, the production numbers from 2023 to 2037 can be calculated and are presented in table 8.3.

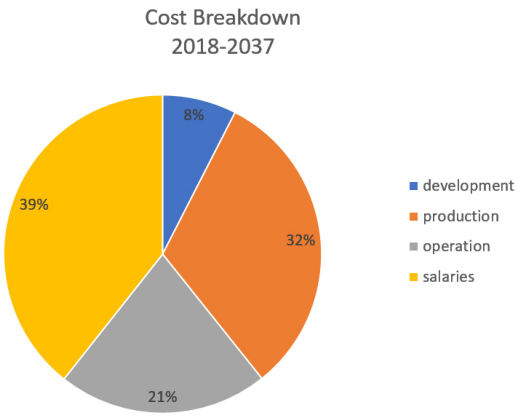

Figure 8.3: Cost breakdown structure 2018-2037

Secondly, learning curves are applied to the production costs of the balloon, the interface and the rocket. A learning curve can be described by eq. (8.8), which takes into account a reduction in cost as the series number of the product increase.

$$C_y = C_0 \cdot SN^{bl} \tag{8.8}$$

Where C_y is the unit cost, C_0 is the first unit cost, SN is the serial number and bl is the slope of the learning curve. bl is assumed to be equal to -0.3219, which represents a learning factor of 80%, a typical number in the aerospace industry according to [57]. Equation 8.8 is now applied to the production costs of the balloon, rocket and interface and the respective learning curves are shown in fig. 8.4. As it can be noticed, the learning curve of the rocket has a bigger slope than the one of the

[7] https://rocketlabusa.com/

Year	Number of launches	Interface	Balloon	Rocket
2023	1	2	2	2
2024	3	0	1	3
2025	7	1	2	7
2026	12	1	3	12
2027	17	1	4	17
2028	23	2	6	23
2029	29	3	8	29
2030	33	3	9	33
2031	35	3	10	35
2032	39	4	11	39
2033	40	3	10	40
2034	43	4	12	43
2035	44	4	12	44
2036	46	4	12	46
2037	49	5	14	49
Total:	421	40	116	422

Table 8.3: Production table for the subsystems composing the ALTAR system for each operational year.

other systems. This is mainly due to the fact that the rocket is composed by three solid engines that are similar enough to be considered to contribute equally to the learning process during production. Therefore, even if in total 422 rockets will be produced, for the learning curve it is like this number would be multiplied by three.

Thirdly, the development costs have to be divided between the five years of development. This is done by assuming that each year, from 2018 to 2023, the same expenses for development will be made. This simplification is necessary because at this stage of the design, it is out of scope to estimate a development cost distribution over time. Finally, all of the costs are corrected for inflation according to forecasts of monetary devaluation in the Euro zone [8].

In fig. 8.3, the total cost breakdown from 2018 to 2037 is presented in percentages and a detailed cost breakdown per year is presented in table 8.4. It can be noted how the production cost of the rocket, the Helium cost and costs associated to salaries are dominant. This is explained by the fact that the rocket and Helium are expendable, whereas salaries are also accounting for part of the operation costs.

8.3.7. FINANCING

In order to finance the project, capital must be raised. A simplified financing model was constructed that is based on the following assumptions or decisions:

- Capital is raised in two different moments, once in 2018 to cover the development costs, once in 2023 to cover the company losses of the first years of activity;
- Capital is raised from investors selling them ownership share of the company and from banks in the form of fixed interest rate (FIR) debt;
- Dividends are paid to investors anytime a profit is made from the company;

[8] https://knoema.com/zobdrl/euro-area-inflation-forecast-2015-2020-and-up-to-2060-data-and-charts

Year	DEVELOPMENT			PRODUCTION			OPERATION				SALARIES	TOTAL
	Rocket	Balloon	Interface	Rocket	Balloon	Interface	Maintenance	Helium	Transportation	LP		
2018	742	150	45	0	0	0	0	0	0	0	0	937
2019	742	150	45	0	0	0	0	0	0	0	0	937
2020	742	150	45	0	0	0	0	0	0	0	0	937
2021	742	150	45	0	0	0	0	0	0	0	0	937
2022	742	150	45	0	0	0	0	0	0	0	0	937
2023	0	0	0	525	15	54	1	4	0	1	1412	2013
2024	0	0	0	532	6	0	4	18	1	4	1440	2005
2025	0	0	0	899	10	22	8	50	3	11	1470	2474
2026	0	0	0	1150	13	21	16	99	6	22	1499	2828
2027	0	0	0	1288	16	21	23	171	10	39	1530	3098
2028	0	0	0	1439	21	40	31	270	16	61	1561	3439
2029	0	0	0	1545	25	56	39	392	24	89	1593	3761
2030	0	0	0	1538	25	53	46	527	32	119	1625	3965
2031	0	0	0	1464	25	50	50	671	40	152	1658	4110
2032	0	0	0	1488	26	63	56	833	50	189	1692	4397
2033	0	0	0	1410	22	46	61	995	60	225	1726	4544
2034	0	0	0	1414	25	59	65	1175	71	266	1761	4836
2035	0	0	0	1361	24	57	68	1355	82	307	1797	5050
2036	0	0	0	1347	23	55	73	1544	93	350	1833	5317
2037	0	0	0	1363	26	67	78	1746	105	396	1870	5652
Cum.	3710	750	225	18765	301	663	620	9848	593	2232	24466	62174

Table 8.4: Cost breakdown per year where numbers are expressed in €10k.

Figure 8.4: Production cost reduction as the serial number of the unit produced increases representing the learning curve effect.

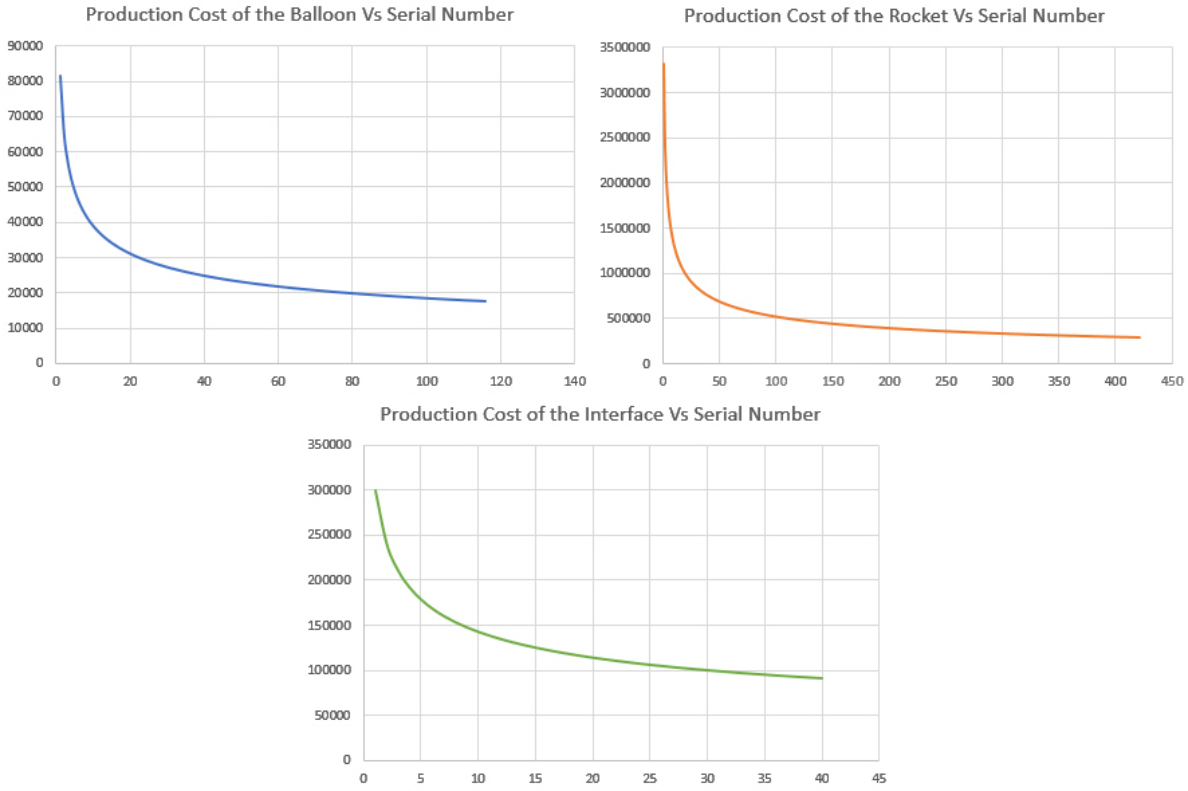

- The development debt is paid back starting from 2029 (10 financial years after the debt is issued);
- The second debt is paid back starting from 2033 (9 financial years after the debt is issued);
- The FIR is assumed to be 6% yearly. This is a very conservative number for the European area (comparable to the FIR before the 2008 crisis) according to current interest rates for issued debts as taken from an ECB report of January 2016 [58];
- Debt payments to the bank occurs yearly and their amount is constant for each of the two debts.

To decide about the financial structure of the company, it was decided that as little capital as possible should be borrowed from banks, keeping nonetheless control over the company. In order to achieve this, 49.5% of the company was decided to be sold to investors in the form of LLPs (Limited Liability Partnership), whereas 50.5% of the company should be owned by their founders, which would finance the business by debt from the banks. The owners would have unlimited liability whereas the partners (investors) would have limited liability corresponding to the money they invested in the company. In this way, the financial time line of the project can be drawn and numbers calculated, as shown in table 8.5, where PPMT indicates the principal payment and IPMT indicates the interest one. It can be noticed that the total principal payment is bigger than the total debt borrowed from the bank. This is due to the fact that for some years the debt cannot be paid back and therefore the interests keep accumulating making the total principal bigger.

Table 8.5: The Financial time line. Positive numbers represents money received by the company, negative numbers represents money that the company pay to the banks. All the numbers in the table are expressed in €10k.

Financial Year	**Capital from Debt**	**Capital from Investors**	**PPMT**	**IPMT**
2018	2366	2319	0	0
2019	0	0	0	0
2020	0	0	0	0
2021	0	0	0	0
2022	0	0	0	0
2023	3182	3247	0	0
2024	0	0	0	0
2025	0	0	0	0
2026	0	0	0	0
2027	0	0	0	0
2028	0	0	0	0
2029	0	0	-321	-254
2030	0	0	-341	-235
2031	0	0	-361	-214
2032	0	0	-383	-193
2033	0	0	-1192	-499
2034	0	0	-1264	-427
2035	0	0	-1340	-352
2036	0	0	-1420	-271
2037	0	0	-1505	-186
Total:	5548	5566	-8127	-2632

Table 8.6: The Income Statement Forecast for each year until the end of the ALTAR program. Numbers are expressed in €10k.

Financial Year	Sales	COGS	Gross Profit	Operating Expense	EBIT	IPMT	EBT	Tax Expense	NI
2018	0	-937	-937	0	-937	0	-937	-234	-703
2019	0	-937	-937	0	-937	0	-937	-234	-703
2020	0	-937	-937	0	-937	0	-937	-234	-703
2021	0	-937	-937	0	-937	0	-937	-234	-703
2022	0	-937	-937	0	-937	0	-937	-234	-703
2023	152	-594	-442	-1419	-1860	0	-1860	-465	-1395
2024	466	-538	-72	-1468	-1539	0	-1539	-385	-1154
2025	951	-932	19	-1542	-1523	0	-1523	-381	-1142
2026	1779	-1185	594	-1642	-1049	0	-1049	-262	-787
2027	2640	-1325	1315	-1773	-458	0	-458	-114	-343
2028	3535	-1500	2035	-1940	96	0	96	24	72
2029	4466	-1625	2840	-2136	705	2542	450	113	338
2030	5257	-1616	3642	-2349	1293	2349	1058	264	793
2031	5722	-1539	4183	-2571	1612	2145	1397	349	1048
2032	6385	-1577	4808	-2819	1989	1928	1796	449	1347
2033	6887	-1478	5409	-3067	2343	4990	1844	461	1383
2034	7407	-1499	5908	-3338	2570	4274	2143	536	1607
2035	7751	-1441	6309	-3608	2701	3516	2350	587	1762
2036	8304	-1425	6879	-3893	2986	2712	2715	679	2036
2037	8876	-1456	7420	-4196	3224	1860	3038	759	2278

8.3.8. INCOME STATEMENT FORECAST

Now that all the expenses have been computed, an income statement of the company prediction for each year of activities can be generated and it it illustrated in table 8.6. Here, sales are calculated by targeting the required price per kilo to SSO of €36,000 (see section 5.5) and applying a contingency of 10% as suggested by table 4.2, that results in a price of €32,000. Then, the sales per launch can be calculated, knowing that at least 47 kg to SSO will be sent each launch (see section 5.1, and the number of launches per year. COGS or cost of goods sold, that comprehend production costs. IPMT is taken from table 8.5 and they are not subject to taxation. Taxes are calculated assuming a tax rate of 25%, as common for Dutch industries with declared revenues greater than €200,000 [9]. The final column of table 8.6 shows the predicted net income (NI) of the company, which can be seen to be positive starting from year 2025.

8.3.9. PROJECT PROFITABILITY

To calculate the company's profit, eq. (8.9) can be used. It has to be noticed that profit is calculated only for the years when the NI is positive, in fact, negative income of the other years is covered by the debt and investments of the partners as explained in section 8.3.7.

$$profit = NI - PPMT€ \tag{8.9}$$

As can be seen in table 8.7, each year profit is payed out as dividends to the partners for a maximum of 49.5% and retained from the company for a maximum of 50.5%. The ROI up to 2037 is calculated

[9] https://www.duijntax.com/en/dutch-corporate-income-tax-rate

Table 8.7: Company profit forecast per year from 2028 to 2037, expressed in €10k.

Financial Year	NI	PPMT	Profit	Dividends to investors	Retained Earnings
2028	72	0	72	36	36
2029	338	321	16	8	8
2030	793	341	453	224	229
2031	1048	361	687	340	347
2032	1347	383	964	477	487
2033	1383	1192	191	94	96
2034	1607	1264	344	170	173
2035	1762	1340	423	209	213
2036	2036	1420	616	305	311
2037	2278	1505	773	383	391
Total:	12665	8127	4538	2246	2292

as the sum of dividends payed to investors divided by the sum that they invested in the company and results to be equal to 33.9%, which is really appealing for investors and therefore could attract capital easily.

This page is intentionally left blank.

9

Conclusions and Recommendations

The on-going growth of the small satellite market increases the demand for a flexible and affordable launcher for small payloads. The main purpose of this report was to investigate whether or not it is possible to design a small-payload launch system with the given requirements that were partially derived from a thorough market analysis. The driving requirements were that this launch system should be able to put a payload of 35 kg in to a sun-synchronous orbit at an altitude of 600 km, at a price of at most 50 k$/kg. Additionally, flexibility and sustainability should be integrated in case this does not conflict with the cost requirement.

The final launcher design consists of a three stage solid rocket booster that will be carried to an altitude of approximately 35 km with a stratospheric balloon. By launching from this altitude, at which 99% of the atmosphere is covered, the launcher leaps over the densest parts of the atmosphere allowing for a reduction in gravity and drag losses. This solution allows to launch the stratospheric balloon from international waters virtually anywhere in the world. Additionally, pollution of the lower layers of the atmosphere is prevented, making it a sustainable and innovative solution to the current market demand.

The launch service is able to put a payload of 47 kg in to the nominal sun-synchronous orbit at an altitude of 600 km at a price of 40 k$/kg. This makes the launch service cost competitive, as this is a 9% cost reduction with respect to the current average market price, exceeding the requirements set at the beginning of this project.

The capabilities of the launcher service extend from bringing a payload of 72 kg in to an orbit at an altitude of 300 km and an inclination of 38.5° to bringing a payload of 43 kg to a sun-synchronous orbit at an altitude of 900 km. This wide range of capability allows to account for varying customer and market demand.

This launch service distinguishes itself from other launch providers by being exceptionally sustainable. This is achieved by making use of helium for the stratospheric balloon and mainly solid propellants for the first three rocket stages. Helium is a non-toxic and inert gas and is also the second most abundant chemical element in the universe. The use of solid propellant is also less harmful and less dangerous than the use of hypergolic propellants, bi-propellants and mono-propellants. The re-usable stratospheric balloon will carry the rocket far above the ground, allowing to conserve the environment by preventing pollution to the lower inhabited layers of the atmosphere.

An additional feature of the launch service is that it requires merely 6 months of notice. This provides a solution for the piggyback problem in which the launch date, to which the small satellite manufacturers have to stick, is set for the big satellites.

ALTAR proves to be a sustainable, innovative, flexible and a cost efficient solution to a rising demand for a dedicated small-payload launcher.

To conclude, in case this research is used as a starting point in further works, some recommendations need to be addressed before beginning phase B of the design process:

1. A more detailed study on the possibility of using hydrogen as balloon gas should be performed. The high price of helium and the amount of it needed produces a very high cost that could be reduced if the use of hydrogen is chosen.
2. A more accurate drift model for the balloon shall be investigated. This will allow to perform a more accurate trajectory estimation and an optimisation of the launch location within international waters.
3. A guidance program for the ascent and descent of the balloon shall be investigated. This will allow for a predicted ascent and to predict where and when the balloon will land and where and were the ship would need to be.
4. An optimisation of the nose cone design for the required payload should be performed. As the aerodynamic loads are small, the payload fairing is currently over-designed and weighs as much as the weight the aerodynamic loads would create.
5. A more thorough investigation shall be performed on the separation mechanism between stages and between the balloon and rocket. Currently, it exceeds the scope of this design phase, but the use of pyro-bolts or similar devices might impose extra loads in the structure that have not been taken into account until now.
6. A detailed design of the nozzle wall contour and of the thermal protection in it should be performed.
7. The use of safer mono-propellants for the OMS should be investigated. Hydrazine is a toxic chemical that imposes safety problems during handling, which needs to be taken into account. If possible, the use of this type of highly toxic propellants should be avoided.
8. The interfaces between the TVC and the nozzle should be design and checked if it is feasible for the case here presented.
9. Load transitions between parts, specifically between interstages and tanks should be investigated to check for necessary extra weight in these zones.

BIBLIOGRAPHY

[1] Kulu, E., "Nanosatellite & CubeSat Database," Online Database, URL: http://www.nanosats.eu, [cited 24 May 2017].

[2] Doncaster, B., Williams, C., and Shulman, J., "2017 Nano/Microsatellite Market Forecast," SpaceWorks Enterprises, Inc., Atlanta, Georgia, USA, Feb. 2017.

[3] Bryce Space and Technology, "State of the Satellite Industry Report 2016," Satellite Industry Association, June 2016.

[4] "UCS Satellite Database," Online Database, Union of Concerned Scientists, Cambridge, Massachusetts, URL: http://www.ucsusa.org/nuclear-weapons/space-weapons/satellite-database, [cited 3 May 2017].

[5] Shambalov, A., Sanghera, B. S., Foulds, D. A., Salvi, G., Vadillo, J. N., Reverda, M., Johnson, N. A., van den Berg, R. J. F., Park, S. J., and Ge, Z. X., "Next Generation Affordable Small-Payloads Launch System, The Midterm Report," TU Delft, Delft, The Netherlands, June 2017.

[6] Roy, A. E., "Luni-Solar Perturbations of an Earth Satellite," *Astrophysics and Space Science*, vol. 4, Aug. 1969, pp. 375–386.

[7] Martin Marietta Corp., Denver, Colorado, *Program to Optimize Simulated Trajectories, Volume 1: Formulation Manual*, Apr. 1975.

[8] Shambalov, A., Sanghera, B. S., Foulds, D. A., Salvi, G., Vadillo, J. N., Reverda, M., Johnson, N. A., van den Berg, R. J. F., Park, S. J., and Ge, Z. X., "Next Generation Affordable Small-Payloads Launch System, The Baseline Report," TU Delft, Delft, The Netherlands, May 2017.

[9] "Space Systems Engineering - Margins and Contingency Module," National Aeronautics and Space Administration, 2008, URL: https://spacese.spacegrant.org/uploads/Margins%20Module/16.%20Margins_Module_V1.0.ppt.

[10] Yajima, N., Izutsu, N., Imamura, T., and Abe, T., *Scientific Ballooning*, Corona Publishing Co., Ltd., 2004.

[11] Brasefield, C., "Winds at Altitudes up to 80 Kilometers," Journal of Geophysical Research, Volume 59, Fort Monmouth, N. J., June 1954.

[12] Toyobo Corporation, Ltd., Osaka, Japan, *PBO Fyber Zylon: Technical Information*, 2005, URL: http://www.toyobo-global.com/seihin/kc/pbo/zylon-p/bussei-p/technical.pdf.

[13] Callister, W. D. and Rethwisch, D. G., *Material Science and Engineering*, 9th ed., J. Wiley & Sons Inc., 2014.

[14] Orbital Sciences Corporation, *Pegasus User's Guide*, 5th ed., August 2000, URL: http://www.brown.edu/Departments/Engineering/Courses/en176/2003%20Lectures/Meeting%203/peg-user-guide.pdf.

[15] Larson, W. and Wertz, J., *Space Mission Analysis and Design*, Kluwer Academic Publishers, Dordrecht, Boston, London, 2011.

[16] Anis, A., "Cold Gas Propulsion System - An Ideal Choice for Remote Sensing Small Satellites," *Remote Sensing - Advanced Techniques and Platforms*, 2012.

[17] Humble, R. W., Henry, G. N., and Larson, W. J., *Space propulsion analysis and design*, McGraw-Hill, New York, 2007.

[18] Sutton, G. P. and Biblarz, O., *Rocket Propulsion Elements*, 8th ed., John Wiley & Sons Inc., 2010.

[19] Spores, R. A., "Green Propellant Infusion Mission Propulsion System Development," *49th AIAA/ASME/SAE/ASEE Joint Propulsion Conference*, American Institute of Aeronautics and Astronautics, 2013, URL: https://doi.org/10.2514/6.2013-3849.

[20] Planetary Systems Cooperation, State Spring, Maryland, USA, *User's Manual for Mark II Lightband*, July 2014.

[21] MOOG CSA Engineering, Mountain View, California, USA, *SoftRide Shock and Vibration Isolation Systems*, Nov. 2015.

[22] Saw, A. and Al-Obaid, A., "Drag of Conical Nose at Supersonic Speeds," Online article, Subang Jaya, Malaysia, July 2013.

[23] de Córdoba, S. S. F., "100km Altitude Boundary for Astronautics," Online Database, URL: http://www.fai.org/icare-records/100km-altitude-boundary-for-astronautics, [cited 12 June 2017].

[24] Jacchia, L., "New Static Models of the Thermosphere and Exosphere with Empirical Temperature Profiles," *SAO Special Report*, vol. 313, May 1970, pp. 53–111.

[25] Benson, T., "Rocket Aerodynamics," Online Database, URL: https://spaceflightsystems.grc.nasa.gov/education/rocket/rktaero.html, [cited 9 June 2017].

[26] Hankey, W., *Re-entry Aerodynamics*, AIAA Institute, 1988.

[27] Titterton, D. and Weston, J., *Strapdown Inertial Navigation Technology*, 2nd ed., Radar, Sonar and Navigation Series, The Institution of Engineering and Technology, London, UK, 2004.

[28] "Launch Vehicle Catalog," Electronic database, EADS SPACE Transportation, 2004, 15th revision.

[29] "Safran's SpaceNaute navigation system chosen for new Ariane 6 launch vehicle," Press release, Safran, URL: https://www.safran-electronics-defense.com/media/safrans-spacenaute-navigation-system-chosen-new-ariane-6-launch-vehicle-20161130.

[30] Facciano, A. B., Seybold, K. G., Westberry-Kutz, T. L., and Widmer, D. O., "Jet Vane Control System Prototype Hardware Development for the Evolved Seasparrow Missile," Tech. rep., Raytheon Missile Systems, 2000, URL: http://www.dtic.mil/dtic/tr/fulltext/u2/a386519.pdf.

[31] Almatech, "Thrust Vector Control Systems for Solid Propellant De-Orbit Motors," , March 2015, URL: https://indico.esa.int/indico/event/73/material/0/8.pdf.

[32] Ahearn, R. L., "Development of Jet Vanes for Solid Propellant Missiles," *SAE Technical Paper*, SAE International, New York, USA, 1962.

[33] Sener Aerospace, *Electro Mechanical Actuators for Aerospace Applications*, 2014, URL: http://www.sener-aerospace.com/EPORTAL_DOCS/GENERAL/SENERV2/DOC-cw53cd2ec89270e/electro-mechanical-actuators-for-aerospace-applications.pdf.

[34] Aerojet Rocketdyne, *Data Sheet Bi-propellant Rocket Engines*, URL: http://www.rocket.com/files/aerojet/documents/Capabilities/PDFs/Bipropellant%20Data%20Sheets.pdf, [cited 12 June 2017].

[35] Orbital Systems, *2.4TSS3-3m S-Band TT&C Antenna System*, 2014, URL: http://www.orbitalsystems.com/wp-content/uploads/2012/09/MA-180-004-2.4TSS3-3m-S-S-Band-TTC-Data-Sheet-B.05.pdf.

[36] Atlanta Services, Software and Designs, *Link Budget Analysis: Error Control & Detection*, August 2013, URL: https://atlantarf.com/Error_Control.php.

[37] Arnold, S. S., Nuzzaci, R., and Gordon-Ross, A., "Energy budgeting for CubeSats with an integrated FPGA," *2012 IEEE Aerospace Conference*, pp. 1–14, pages.

[38] Nock, K., Aaron, K., Heun, M. K., and Pankine, A., "Aerodynamic and Mission Performance of Winged Balloon Guidance System," *Journal of Aircraf*, 2007.

[39] Markish, J., "Valuation Techniques for Commercial Aircraft Program Design," *Journal of Cleaner Production*, vol. 108, June 2002, pp. 169–182.

[40] SpaceX, *Falcon 9 Payload User's Guide - First revision*, 2009, URL: https://www.spaceflightnow.com/falcon9/001/f9guide.pdf.

[41] Orbit - Communication Without Boundaries, *Product Specification AL-1100-LSC*, 2003, URL: http://orbit-cs.com/wp-content/uploads/2015/03/Tri-Band__Product_Specification_V0113N.pdf.

[42] Knacke, T. W., *Parachute Recovery Systems Design Manual*, Para Publishing, Santa Barbara, USA, 1992.

[43] Zandbergen, B., "Aerospace Design & Systems Engineering Elements I," Lecture Notes, revision 1.05, Delft, The Netherlands, Aug. 2015.

[44] S.Turteltaub, "Personal conversation," Personal conversation, Delft, The Netherlands, June 2017.

[45] Hamann, R. and van Tooren, M. J. L., "AE3-S01 Systems Engineering & Technical Management Techniques Part II," Lecture Notes, Issue 1, Delft, The Netherlands, Jan. 2006.

[46] A. Martínez-Romo, J. J. S. B. C. F. R., R. González Mota and Candelas, I. R., "Effect of ultraviolet radiation in the photo-oxidation of High Density Polyethylene and Biodegradable Polyethylene films," *IOPscience*, 2015.

[47] Kinnison, S. T., Harry, *Aviation Maintenance Management*, McGraw-Hill, 2011.

[48] Zandbergen, B., "Aerospace Design & Systems Engineering Elements I Part: Launcher Design and Sizing," Course Reader, Delft, The Netherlands, Sept. 2013.

[49] "Handling and storage of nitrogen tetroxide," Online database, Rocket propulsion laboratory research and technology division, URL: http://www.dtic.mil/dtic/tr/fulltext/u2/404805.pdf, [cited 14 June 2017].

[50] "Health & Environment," Online database, International Tungsten Industry Association, URL: http://www.itia.info/health-environment.html, [cited 13 June 2017].

[51] "Aluminum Sustainability," Online database, The aluminum association, URL: http://www.aluminum.org/aluminum-sustainability, [cited 13 June 2017].

[52] Hamann, R. and van Tooren, M. J. L., "AE3-S01 Systems Engineering & Technical Management Techniques Part I," Lecture Notes, Issue 2, Delft, The Netherlands, Sept. 2006.

[53] Cervone, A. and Gill, E., "Systems Engineering & Aerospace Design," Lecture Slides, Delft, The Netherlands, February 2017.

[54] Euroconsult, "Prospects for the Small Satellite Market Executive Report 2016 Edition," Brochure, Paris, France, 2016.

[55] Girdzijauskas, S. and Streimikiene, D., *Logistic analysis of business cycles, economic bubbles and crises*, chap. 3, IGI Global, 2010, pp. 45–64.

[56] Van Kesteren, M. W., Zandbergen, B. T. C., Naeije, M. C., and Van Kleef, A. J. P., "Design and Analysis of an Airborne, solid Propelled, Nanosatellite Launch Vehicle using Multidisciplinary Design Optimization," *Proceedings of the 6th European Conference for Aeronautics and Space Sciences*, EUCASS, Krakow, Poland, 2015.

[57] Koelle, D. D. E., *Handbook of Cost Engineering and Design of Space Transportation systems*, TransCostSystems, 2013.

[58] Unknown, "Euro area bank interest rate statistics: February 2016," European Central Bank, Directorate Central Communications, Frankfurt am Main, Germany, 2016.

A

HARDWARE

The ALTAR has two main systems, those are the balloon and the rocket. The Gondola and Rocket segments both require avionics and interactions between the components can be seen in fig. A.1. In the hardware diagram, the blue elliptical blocks represent the subsystems and the lines represent interaction between the subsystems and components. More detail of the rocket navigation subsystem can be found in fig. 4.35 and the flow of the electrical power subsystem is shown in fig. 4.41. Furthermore, the components of the data handling system of the product or system can be seen in fig. 4.40.

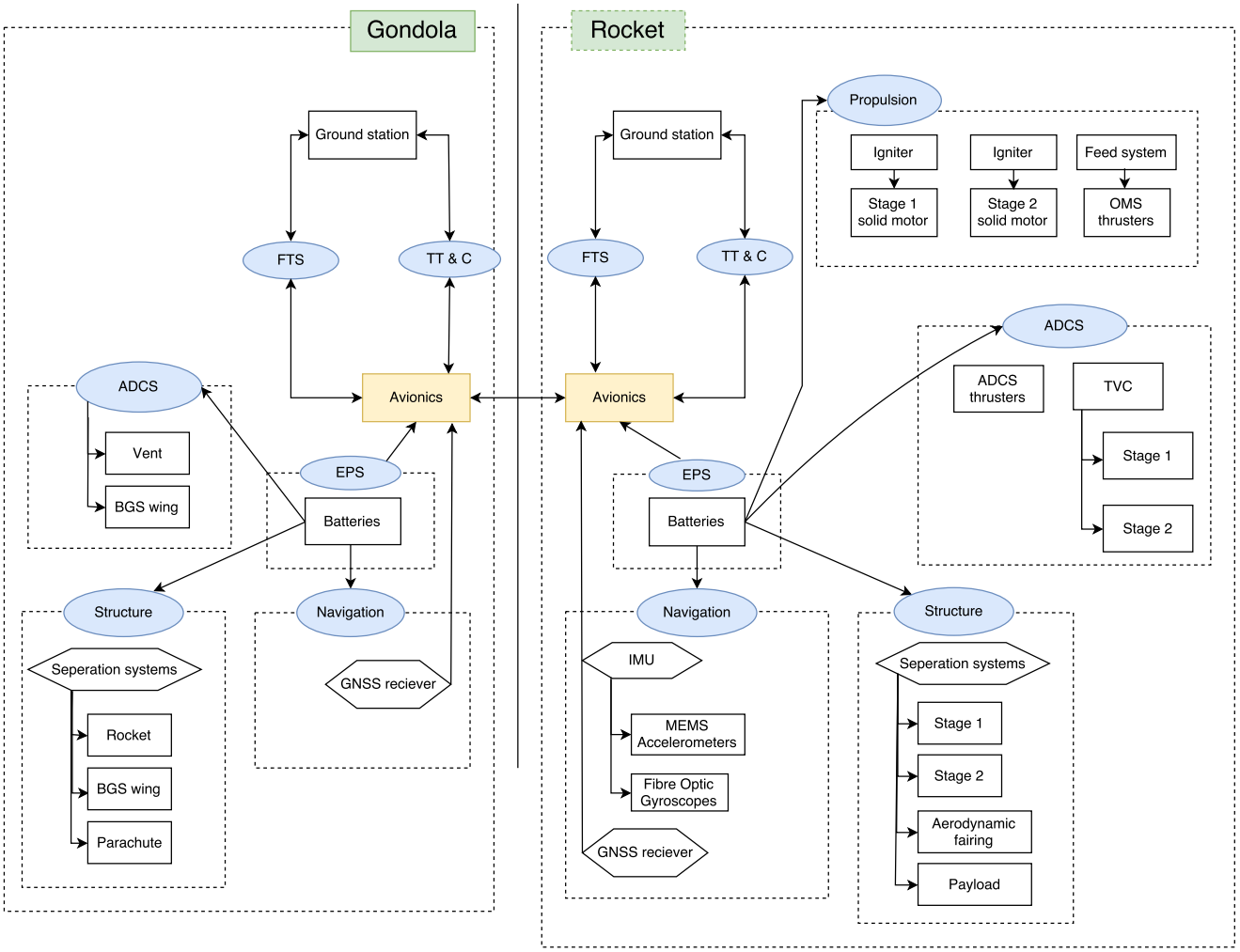

Figure A.1: Illustration of the components of the product or system and their mutual relations and interactions.

This page is intentionally left blank.

B

Task Distribution

Name of Team-member	Sections worked on	Extras
Ruben van den Berg	section 4.5.1 section 4.5.2 section 4.5.3 section 4.5.4 Summary chapter 1 section 5.6 section 4.6.5 chapter 6	Quality Assurance Minutes Introduction
Deacon Foulds	section 4.4.5 section 4.9 section 4.8.1	
Zhouxin Ge	section 4.6 section 4.6.1 section 4.6.2 section 4.6.3 section 4.6.4 section 8.1.2 section 8.1.3 section 4.5.5 section 4.5.6 section 7.2 section 5.3 section 2.2	
Nelson Johnson	Summary section 4.4 section 4.4.1 section 4.4.2 section 4.4.3 section 4.4.4 section 5.8 section 5.8.1 section 5.8.2 section 8.3 section 8.3.1	Full Quality Assurance CATIA Files
Jaime Negro Vadillo	section 4.12.1 section 4.12.2 section 4.12.3 section 7.3 section 8.1 section 8.2	Conclusion and Recommendations,
Sangjae Park	section 2.1 section 4.1 section 4.2.5 section 4.10.1 section 4.10.3 section 4.11.2 section 5.7 appendix A	Jury summary
Martin Reverda	chapter 3 section 4.7.1 section 4.7.2 section 4.4.2 section 5.1	
Giambattista Salvi	section 4.2.2 section 4.2.3 section 4.2.4 section 4.3 section 4.12 section 5.5 section 8.3.2 section 8.3.3 section 8.3.4 section 8.3.5 section 8.3.6 section 8.3.7 section 8.3.8 section 8.3.9	CAD models assembly Parts renderings Cover page.
Bhupinder Sanghera	section 4.1.2 section 4.7.3 section 4.8 section 4.11 section 4.12.4 section 5.2 chapter 9	Preface Acknowledgements Quality Assurance
Anton Shambalov	section 2.1 section 4.2.1 section 4.2.5 section 4.2.6 section 4.8.1 section 4.10 section 4.11 section 5.8 section 5.9 section 7.1	Bibliography